MECHANICS OF ANISOTROPIC CONJUGATE PAIR APPROACH

A Dissertation

by

VEYSEL EREL

Submitted to the Office of Graduate and Professional Studies of
Texas A&M University
in partial fulfillment of the requirements for the degree of

DOCTOR OF PHILOSOPHY

Chair of Committee,	Alan Freed
Committee Members,	Anastasia Muliana
	Micheal Moreno
	Sevan Goenezen
Head of Department,	Andreas A. Polycarpou

December 2019

Major Subject: Mechanical Engineering

ABSTRACT

This thesis proposes conjugate stress/strain pairs, enables to derive constitutive equations without utilizing the invariant theory by using advantages of upper triangular decomposition, improvement for anisotropic materials. Linear small strain and large strain, nonlinear large strain uniaxial composite experimental results have been used to validate transversely isotropic conjugate pair models.

Advantages of anisotropic improvement can be justified as isotropic, and anisotropic models can be obtained from the same strain energy density function. Parameters for a conjugate stress/strain model can be more general than those for a Spencer model, for example, they can be unique for a given data set. The conjugate pair model provides a parameter denoted by n (anisotropic parameter) which has a physical meaning. Conjugate pair models provide linear stress/strain relations for classical rubber like behavior.

To my wonderful parents, my lovely wife and my precious daughter for their tremendous support

ACKNOWLEDGEMENTS

Looking back from the long and demanding journey towards to the finalization of my PhD study, the first person I would like to express my gratitude is my academic advisor, Dr. Alan D. Freed supported and instructed by a mentor like him, who has masterful grasp of his field, is my great pleasure. His positive attitude and smiley face always helped me to figure out difficulties and challenges that I faced during my studies. I have been and will always be benefited through learning from his knowledge and character.

Thanks also to each of my committee members, Dr. Anastasia Muliana who share the experimental data with me, Dr. Micheal Moreno who let me to utilize his laboratory and facilities and valuable comments on our papers, Dr. Sevan Goenezen for sharing their valuable suggestions during my study.

I also wish a very special thanks to my labmate, Mingliang Jiang who helped me a lot to perform uniaxial, biaxial and pure shear experiments.

Finally, I would like to express my very special thanks to my wife, Busra, for her never-ending patience, support, and love. She is the best young mother and the best wife in the world, who has consistently self-sacrificed for us. Last but not least, I would like to thank to my daughter, Melisa, for the peace and happiness she brings to my life each day.

CONTRIBUTORS AND FUNDING SOURCES

Contributors

The polyvinyl-ester data set analyzed for Chapter 4 was provided by Professor Anastasia Muliana. Uniaxial tensile tests were contacted at Biomechanical Environments Laboratory with Mingliang Jiang.

All other work conducted for the thesis (or) dissertation was completed by the student independently.

Funding Sources

Some part of this study was funded by the Texas A&M Engineering Experimental Station.

TABLE OF CONTENTS

Page

LIST OF FIGURES

FIGURE Page

LIST OF TABLES

TABLE Page

1. INTRODUCTION

The conjugate pair approach proposes an easy way to derive constitutive equations for different types of boundary value problems. The rate of mechanical work can be divided into three parts with physical meanings form which constitutive relations can be derived. Researchers do not need to take derivatives of a strain energy density function with respect to their invariants or make complicated calculations.

This proposal begins with a literature review. Continuum mechanics basics, Balance Laws, and differences between simple shear and pure shear experiments is explained. Then, Spencer's fiber model is described via isotropic functions, using the Cayley Hamilton theorem. A uniform extension boundary value problem was solved for one preferred fiber direction. A 2D stiffness matrix was derived for a single, fiber-family material.

In Chapter 2, the conjugate pair model, Srinivasa's upper triangular decomposition, and isotropic and anisotropic conjugate stress/strain pairs are explained. Uniaxial and Biaxial 2D constitutive equations are derived. Experimental procedures, testing protocols, and tools for data analysis are explained explicitly in Chapter 3.

In Chapter 4, small strain experimental data is analyzed and sets of experimental results are compared with Spencer's fiber approach (classical model) and with the conjugate stress/strain model (new model). Material parameter variations have been investigated by statistical analysis. The physical meaning of the strength of anisotropy parameter n is found in Chapter 5. Large strain linear and nonlinear conjugate pair models is discussed in the same chapter. Finite element implementation of the conjugate pair approach is described in Chapter 6. In Chapter 7, main findings and conclusion are addressed.

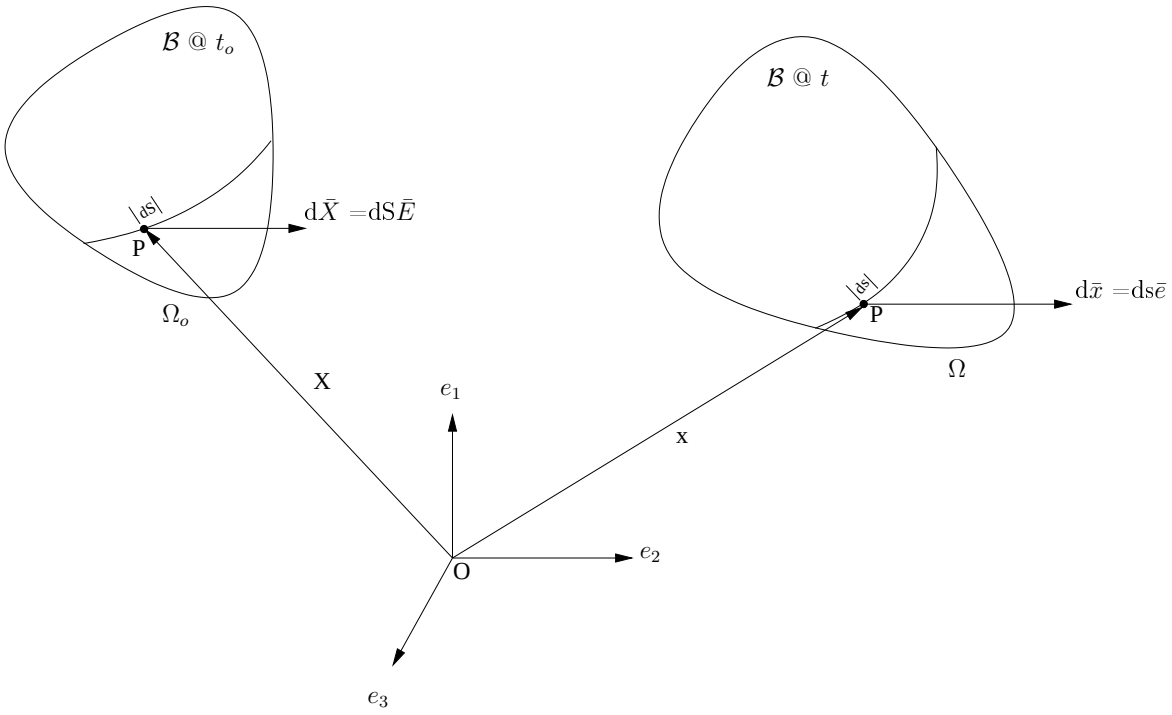

Figure 1.1: Deformation from reference configuration to current configuration

1.1 Continuum Basis

Under the continuum mechanics approach, a body $\mathcal{B} = \{P_k\}$ is designated as a set of material points (P_k) in a three-dimensional Euclidean space ($\mathbf{R}^3$) in which any element of $\mathcal{B}$ has a unique representation. The region in $\mathbf{R}^3$, maintained by the images of the particles, is called a configuration of $\mathcal{B}$. A reference frame associates with an undeformed shape and has an origin located at point O associated with an orthogonal vector basis $\mathbf{e}_i$, i=1,2,3 (coordinate frame). Let a typical particle P be described by its position vector $\mathbf{X}(P)$ in reference frame at reference time (t_o). The domain (Ω_0) of $\mathbf{X}$ that is the region in Euclidean space occupied by $\mathcal{B}$ at time t_o is called reference configuration of $\mathcal{B}$. The motion of a particle relative to reference frame obeys a pair of invertible maps described by the vector function

$$\mathbf{x} = \chi(\mathbf{X}, t). \tag{1.1}$$

As the body moves with time the configuration and position vectors change; thus, the new configuration at time t is called the current configuration of $\mathcal{B}$.

Motion χ is considered to be smooth, which means it is a continuous and differentiable function of position

$$\mathbf{F} = \partial\mathbf{x}/\partial\mathbf{X} = \text{Grad } \mathbf{x} \tag{1.2}$$

where $\mathbf{F}$ is the gradient of motion called the deformation gradient. This tensor transforms a tangent element $\mathrm{d}\mathbf{X}$ from the reference configuration into a tangent element $\mathrm{d}\mathbf{x}$ in the current configuration, as shown in Fig. 1.1, thus

$$\mathrm{d}\mathbf{x} = \mathbf{F}\mathrm{d}\mathbf{X}. \tag{1.3}$$

Let's assume $|\mathrm{d}\mathbf{x}| = \mathrm{ds}$ and $|\mathrm{d}\mathbf{X}| = \mathrm{dS}$, where s and S are the arc lengths for the deformed and initial states, respectively. So, Eq. 1.3 can be written as

$$\lambda\mathbf{e} = \mathbf{F}\mathbf{E} \tag{1.4}$$

which $\mathbf{e} = \mathrm{d}\mathbf{x}/\mathrm{ds}$ and $\mathbf{E}$=$\mathrm{d}\mathbf{X}/\mathrm{dS}$ are unit vectors that are tangent to a line. Thus, stretch can be described as

$$\lambda = \mathrm{d}s/\mathrm{d}S \tag{1.5}$$

which is ratio of a current length ds to its reference length dS of a material element.

In continuum mechanics, the deformation gradient tensor $\mathbf{F}$ plays an important role in describing how small line segments, infinitesimal surface areas, and infinites-

imal volumes transform from the reference configuration to a current configuration. For small line segments, the relationship between these two configuration has been shown at Eq. 1.3. Similarly, assuming a reference, infinitesimal, surface area $\mathrm{d}A$ and its associated current, infinitesimal, surface area $\mathrm{d}a$, their relationship between configurations is described as

$$\mathbf{n}\mathrm{d}a = \det(\mathbf{F})\mathbf{F}^{-\mathrm{T}}\mathbf{N}\mathrm{d}A \tag{1.6}$$

where $\mathbf{N}$ and $\mathbf{n}$ are unit normal vectors to surfaces $\mathrm{d}A$ and $\mathrm{d}a$, respectively. This relation is known as Nanson's formula. Further, the volume relation

$$\mathrm{d}v = \det(\mathbf{F})\mathrm{d}V \tag{1.7}$$

describes how infinitesimal volumes transformation between the initial and current configurations. This relationship shows that the determinant of the deformation gradient is the ratio of the current volume to a reference volume. The conservation of mass requires that $\det(\mathbf{F}) \neq 0$; otherwise, line elements of non-zero length in some reference configuration could be mapped into line elements of zero length in the current configuration*. A different way of saying that a volume change cannot become negative at any stage of deformation is that

$$J = \det(\mathbf{F}) > 0. \tag{1.8}$$

A deformation is said to be isochoric (incompressible) if there is no volume change, i.e., if $\det(\mathbf{F}) = 1$.

*Dr. K.R. Rajagopal explained this during one of his lectures, we cannot take a cube and transform it to a plane.

1.1.1 Stress Principles, Balance Laws and Equilibrium

A deformation of a material body $\mathcal{B}$ is caused by a system of applied forces that are comprised of resultant body forces and contact forces. Applied forces are measured in the current configuration. These forces act on any part $\mathcal{P} \subset \mathcal{B}$ of body $\mathcal{B}$. The body forces are dispersed all around the continuum and act on each particle of the body in its current configuration, and are described by a vector field $\mathbf{b}$. Body forces may be related to gravitational or magnetic forces. On the other hand, $\mathbf{t_n}$ is defined as a distribution of contact forces per unit surface area. It is local and applies on an infinitesimal surface element of area $\mathrm{d}S$.

The total force $\mathcal{F}(\mathcal{P},t)$ and the total torque $\mathcal{T}(\mathcal{P},t)$ acting on a part of the body $\mathcal{P}$ are associated with the momentum and the moment of momentum of a body ($\mathcal{B}$) at its material points. Thus, Euler's law of motion can be shown as [3],

$$\mathcal{F}(\mathcal{P},t) = \int_{\partial\mathcal{P}} \mathbf{t_n} \mathrm{d}a + \int_{\mathcal{P}} \mathbf{b} \mathrm{d}v = \frac{\mathrm{d}}{\mathrm{d}t} \int_{\mathcal{P}} \mathbf{v} \mathrm{d}m \tag{1.9}$$

$$\mathcal{T}(\mathcal{P},t) = \int_{\partial\mathcal{P}} \mathbf{x} \times \mathbf{t_n} \mathrm{d}a + \int_{\mathcal{P}} \mathbf{x} \times \mathbf{b} \mathrm{d}v = \frac{\mathrm{d}}{\mathrm{d}t} \int_{\mathcal{P}} \mathbf{x} \times \mathbf{v} \mathrm{d}m \tag{1.10}$$

where $\mathrm{d}m = \rho \mathrm{d}v$ is the material element of mass with density ρ per unit volume in $\mathcal{B}$ @ t. The principle of balance of mass also equates $\mathrm{d}m = \rho_r \mathrm{d}V$ where ρ_r is the mass density per unit volume V in a reference configuration. Due to the conservation of mass principle, a density relation follows

$$\rho_r = \det(\mathbf{F})\rho. \tag{1.11}$$

After the momentum equation (1.9) was applied to an arbitrary tetrahedral element,

Cauchy's theory of stress leads to

$$\mathbf{t_n} = \mathbf{Tn} \tag{1.12}$$

where $\mathbf{n}$ is the unit normal vector to $\partial\mathcal{P}$ in the current configuration, $\mathbf{T}$ is called Cauchy stress tensor which measures force per unit deformed area, and $\mathbf{t_n}$ is the traction or stress vector, also with units of force per unit deformed area. Hence, the Cauchy stress tensor was derived from the existence of contact force, Eq. 1.12 has to satisfy Euler's law of motion. By using the divergence theory, the momentum relation, Eq. 1.9, becomes

$$\mathrm{div}(\mathbf{T}) + \mathbf{b} = \rho\mathbf{a}. \tag{1.13}$$

This equation, known as Cauchy's first law of motion, is a necessary condition to ensure a balance of linear momentum. The combination of Euler's moment of momentum equation (1.10) with Cauchy's stress principle (1.12) leads to

$$\mathbf{T}^{\mathrm{T}} = \mathbf{T} \tag{1.14}$$

which is known as Cauchy's second law. Under the purely static loading condition, and in an absence of body forces, Cauchy's first law of motion, Eq. (1.10), transforms to

$$\mathrm{div}(\mathbf{T}) = 0 \tag{1.15}$$

which is the condition for quasistatic equilibrium.

The Cauchy stress tensor establishes the contact force ($\mathbf{t_n}$) in the current configuration; however, there are some applications that use a reference configuration. Thus, the engineering stress tensor $\mathbf{P}$, also known as first Piola-Kirchoff stress tensor, is

introduced to establish contact forces in a reference configuration. This engineering stress ($\mathbf{P}$) is not necessary symmetric, like Cauchy stress. The relationship between these tensors is

$$\mathbf{P} = \det(\mathbf{F})\mathbf{T}\mathbf{F}^{\mathrm{T}}. \tag{1.16}$$

1.1.2 Mechanical Energy Principles

Lets apply the mechanical energy principle, neglecting all thermal effects; thus, the total mechanical energy time derivative $E(\mathcal{P},t)$ for any part $\mathcal{P} \subset \mathcal{B}$ of body $\mathcal{B}$ is equal to the rate of working of the applied forces $\Pi(\mathcal{P},t)$

$$E(\mathcal{P},t) = \Pi(\mathcal{P},t) \tag{1.17}$$

where the total mechanical energy contains the total kinetic energy and the total potential energy, according to Hamilton's principle. Thus, these terms may be written as [4]

$$\frac{\mathrm{d}}{\mathrm{d}t}\Big[\int_{\mathcal{P}} \frac{1}{2}\mathbf{v}\cdot\mathbf{v}\mathrm{d}m + \int_{\mathcal{P}} W(\mathbf{F})\mathrm{d}V\Big] = \int_{\partial\mathcal{P}} \mathbf{t_n}\cdot\mathrm{d}a + \int_{\mathcal{P}} \mathbf{b}\cdot\mathbf{v}\mathrm{d}v \tag{1.18}$$

where W($\mathbf{F}$) is the elastic stored energy per unit reference volume, which is also known as the strain-energy density. The equation above can be solved by using Cauchy's stress principle, the divergence theorem and Cauchy's first law to develop explicit formulas for both Cauchy stress and the first Piolo-Kirchoff stress. Due to the dependence of W on the deformation gradient, the rate $\partial W(\mathbf{F})/\partial t$ can be expressed as

$$\frac{\partial W}{\partial t} = \mathrm{tr}\Big(\mathbf{F}\frac{\partial W}{\partial \mathbf{F}}\mathbf{L}\Big) \tag{1.19}$$

where $\mathbf{L}$ is velocity gradient tensor, $\mathbf{L} = grad\mathbf{v} = \dot{\mathbf{F}}\mathbf{F}^{-\mathbf{1}}$.

A hyperelastic/Green elastic solid is a material whose strain energy (elastic po-

tential) can be expressed as a function of

$$W(\mathbf{X},t) = W(\mathbf{F}(\mathbf{X},t),\mathbf{X}) \tag{1.20}$$

Theorem [3]: For elastic bodies the work assumption implies that there exists a function

$$W : \tau^{+} \cdot \mathcal{B} \ @ \ t \quad P = \left[\frac{\partial W(\mathbf{F},\mathbf{X})}{\partial \mathbf{F}}\right]^{\mathrm{T}} \tag{1.21}$$

After introducing basic principles of continuum mechanics. Polar and upper-triangular decomposition have been compared and contrasted for the pure shear and simple shear deformation.

1.2 Polar Decomposition and Upper Triangular Decomposition

In 2012, Srinivasa [5] demonstrated that constitutive equations for Green elastic materials can be derived from a distortion tensor that arises from an upper-triangular decomposition of the deformation gradient. This decomposition doesn't require an eigen analysis, in addition, it is very simple, fast and widely applicable. It proposes that the total deformation can be decomposed into physically apparent, meaningful, and simple constituents. The polar and upper-triangular decompositions are explained in this section, and applied to simple shear and pure shear deformations to observe their similarities and differences.

Let the gradient of motion be $\mathbf{F}$. Then the polar decomposition theorem implies

$$\mathbf{F} = \mathbf{RU} = \mathbf{VR} \tag{1.22}$$

where $\mathbf{R}$ is an orthogonal tensor and $\mathbf{U}$ and $\mathbf{V}$ are the symmetric, positive-definite, right- and left-stretch tensors, respectively. To quantify these rotation and stretch tensors an eigen analysis is required. For this reason, Green's deformation tensor

($\mathbf{C} = \mathbf{F}^{\mathsf{T}}\mathbf{F}$) needs to be calculated first, which is equal to $\mathbf{U}^2$. Then one performs an eigenvector/eigenvalue analysis using the conventional equation ($\mathbf{Ax} = \lambda\mathbf{x}$). Eigenvectors ($\mathbf{x_i}$) form columns within the rotation matrix ($\mathbf{R}$), while the eigenvalues (λ_i) are the principal stretches belonging to $\mathbf{U}$ and $\mathbf{V}$. The stretch tensor ($\mathbf{U}$) and its inverse ($\mathbf{U}^{-1}$) can be obtaioned through calculating the square root of Green's deformation tensor using the Cayley-Hamilton theorem [6], with $\mathbf{R} = \mathbf{F}\mathbf{U}^{-1}$ following thereafter. This way is a Lagrangian approach for quantifying the rotation and right-stretch tensors. An Eulerian way can be accomplished by starting with the Finger deformation tensor ($\mathbf{B} = \mathbf{F}\mathbf{F}^{\mathsf{T}}$) and employing the same procedure.

On the other hand, Gram-Schmitdt (upper triangular) factorization decomposes a matrix into a product of a rotation and an upper-triangular matrix, where $\mathbf{Q}$ is a proper orthogonal matrix and $\mathbf{R}$ is an upper-triangular matrix. As this applies to the deformation gradient $\mathbf{F}$, we adopt the notation of Srinivasa [5], viz., $\mathbf{F} = \mathbf{Q}\tilde{\mathbf{F}}$ where $\mathbf{Q}$ is orthogonal and $\tilde{\mathbf{F}}$ is upper triangular. This deformation interpretation can be deconstructed into physically apparent, meaningful, and simple entities.

Rotation $\mathbf{Q}$ arising from a Gram-Schmidt decomposition of $\mathbf{F}$ is distinct from the rotation $\mathbf{R}$ coming from a polar decomposition of $\mathbf{F}$!

A Cholesky factorization the right Cauchy-Green deformation tensor $\mathbf{C} = \mathbf{F}^{\mathsf{T}}\mathbf{F} = \tilde{\mathbf{F}}^{\mathsf{T}}\tilde{\mathbf{F}}$ establishes the components of distortion that in the 2D case are [5]

$$[\tilde{\mathbf{F}}] = \begin{bmatrix} a & a\gamma \\ 0 & b \end{bmatrix}, \quad a = \sqrt{C_{11}}, \quad b = \sqrt{C_{22} - C_{12}^2/C_{11}}, \quad \gamma = C_{12}/C_{11} \tag{1.23}$$

where all parameters have physical meaning, such as: a is an elongation in the 1-direction, b is an elongation in the 2-direction, both measured from a reference gage of unit length, and γ is the magnitude of shear in the 12-plane. A practical side of

these parameters is that an experimentalist can measure them directly. Elongations a and b are equivalent to stretches λ_1 and λ_2 *only* when there is an absence of shear.

Conveniently, the elongations a and b, and the shear γ can all be calculated in terms of entities from the deformation gradient as [7]

$$a = \sqrt{F_{11}^2 + F_{21}^2}, \quad b = \frac{F_{11}F_{22} - F_{12}F_{21}}{\sqrt{F_{11}^2 + F_{21}^2}}, \quad \gamma = \frac{F_{11}F_{12} + F_{21}F_{22}}{F_{11}^2 + F_{21}^2} \tag{1.24}$$

as can the trigonometric functions

$$\sin\theta = \frac{-F_{21}}{\sqrt{F_{11}^2 + F_{21}^2}}, \quad \cos\theta = \frac{F_{11}}{\sqrt{F_{11}^2 + F_{21}^2}} \tag{1.25}$$

which populate rotation

$$\mathbf{Q} = \begin{bmatrix} \cos\theta & \sin\theta \\ -\sin\theta & \cos\theta \end{bmatrix} \quad \text{obeying} \quad \mathbf{Q} = \mathbf{F}\tilde{\mathbf{F}}^{-1} \tag{1.26}$$

with θ being that angle by which the material coordinate axes $\tilde{\mathbf{e}}_i$ (wherein a, b and γ are measured) rotate about the reference coordinate axes $\mathbf{e}_i$ (wherein the observer resides).

Freed [8] applied the **QR** decomposition to solve different boundary conditions. The upper-triangular decomposition introduces a new theoretical framework, which is called experimentor's frame. This new coordinate frame coincides with the Eulerian frame for deformations without any rotation, such as uniaxial and biaxial tension/compression deformations. Disparity between the Eulerian and experimentor's frames can be easily visualized under simple shear and pure shear deformations. Simple/pure shear deformations are now reviewed to clarify rotation tensor differences as they pertain to the polar/upper-triangular decompositions.

1.2.1 Simple Shear Deformation

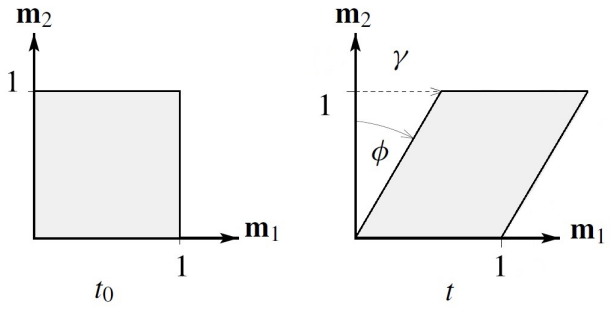

Figure 1.2: Simple shear deformation where shear strain is given by $\gamma = \tan\phi$. [1]

The deformation gradient of a planar material subjected to a simple shear (shown in Fig. 1.2) is quantified by the matrix

$$[\mathbf{F}] = \begin{bmatrix} 1 & \gamma \\ 0 & 1 \end{bmatrix} \tag{1.27}$$

while the Green deformation tensor $\mathbf{C} = \mathbf{F}^{\mathsf{T}}\mathbf{F}$ and the Finger deformation tensor $\mathbf{B} = \mathbf{F}\mathbf{F}^{\mathsf{T}}$ have components of

$$[\mathbf{C}] = \begin{bmatrix} 1 & \gamma \\ \gamma & 1+\gamma^2 \end{bmatrix} \quad \text{and} \quad [\mathbf{B}] = \begin{bmatrix} 1+\gamma^2 & \gamma \\ \gamma & 1 \end{bmatrix} \tag{1.28}$$

. The rotation tensor $\mathbf{R}$ (the product of a polar decomposition, which requires an eigen analysis) and the rotation tensor $\mathbf{Q}$ (the outcome of an upper-triangular decomposition, which does not require an eigen analysis) are distinct, viz.,

$$[\mathbf{R}] = \frac{1}{\sqrt{4+\gamma^2}} \begin{bmatrix} 2 & \gamma \\ -\gamma & 2 \end{bmatrix}, \quad [\mathbf{Q}] = \begin{bmatrix} 1 & 0 \\ 0 & 1 \end{bmatrix} \tag{1.29}$$

1.2.2 Pure Shear Deformation (Strength of Materials)

In a pure shear deformation (as introduced in strength of materials), the difference between all three coordinate frames can be easily visualized. The Lagrangian, Eulerian, and experimentor's frames are all illustrated in Fig. 1.3.

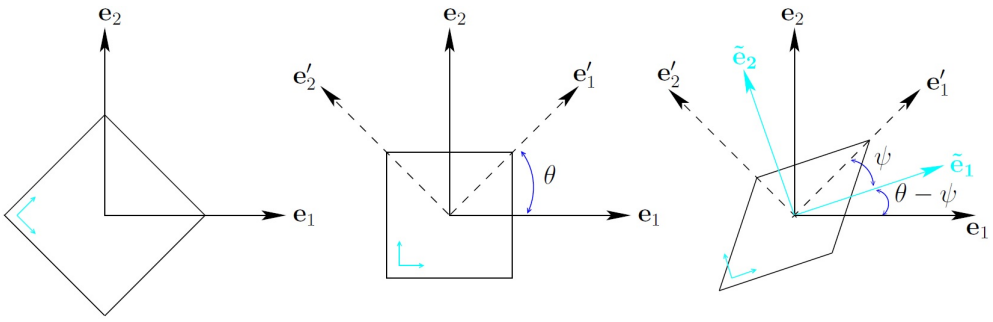

Figure 1.3: The figure at the left shows a Lagrangian viewpoint ($\mathbf{e}$, solid lines), the figure in the middle shows an Eulerian viewpoint ($\mathbf{e}'$, dashed lines), and the figure at the right shows an experimentor's viewpoint ($\tilde{\mathbf{e}}$, colored lines) [1]

Let the square in the left graphic of Fig. 1.3 be placed in a Lagrangian frame. A small reference frame, the experimentor's coordinates, is drawn in one corner of the square. This square is then rotated by an angle θ (in this case, 45°). The rotated square can be observed in the middle graphic of Fig. 1.3. The dashed lines represent the Eulerian frame. Afterwords we deform the square by pulling an amount of λ on two opposing corners and proportionally pushing by an amount of $(1/\lambda)$ on the other two opposing corners, as formulated in strength of materials. We then zoom in and

move the small axes from the corner to the center of the square. The colored lines are the experimentor's frame, with angle ψ being the rotation between the Eulerian and experimentor's axes. Rotation tensors for both frames can be described as

$$[\mathbf{R}] = \frac{1}{\sqrt{2}} \begin{bmatrix} 1 & 1 \\ -1 & 1 \end{bmatrix}, \quad [\mathbf{Q}] = \frac{1}{\sqrt{\lambda^2 + 1/\lambda^2}} \begin{bmatrix} \lambda & 1/\lambda \\ -1/\lambda & \lambda \end{bmatrix} = \begin{bmatrix} \cos\phi & \sin\phi \\ -\sin\phi & \cos\phi \end{bmatrix} \tag{1.30}$$

where $\theta = 45^\circ$ so $\sin\theta = \cos\theta = 1/\sqrt{2}$ and where λ is the stretch in the $\mathbf{e}_1'$ direction.

1.3 Spencer's Fiber Approach

Spencer's [9] fiber model is one of the pioneering studies in fiber reinforced materials. Before his study researchers, such as Adkins and Rivlin (1955) and Green and Adkins (1960), assumed fibers to be infinitesimally thin. Their fibers do not occupy any volume and are localized in an isotropic material. "The result of these assumptions is that the material is constrained isotropic material" [9, pp. 79].

Spencer's fiber model has no constraints and is appropriate for densely distributed fibers. He states that the strain energy function W is a function of the deformation gradient $F_{iR} = \partial x_i / \partial X_R$ and an initial fiber direction a_R. Because a material response does not depend upon one's frame of reference, the strain energy function has to be invariant under any rigid body rotation of the deformed configuration. For example, a position vector rotates according to

$$\bar{x}_i = Q_{iJ} x_J \tag{1.31}$$

where x_i is the current position of a particle position in the deformed body, Q_{iJ} is an arbitrary proper orthogonal matrix, and $\bar{x}_i$ is the particle's position after the rigid

body rotation. Thus

$$W(\partial x_i/\partial X_R, a_R) = W(\partial \bar{x}_i/\partial X_R, \bar{a}_R) \tag{1.32}$$

for any Q_{iJ} that satisfies $Q_{iK}Q_{jK} = I_{ij}$ and $\det(\mathbf{Q}) = 1$. This suggests W is a function of Green's deformation tensor $C_{RS} = F_{iR}F_{iS}$ and the initial fiber direction a_R. The deformation gradient tensor does not obey an isotropic function rule, but the Green deformation tensor does. Thus, if a strain energy function is a function of the Green deformation tensor, then the constitutive equations will be directly isotropic ($\bar{\mathbf{C}} = \mathbf{Q}.\mathbf{C}.\mathbf{Q}^{\mathbf{T}}$).

Let $\bar{x}_R$ be the position of a particle in an undeformed body after a rigid body rotation, and let $\bar{a}_R$ be the fiber direction in the undeformed rotated body. Spencer assumed that anisotropic properties of a material only come from fibers, then

$$W(C_{RS}, a_R) = W(\bar{C}_{RS}, \bar{a}_R). \tag{1.33}$$

If the above equation holds, then W does not depend upon rigid rotations. W is an isotopic function of C_{RS} and a_R and can therefore be replaced by a set of isotropic invariants of these tensor fields. Furthermore, because a_R is not a material property, W has to be an even function of $\mathbf{a}$ (fiber direction) in order for it to represent an isotropic invariant. That is, a fiber has no preferred direction. It should be replaced by the vector product $a_R a_S$. In that case, C_{RS} and $a_R a_S$ are symmetric second-order tensors; thus in the 3D case, W can be expressed as a function of ten invariants [9]

$$\begin{aligned} &\mathrm{tr}\mathbf{C}, \mathrm{tr}\mathbf{C}^2, \mathrm{tr}\mathbf{C}^3, \mathrm{tr}(\mathbf{aa}), \mathrm{tr}(\mathbf{aa})^2, \mathrm{tr}(\mathbf{aa})^3, \\ &\mathrm{tr}(\mathbf{aa})\mathbf{C}, \mathrm{tr}(\mathbf{aa})\mathbf{C}^2, \mathrm{tr}(\mathbf{aa})^2\mathbf{C}, \mathrm{tr}(\mathbf{aa})^2\mathbf{C}^2 \end{aligned} \tag{1.34}$$

where

$$C_{RS} = \frac{\partial x_i}{X_R}\frac{\partial x_i}{X_S}, \quad \mathbf{C} = [C_{RS}], \quad (\mathbf{aa}) = [a_R a_S]. \tag{1.35}$$

Since **a** is a unit vector

$$\begin{gathered}(\mathbf{aa}) = (\mathbf{aa})^2 = (\mathbf{aa})^3 = ..., \\ \mathrm{tr}(\mathbf{aa}) = \mathrm{tr}(\mathbf{aa})^2 = \mathrm{tr}(\mathbf{aa})^3 = ... = 1\end{gathered} \tag{1.36}$$

and the number of independent moment invariants in Eq. (1.34) reduces to five:

$$\mathrm{tr}(\mathbf{C}), \mathrm{tr}(\mathbf{C}^2), \mathrm{tr}(\mathbf{C}^3), \mathrm{tr}(\mathbf{aa})\mathbf{C}, \mathrm{tr}(\mathbf{aa})\mathbf{C}^2. \tag{1.37}$$

The invariants shown above can be written as a different set

$$\begin{gathered}J_1 = \mathrm{tr}(\mathbf{C}), \quad J_2 = \frac{1}{2}\{\mathrm{tr}(\mathbf{C})^2 - \mathrm{tr}(\mathbf{C}^2)\}, \quad J_3 = \mathrm{tr}(\mathbf{aa})\mathbf{C}^2, \\ K_1 = \det \mathbf{C}, \quad K_2 = \mathrm{tr}(\mathbf{aa})\mathbf{C}.\end{gathered} \tag{1.38}$$

according to the Cayley-Hamilton theorem. Thus, W can also be a function of the J_1, J_2, J_3, K_1, K_2 invariants, which have greater physical appeal. If the applied fibers are inextensible, i.e., stretch $\lambda = 1$ in the fiber direction, and if the material is incompressible, i.e., $\rho = \rho_o$ and therefore detF=1, then

$$K_1 = 1, \quad K_2 = 1. \tag{1.39}$$

The Finger deformation tensor and fiber direction, as Eulerian fields, are defined below

$$B_{ij} = \frac{\partial x_i}{\partial X_R}\frac{\partial x_j}{\partial X_R}, \quad a_i = \frac{\partial x_i}{\partial X_R}a_R. \tag{1.40}$$

Like invariants to Eq. (1.38) can be written for these fields

$$\begin{aligned} J_1 = \mathrm{tr}(\mathbf{B}) = B_{ii}, \quad J_2 = \frac{1}{2}\{(\mathrm{tr}\mathbf{B})^2 - \mathrm{tr}(\mathbf{B}^2)\} = \frac{1}{2}\{B_{ii}^2 - B_{ik}B_{ik}\}, \\ J_3 = \mathrm{tr}(\mathbf{aa})\mathbf{B} = a_i B_{ik} a_k, \quad K_1 = \det(\mathbf{B}), \quad K_2 = \mathrm{tr}(\mathbf{aa}) = a_i a_i \end{aligned} \tag{1.41}$$

with $K_1 = 1$ if the material is incompressible and $K_2 = 1$ if the fibers are inextensible. The relationship between second Piola-Kirchhoff Stress and Cauchy stress is

$$\mathbf{S}(X,t) = \det(\mathbf{F})[\mathbf{F}^{-1}][\mathbf{T}(x,t)][\mathbf{F}^{-1}]^T \tag{1.42}$$

because the push-forward operator of a weighted contravariant tensor is [10]

$$T_{ij} = \frac{1}{\det(F)} \frac{\partial x_i}{\partial X_R} \frac{\partial x_j}{\partial X_S} S_{RS}. \tag{1.43}$$

Elastic constitutive equations expressed in terms of the second Piola-Kirchhoff stress and the Green strain are described by

$$S_{RS} = \frac{1}{2}\Big(\frac{\mathrm{d}W(E)}{\mathrm{d}E_{RS}} + \frac{\mathrm{d}W(E)}{\mathrm{d}E_{SR}}\Big). \tag{1.44}$$

The Green strain, determinant of the deformation gradient, and the K_1 invariant are described by

$$E_{RS} = \frac{1}{2}\Big(C_{RS} - \delta_{RS}\Big), \quad \det(\mathbf{F}) = \sqrt{\det(\mathbf{C})}, \quad K_1 = \det(\mathbf{C}). \tag{1.45}$$

Taking the derivative of Green Strain, $2\mathbf{dE} = \mathbf{dC}$, and plugging it into Eq. (1.44) combined with Eq. (1.43) leads to

$$T_{ij} = {K_1}^{-\frac{1}{2}} \frac{\partial x_i}{\partial X_R} \frac{\partial x_j}{\partial X_S} \Big(\frac{\mathrm{d}W}{\mathrm{d}C_{RS}} + \frac{\mathrm{d}W}{\mathrm{d}C_{SR}}\Big). \tag{1.46}$$

Due to the inextensible and incompressible constraints, two Lagrange multipliers should be introduced, viz., p and t, such that W is replaced by

$$W-\frac{1}{2}p(K_1-1)+\frac{1}{2}t(K_2-1). \tag{1.47}$$

Inserting value K_1 into Eq. (1.46) and using the chain rule to represent the strain energy density in terms of invariants J_1, J_2, J_3 results in

$$\begin{aligned} T_{ij}=\frac{\partial x_i}{\partial X_R}\frac{\partial x_j}{\partial X_S}\Big\{W_1\big(\frac{\partial J_1}{\partial C_{RS}}+\frac{\partial J_1}{\partial C_{SR}}\big)+W_2\big(\frac{\partial J_2}{\partial C_{RS}}+\frac{\partial J_2}{\partial C_{SR}}\big)+W_3\big(\frac{\partial J_3}{\partial C_{RS}}+\frac{\partial J_3}{\partial C_{SR}}\big) \\ -\frac{1}{2}p\big(\frac{\partial K_1}{\partial C_{RS}}+\frac{\partial K_1}{\partial C_{SR}}\big)+\frac{1}{2}t\big(\frac{\partial K_2}{\partial C_{RS}}+\frac{\partial K_2}{\partial C_{SR}}\big)\Big\} \end{aligned} \tag{1.48}$$

where $W_1=\partial W/\partial J_1, W_2=\partial W/\partial J_2$, and $W_3=\partial W/\partial J_3$. Inserting Eq. (1.38) values into the above Cauchy stress equation results in the following gradients

$$\begin{aligned} &\frac{\partial J_1}{\partial C_{RS}}=\frac{\partial \mathrm{tr}\mathbf{C}}{\partial C_{RS}}=\delta_{RS}, \\ &\frac{\partial J_2}{\partial C_{RS}}=\frac{\partial \frac{1}{2}\big((\mathrm{tr}\mathbf{C})^2-\mathrm{tr}\mathbf{C}^2\big)}{\partial C_{RS}}=\mathrm{tr}\mathbf{C}\delta_{RS}-C_{RS}=J_1\delta_{RS}-C_{RS}, \\ &\frac{\partial J_3}{\partial C_{RS}}=\frac{\partial \mathrm{tr}(\mathbf{aa})\mathbf{C}^2}{\partial C_{RS}}=a_RC_{SI}a_I+a_IC_{IR}a_S, \\ &\frac{\partial K_1}{\partial C_{RS}}=\frac{\partial \det(\mathbf{C})}{\partial C_{RS}}=\det(\mathbf{C})\mathbf{C}^{-\mathrm{T}}=J_2\delta_{RS}-J_1C_{RS}+C_{RI}C_{IS}, \\ &\frac{\partial K_2}{\partial C_{RS}}=\frac{\partial \mathrm{tr}(\mathbf{aa})\mathrm{C}}{\partial C_{RS}}=a_Ra_S. \end{aligned} \tag{1.49}$$

Pushing forward the invariant derivatives of Eq. (1.49) with $\frac{\partial x_i}{\partial X_R}\frac{\partial x_j}{\partial X_S}$ produces

$$\begin{aligned}
&\frac{\partial x_i}{\partial X_R}\frac{\partial x_j}{\partial X_S}\delta_{RS} = B_{ij},\\
&\frac{\partial x_i}{\partial X_R}\frac{\partial x_j}{\partial X_S}(J_1\delta_{RS} - C_{RS}) = J_1 B_{ij} - B_{ik}B_{jk},\\
&\frac{\partial x_i}{\partial X_R}\frac{\partial x_j}{\partial X_S}(a_R C_{SI} a_I + a_I C_{IR} a_S) = a_i B_{jk} a_k + a_j B_{ik} a_k,\\
&\frac{\partial x_i}{\partial X_R}\frac{\partial x_j}{\partial X_S}(J_2\delta_{RS} - J_1 C_{RS} + C_{RI}C_{IS}) = \delta_{ij},\\
&\frac{\partial x_i}{\partial X_R}\frac{\partial x_j}{\partial X_S}a_R a_S = a_i a_j.
\end{aligned} \tag{1.50}$$

After plugging the equalities above, Cauchy stress can be expressed as

$$\begin{aligned}
T_{ij} = 2(W_1 + J_1 W_2)B_{ij} - 2W_2 B_{ik}B_{jk} + 2W_3(a_i B_{jk} a_k + a_j B_{ik} a_k)\\
- p\delta_{ij} + t a_i a_j.
\end{aligned} \tag{1.51}$$

After subtracting out the Lagrange multipliers, a reaction stress (R_{ij}) can be identified

$$T_{ij} = -p\delta_{ij} + t a_i a_j + R_{ij}. \tag{1.52}$$

Because the Lagrange multipliers contain pressure and fiber stress, the reaction stresses R_{ii} and $a_i a_j R_{ij}$ will be zero. Therefore R_{ij} should be modified to satisfy these conditions.

$$\begin{aligned}
R_{ij} =& 2(W_1 + J_1 W_2)B_{ij} - 2W_2 B_{ik}B_{jk} + 2W_3(a_i B_{jk} a_k + a_j B_{ik} a_k) -\\
&\{(J_1 - J_3)W_1 + (J_2 + 1)W_2\}\delta_{ij} +\\
&\{(J_1 - 3J_3)W_1 - (J_2 - 3)W_2 - 4J_3 W_3\} a_i a_j
\end{aligned} \tag{1.53}$$

which is Spencer's constitutive equation.

1.3.1 Validation with 2D Fiber Model

The Model that is derived above for the 3D case can be used for 2D plane strain.

Proof: Consider a bi-axial experiment obeying a plane strain condition whose fibers are located in the x_1 and x_2 direction so that

$$a_3 = 0, B_{13} = B_{23} = 0, B_{33} = 1. \tag{1.54}$$

The 3D Finger deformation tensor now has components of

$$\begin{bmatrix} B_{11} & B_{12} & 0 \\ B_{21} & B_{22} & 0 \\ 0 & 0 & 1 \end{bmatrix}, \quad J_1 = B_{11} + B_{22} + 1, \quad J_2 = B_{11} + B_{22} + B_{11}B_{22} - B_{12}^2. \tag{1.55}$$

Therefore the determinant of the 2D plane-strain Finger deformation tensor is $\det(\mathrm{B}) = B_{11}B_{22} - B_{12}^2 = 1$ impliying that

$$J_1 = J_2 = B_{11} + B_{22} + 1 \tag{1.56}$$

with the relationship between J_2 and J_3 being $J_3 = J_2 - 2$ and the shear strain relationship becomes $\gamma^2 = J_3 - 1$ [9]. Thus, a plane strain bi-axial experiment can be signified directly in terms of γ. The strain energy density becomes a function of γ.

1.3.2 One Preferred Direction Fiber Uniform Extension

Consider rectangular block that contains fibers perpendicular to the X_3 direction. Initial fiber position has a ϕ degree angle to the X_1 direction, as seen Fig. 1.4.

Uniaxial extension has been applied in the X_1 direction. The relation between

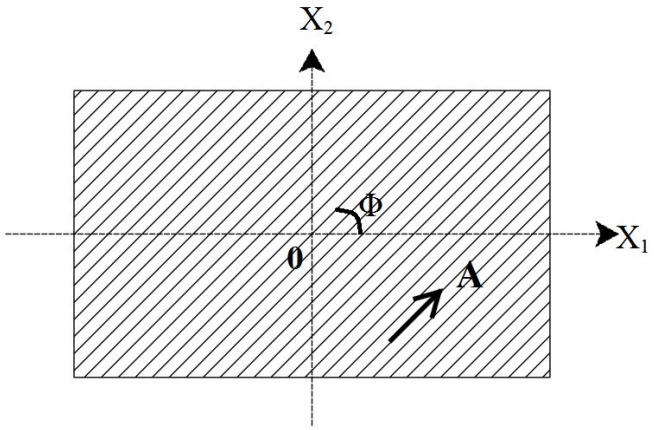

Figure 1.4: Lagrangian configuration of a rectangular part that is reinforced with a one preferred direction of straight fibers

initial and final configurations is

$$x_1 = \lambda_1 X_1, \quad x_2 = \lambda_2 X_2, \quad x_3 = \lambda_3 X_3. \tag{1.57}$$

initial and final fiber directions is

$$A = (\cos\phi, \sin\phi, 0), \quad a = (\cos\theta, \sin\theta, 0). \tag{1.58}$$

where $\cos\theta = \lambda_1 \cos\phi$, and $\sin\theta = \lambda_2 \sin\phi$, and constraint conditions $\lambda_1\lambda_2\lambda_3 = 1$, and $\lambda_1^2 \cos^2\phi + \lambda_2^2 \sin^2\phi = 1$, produces a Finger deformation tensor with components of

$$B_{11} = \lambda_1^2, \quad B_{22} = \lambda_2^2, \quad B_{33} = \lambda_3^2, \quad B_{ij} = 0 \ (i \neq j). \tag{1.59}$$

Therefore the invariants at Eq. (1.37) can be written as

$$J_1 = \lambda_1^2 + \lambda_2^2 + \lambda_3^2, \quad J_2 = \lambda_1^{-2} + \lambda_2^{-2} + \lambda_3^{-2}, \quad J_3 = \lambda_1^2 \cos^2\phi + \lambda_2^2 \sin^2\phi \tag{1.60}$$

. Plugging these invariants into the Cauchy stress equation (1.51) leads to

$$\begin{aligned}
T_{11} &= 2W_1\lambda_1^2 + 2W_2(\lambda_2^2+\lambda_3^2)\lambda_1^2 + 4W_3\lambda_1^4\cos^2\phi - p + t\lambda_1^2\cos^2\phi \\
T_{22} &= 2W_1\lambda_2^2 + 2W_2(\lambda_3^2+\lambda_1^2)\lambda_2^2 + 4W_3\lambda_2^4\sin^2\phi - p + t\lambda_1^2\sin^2\phi \\
T_{33} &= 2W_1\lambda_3^2 + 2W_2(\lambda_1^2+\lambda_2^2)\lambda_3^2 - p \\
T_{12} &= \lambda_1\lambda_2\sin\phi\cos\phi\{2(\lambda_1^2+\lambda_2^2)W_3 + t\} \\
T_{13} &= t_{23} = 0.
\end{aligned} \tag{1.61}$$

By assuming a strain energy function that is a scalar function of the fiber direction vectors and that is a quadratic function of the infinitesimal strain tensor, the constitutive equation for a transversely isotropic, linear, elastic material with a single preferred fiber direction is

$$\begin{aligned}
T_{ij} = \lambda e_{kk}\delta_{ij} + 2\mu_t e_{ij} + \alpha(a_k a_m e_{km}\delta_{ij} + e_{kk}a_i a_j) + \\
2(\mu_l - \mu_t)(a_i a_k e_{kj} + a_j a_k e_{ki}) + \beta a_k a_m e_{km} a_i a_j.
\end{aligned} \tag{1.62}$$

To calculate T_{11} and T_{22}, let i= 1,2, and j= 1,2, respectively, assume a fiber in the 1 direction,viz., a=$[1,0]^T$, thus $a_1 a_1 = 1$ otherwise $a_i a_j = 0$, and therefore one gets

$$\begin{aligned}
T_{11} &= \lambda(e_{11}+e_{22}) + 2\mu_t e_{11} + \alpha(e_{11} + (e_{11}+e_{22})) + \\
&\quad 2(\mu_l - \mu_t)(e_{11}+e_{11}) + \beta e_{11}, \\
T_{11} &= \lambda(e_{11}+e_{22}) + 2\mu_t e_{11} + \alpha(2e_{11}+e_{22}) + 4(\mu_l - \mu_t)e_{11} + \beta e_{11}, \\
T_{22} &= \lambda(e_{11}+e_{22}) + 2\mu_t e_{22} + \alpha e_{11} \\
T_{12} &= 2\mu_t e_{12} + 2(\mu_l - \mu t)e_{12}
\end{aligned} \tag{1.63}$$

The 2 dimensional, linear elastic, transversely isotropic, constitutive equation can be

written as the linear system of equations

$$\begin{bmatrix} e_1 \\ e_2 \\ e_3 \end{bmatrix} = \begin{bmatrix} \dfrac{1}{\lambda+2\alpha+\beta+4\mu_l-2\mu_t} & \dfrac{1}{\lambda+\alpha} & 0 \\ \dfrac{1}{\lambda+\alpha} & \dfrac{1}{\lambda+2\mu_t} & 0 \\ 0 & 0 & 2\mu_l \end{bmatrix} \begin{bmatrix} T_1 \\ T_2 \\ T_{12} \end{bmatrix}. \tag{1.64}$$

This compliance matrix is exactly the same as the one would derive for a conventional, transversely isotropic, strain-stress response. In that case

$$E_1 = \lambda+2\alpha+\beta+4\mu_l-2\mu_t, \quad E_2 = \lambda+2\mu_t, \quad G_{12} = 2\mu_l \tag{1.65}$$

that by plugging in these values, compliance matrix becomes,

$$\begin{bmatrix} \dfrac{1}{E_1} & \dfrac{-\nu_{21}}{E_2} & 0 \\ \dfrac{-\nu_{12}}{E_1} & \dfrac{1}{E_2} & 0 \\ 0 & 0 & \dfrac{1}{G_{12}} \end{bmatrix}. \tag{1.66}$$

There are 5 material constants; however, the compliance matrix is symmetric due to transverse isotropy, i.e., $\dfrac{\nu_{21}}{E_2} = \dfrac{\nu_{12}}{E_1}$, and therefore there are four, independent, material parameters that need to be calculated.

2. THE CONJUGATE PAIR FIBER APPROACH

Conjugate variables/pairs have been widely used to express the internal energy of a system in thermodynamics. Pressure/volume and temperature/entropy are the most common conjugate pairs, and the product of these two quantities contribute to a state function that has a unit of energy or power. A small increment in the energy is the product of pressure (the propulsive force) times a volume change (the associated displacement). Pressure is an intensive property, which is point-wise defined; whereas volume is an extensive property which means it depends on the amount of substance.

A similar situation applies to mechanical systems, If we consider the pressure as a stress, and the small volume change as a strain increment, stress and strain-rate pairs can be used to represent a potential energy (strain energy) change with respect to time. The work done is stored as an elastic strain energy. In general, the mechanical work done δW is not an exact differential; however, under the Green elastic (hyperelastic) material assumption there exists a scalar function $W(\mathbf{F})$ strain energy such that

$$\mathrm{d}W(\mathbf{F}) = tr\Big(\frac{W(\mathbf{F})}{\mathbf{F}}\mathrm{d}\mathbf{F}\Big) \tag{2.1}$$

where $d\mathbf{F}$ is the material derivative of $\mathbf{F}$. There are many ways to express stress and strain conjugate pairs, each defined stress has an associated strain pair such that

$$\mathrm{d}W = \mathrm{tr}(\mathbf{P}^{\mathbf{T}}\mathrm{d}\mathbf{F}) = \mathrm{tr}(\mathbf{S}\mathrm{d}\mathbf{E}) = \mathrm{tr}(\mathbf{T}\mathrm{d}\ln\mathbf{U}) \tag{2.2}$$

where $\ln\mathbf{U}$ is Hencky strain. In the early twentieth century Caratheodory [11], applied Pfaffis' equation to represent theormodynamic concepts in a mathematical approach which introduces integrating factors to make an inexact differential equation

exact. Caratheodory's axiomatic approach to thermodynamics has the consequence that a change in the internal energy of a body deformed in an adiabatic enclosure is independent of path; therefore the differentials are exact and the second law becomes Pfaffian equation wherein temperature is the integrating factor. Consequently, strain rate must be an exact differential. In other words, strain is a two-state field. It is not depend upon the path followed and as such, strain rate can be integrated without full knowledge of path.

2.1 Introduction

Conjugate, stress/strain, base-pairs theory gives us a chance to decompose the strain energy density into distinct parts. Each part is described by a different stress/strain conjugate pair and each part has a physical meaning that comes directly from experiment. Therefore, constitutive equations can be developed by using these outstanding advantages of conjugate pairs without a need to introduce tensor invariants.

In 1976, McLellan [12] utilized an upper-triangular decomposition of the deformation gradient, and demonstrated that the work done can be described by six strain parameters for an isotropic Green elastic solids. Later, Srinivasa [5] applied an equivalent factorization, and extended it for transversely isotropic, and orthotropic, Green elastic materials. His factorization strategy took advantage of Cholesky factorization to obtain direct relations between the deformation gradient and upper-triangle distortion tensor. Since then, Freed [8] employed this decomposition to solve various boundary conditions such as pure shear and simple shear deformations. Freed *et al.* [7] decomposed these conjugate pairs into three meaningful modes of deformation which are dilation, squeeze (pure shear) and simple shear.

The conventional way to decompose the strain-energy density is to break it into

hydrostatic and deviatoric parts as

$$\mathbf{A}_{hydrostatic} = \frac{1}{3}\mathrm{tr}(\mathbf{A})\mathbf{I}, \qquad \mathbf{A}_{deviaotoric} = \mathbf{A} - \frac{1}{3}\mathrm{tr}(\mathbf{A})\mathbf{I} \tag{2.3}$$

respectively, where $\mathbf{A}$ is an arbitrary symmetric matrix and $\mathbf{I}$ is the identity matrix. Dilatation deformation corresponds to the hydrostatic portion, while pure shear and simple shear match with the deviatoric portion. In classical theory, the deviatoric portion can not decompose into the pure and simple shear deformations; whereas the conjugate pair approach provides a means whereby pure and simple shear deformations can be decomposed. A decomposition of classical, transversely isotropic, strain-energy function decomposition will be investigated at following chapters.

In this chapter, the conjugate stress/strain basis pairs for isotropic and anisotropic materials are derived. Encoding/decoding maps that transform conjugate pairs into tensor components and vice versa are then described. Uniaxial and biaxial boundary-value problems are solved under an explicit elasticity assumption.

2.2 Conjugate stress/strain pairs

Derivation of the conjugate stress/strain pairs starts with a notable strain-energy density rate (stress power) description of [3]

$$\dot{W} = \mathrm{tr}(\mathbf{P}^{\mathsf{T}}\dot{\mathbf{F}}) \tag{2.4a}$$

Multiplying by $\mathbf{I}$, specifically $\mathbf{F}\mathbf{F}^{-1}$, and using properties of the trace gives

$$\dot{W} = \mathrm{tr}(\mathbf{P}^{\mathsf{T}}\dot{\mathbf{F}}) = \mathrm{tr}(\mathbf{F}\,\mathbf{P}^{\mathsf{T}}\dot{\mathbf{F}}\,\mathbf{F}^{-1}) = \mathrm{tr}(\mathbf{S}\,\mathbf{L}) \tag{2.4b}$$

where, because the Kirchhoff stress $\mathbf{S} = \det(\mathbf{F})$ is symmetric, it follows that

$$\mathbf{S} = \mathbf{P}\mathbf{F}^{\mathsf{T}} = \mathbf{F}\mathbf{P}^{\mathsf{T}}. \tag{2.4c}$$

Introducing an upper-trianglar decomposition of deformation gradient, and taking its material derivative, leads to

$$\dot{\mathbf{F}} = \dot{\mathbf{Q}}\tilde{\mathbf{F}} + \mathbf{Q}\dot{\tilde{\mathbf{F}}}. \tag{2.4d}$$

Plugging this relationship into the strain-energy equation produces

$$\dot{W} = \mathrm{tr}(\mathbf{S}\dot{\mathbf{F}}\mathbf{F}^{-1}) = \mathrm{tr}(\mathbf{S}\dot{\mathbf{Q}}\tilde{\mathbf{F}}\tilde{\mathbf{F}}^{-1}\mathbf{Q}^{-1}) + \mathrm{tr}(\mathbf{S}\mathbf{Q}\dot{\tilde{\mathbf{F}}}\tilde{\mathbf{F}}^{-1}\mathbf{Q}^{-1}) \tag{2.4e}$$

where the first trace on the right-hand side is equal to zero because

$$\mathrm{tr}(\mathbf{S}\dot{\mathbf{Q}}\mathbf{Q}^{\mathsf{T}}\tilde{\mathbf{F}}\tilde{\mathbf{F}}^{-1}) = \mathrm{tr}(\mathbf{S}\dot{\mathbf{Q}}\mathbf{Q}^{\mathsf{T}}) = 0 \tag{2.4f}$$

since the trace between a symmetric tensor ($\mathbf{S}$) and a skew-symmetric tensor ($\dot{\mathbf{Q}}\mathbf{Q}^{\mathsf{T}}$) is zero. Consequently, only the second trace on the right-hand side persists

$$\dot{W} = \mathrm{tr}(\mathbf{Q}^{\mathsf{T}}\mathbf{S}\mathbf{Q}\dot{\tilde{\mathbf{F}}}\tilde{\mathbf{F}}^{-1}) = \mathrm{tr}(\tilde{\mathbf{S}}\tilde{\mathbf{L}}) \tag{2.4g}$$

wherein $\tilde{\mathbf{S}} \coloneqq \mathbf{Q}^{\mathsf{T}}\mathbf{S}\mathbf{Q}$ is symmetric and $\tilde{\mathbf{L}} \coloneqq \dot{\tilde{\mathbf{F}}}\tilde{\mathbf{F}}^{-1}$ is upper-triangular so that

$$\dot{W} = \mathrm{tr}\left(\begin{bmatrix} \tilde{S}_{11} & \tilde{S}_{12} \\ \tilde{S}_{12} & \tilde{S}_{22} \end{bmatrix}\begin{bmatrix} \tilde{L}_{11} & \tilde{L}_{12} \\ 0 & \tilde{L}_{22} \end{bmatrix}\right) = \tilde{S}_{11}\tilde{L}_{11} + \tilde{S}_{12}\tilde{L}_{12} + \tilde{S}_{22}\tilde{L}_{22} \tag{2.4h}$$

Each of these stress/strain-rate terms corresponds to a different deformation mode (different experiments). If we decompose the distortion tensor $\tilde{\mathbf{F}}$ into a product of three fundamental modes of deformation, e.g., $\tilde{\mathbf{F}} = \tilde{\mathbf{F}}^{\circ}\tilde{\mathbf{F}}^{\square}\tilde{\mathbf{F}}^{\angle}$ with matrix components [7]

$$\tilde{\mathbf{F}}^{\circ}\tilde{\mathbf{F}}^{\square}\tilde{\mathbf{F}}^{\angle} = \begin{bmatrix} \sqrt{ab} & 0 \\ 0 & \sqrt{ab} \end{bmatrix} \begin{bmatrix} \sqrt{a/b} & 0 \\ 0 & \sqrt{b/a} \end{bmatrix} \begin{bmatrix} 1 & \gamma \\ 0 & 1 \end{bmatrix} = \begin{bmatrix} a & a\gamma \\ 0 & b \end{bmatrix} \tag{2.5}$$

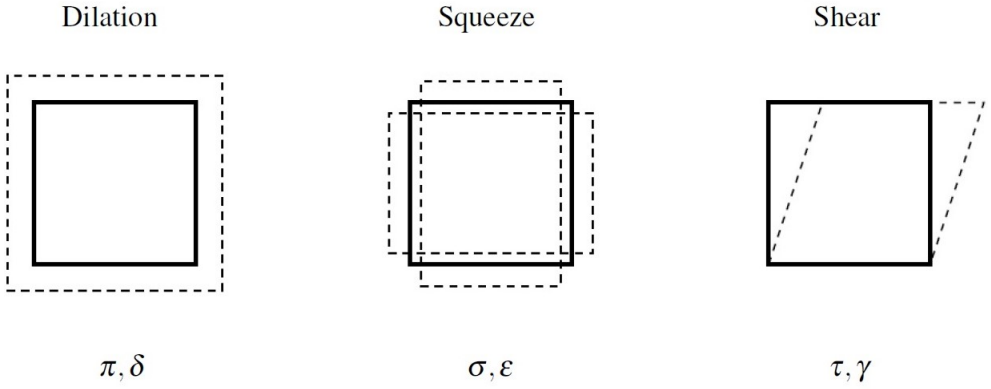

Figure 2.1: The three different modes of deformation that exist for a 2D strain-energy density when deconstructed as independent, thermodynamic, conjugate pairs [1].

where π, σ and τ are the stresses that are conjugate to strains δ, ϵ and γ, which are defined below. The first matrix $\tilde{\mathbf{F}}^{\circ}$ corresponds to a dilation (hydrostatic like) motion, the second matrix $\tilde{\mathbf{F}}$ corresponds to a squeeze (pure-shear like) motion, and the third matrix $\tilde{\mathbf{F}}^{\angle}$ correlates to a simple shear motion. With this proposed strain energy and distortion tensor $\tilde{\mathbf{F}}$ decomposition, the deviatoric portion of a deformation is able to be described as pure shear and simple shear deformation, independently.

Now we have enough information to construct each conjugate pair by writing the rate of strain-energy density out in terms of these pairs.

2.3 Stress/Strain Basis Pairs for Isotropic Materials

This idea was proposed by Freed, Erel and Moreno [7] in their first, conjugate, stress/strain pairs paper which was published in 2016. It provided an unique set of conjugate, stress/strain, basis pairs suitable for isotropic planar materials. The strain energy density of a membrane (2D deformation) was found to decompose into three separable parts, viz.

$$\begin{aligned} \dot{W} &= \widetilde{S}_{11}\,\dot{a}/a + \widetilde{S}_{22}\,\dot{b}/b + \widetilde{S}_{12}\,a\dot{\gamma}/b \\ &= \pi\dot{\delta} + \sigma\dot{\varepsilon} + \tau\dot{\gamma} \end{aligned} \tag{2.6}$$

where $\tilde{S} = Q^{\mathrm{T}} S Q$, with $\mathbf{S}$ being the Kirchhoff stress, and $\tilde{S}$ being its counterpart when rotated into the experimentor's frame by $\mathbf{Q}$, which comes from $\mathrm{F} = \mathbf{Q}\tilde{\mathbf{F}}$. A stress basis is defined by

$$\pi = \widetilde{S}_{11} + \widetilde{S}_{22} \tag{2.7a}$$

$$\sigma = \widetilde{S}_{11} - \widetilde{S}_{22} \tag{2.7b}$$

$$\tau = (a/b)\,\widetilde{S}_{12} \tag{2.7c}$$

whose associated strain-rate basis becomes

$$\delta = \ln\sqrt{ab} \qquad \dot{\delta} = \tfrac{1}{2}\big(\dot{a}/a + \dot{b}/b\big) \tag{2.7d}$$

$$\varepsilon = \ln\sqrt{a/b} \qquad \dot{\varepsilon} = \tfrac{1}{2}\big(\dot{a}/a - \dot{b}/b\big) \tag{2.7e}$$

$$\gamma \qquad\qquad \dot{\gamma} \tag{2.7f}$$

where δ, ε and γ are each two-state fields that are independent of path, and therefore, each is a thermodynamically viable measure for strain. From these stress/strain conjugate pairs, Freed, et al. [7] derived a set of non-linear and implicit constitutive equations that describes isotropic elastic membranes of biologic origin. Experimental data from porcine myodarcardium and visceral pleural membrane were used to validate the theory. Furthermore, Abaqus UMAT and FEBio plug-ins have been written to confirm the theory numerically. This numerical validation method is explained in Chapter 6. Conversion maps between tensor components and their thermodynamic coordinates (conjugate pairs) can be described as a linear system of equations that are

$$\begin{bmatrix} \pi \\ \sigma \\ \tau \end{bmatrix} = \begin{bmatrix} 1 & 1 & 0 \\ 1 & -1 & 0 \\ 0 & 0 & a/b \end{bmatrix} \begin{bmatrix} \widetilde{S}_{11} \\ \widetilde{S}_{22} \\ \widetilde{S}_{12} \end{bmatrix} \tag{2.8}$$

and

$$\begin{bmatrix} \dot{\delta} \\ \dot{\epsilon} \\ \dot{\gamma} \end{bmatrix} = \frac{1}{2} \begin{bmatrix} 1 & 1 & 0 \\ 1 & -1 & 0 \\ 0 & 0 & 2 \end{bmatrix} \begin{bmatrix} \dot{a}/a \\ \dot{b}/b \\ \dot{\gamma} \end{bmatrix} \tag{2.9}$$

both of which are invertible.

2.4 Stress/Strain Basis Pairs for Anisotropic Materials

Most materials are anisotropic, so we seek an augmentation to the stress/strain basis pairs of Eq. (2.7) that would be appropriate for these materials. Transversely isotropic behavior is achieved by introducing an anisotropic parameter n into the stress and strain basis-pair equation (2.7) which are independent from constitutive relations. As discussed before in §1.1.3, the conventional method has five material

parameters. What we propose has one less material parameter, and these parameters have different physical interpretations. Such an extension must remain compliant with the stress power of Eq. (2.6).

Let n denote the extent of anisotropy, then an admissible stress basis is

$$\pi = \tfrac{1}{n}\,\widetilde{S}_{11} + n\,\widetilde{S}_{22} \tag{2.10a}$$

$$\sigma = \tfrac{1}{n}\,\widetilde{S}_{11} - n\,\widetilde{S}_{22} \tag{2.10b}$$

$$\tau = (a/b)\,\widetilde{S}_{12} \tag{2.10c}$$

whose associated strain basis (and strain-rate basis) is

$$\delta = \ln\sqrt{a^n b^{1/n}} \qquad \dot{\delta} = \tfrac{1}{2}\Big(n\,\dot{a}/a + \tfrac{1}{n}\,\dot{b}/b\Big) \tag{2.10d}$$

$$\varepsilon = \ln\sqrt{a^n/b^{1/n}} \qquad \dot{\varepsilon} = \tfrac{1}{2}\Big(n\,\dot{a}/a - \tfrac{1}{n}\,\dot{b}/b\Big) \tag{2.10e}$$

$$\gamma \qquad\qquad \dot{\gamma} \tag{2.10f}$$

which collectively reduce to Eq. (2.7) at the isotropic boundary of $n = 1$. If $n > 1$ then the 1-direction has a stiffer response than the 2-direction, and if $n < 1$ then the 2-direction has a stiffer response than the 1-direction.

The conjugate, stress/strain, base pairs for a planar state were derived from a strain energy density by Dr. Freed in [7]. Equation (2.10) preserves the rate by which work is done on a deformable solid by stressing it, specifically

$$\dot{W} = \pi\dot{\delta} + \sigma\dot{\epsilon} + \tau\dot{\gamma} = \tilde{S}_{11}\dot{a}/a + \tilde{S}_{22}\dot{b}/b + \tilde{S}_{12}a\dot{\gamma}/b \tag{2.11}$$

In other words, the base pairs from Eq. (2.10) are thermodynamically admissible. The same strain energy density expression is obtained for both the isotropic and

anisotropic cases. Both obey the laws of thermodynamics.

The stress/strain base pairs demonstrate an one-to-one mapping property between tensor components and thermodynamics variables, per our hypothesis. An encoding/decoding relation can be seen as

$$\begin{bmatrix} \pi \\ \sigma \\ \tau \end{bmatrix} = \begin{bmatrix} \frac{1}{n} & n & 0 \\ \frac{1}{n} & -n & 0 \\ 0 & 0 & a/b \end{bmatrix} \begin{bmatrix} \widetilde{S}_{11} \\ \widetilde{S}_{22} \\ \widetilde{S}_{12} \end{bmatrix} \tag{2.12}$$

while the rates of the extensive variables map as

$$\begin{bmatrix} \dot{\delta} \\ \dot{\epsilon} \\ \dot{\gamma} \end{bmatrix} = \frac{1}{2} \begin{bmatrix} n & \frac{1}{n} & 0 \\ n & -\frac{1}{n} & 0 \\ 0 & 0 & 2 \end{bmatrix} \begin{bmatrix} \dot{a}/a \\ \dot{b}/b \\ \dot{\gamma} \end{bmatrix} \tag{2.13}$$

and we notice that the anisotropic parameter n is introduced as a characteristic of the encoding/decoding map not through the constitutive equation itself, which remains isotropic. This result illustrates how constitutive equations can be derived without the aid of invariant theory, as developed by Spencer [9] and others.

2.5 Boundary Value Problems

In this section well-known boundary value problems are investigated from which one can construct consititive equations using the conjugate pair approach. At the end of this section, we will have derived the stress/strain relations by which one can validate the proposed theory. This part demonstrates how theory can inform experiments.

Consider a Helmholtz free-energy density A for planar membranes that are under

isothermal adiabatic conditions as explained by [7]

$$\rho_0 A = -C(T\ln(T/T_0) - (T - T_0)) + 2K(\delta - \alpha(T - T_0))^2 + M\epsilon^2 + \frac{1}{2}G\gamma^2 \qquad (2.14)$$

where C is heat capacity, T is measured temperature, T_0 is initial temperature, and α is the coefficient of thermal expansion. Upon neglecting the effect of temperature and thermal strain, equation (2.14) simplifies as

$$\rho_0\, A = 2K\delta^2 + M\epsilon^2 + \tfrac{1}{2}G\gamma^2. \qquad (2.15)$$

A Green elastic solids assumes that Helmholtz free-energy A can be written as a function of temperature and strain as

$$\rho_0\, \mathrm{d}A = -\rho_0 S\mathrm{d}T + \mathrm{d}W. \qquad (2.16)$$

This is an explicit form of Helmholtz free-energy function. To consider implicit elasticity, temperate, strain and stress should all be function of stored energy [13]. In terms of a decomposition in work, the second law of thermodynamics now takes on a form of

$$\rho_0 \quad \frac{\partial A}{\partial T}\mathrm{d}T + \frac{\partial A}{\partial \delta}\mathrm{d}\delta + \frac{\partial A}{\partial \varepsilon}\mathrm{d}\varepsilon + \frac{\partial A}{\partial \gamma}\mathrm{d}\gamma\Big) = -\rho_0 S\mathrm{d}T + \pi\mathrm{d}\delta + \sigma\mathrm{d}\epsilon + \tau\mathrm{d}\gamma. \qquad (2.17)$$

After substituting Eq. (2.15) into the right-hand side of equation (2.17) for the second law of thermodynamics, the constitutive equations of Freed, Erel and Moreno [7] evolve

$$\pi = 4K\delta \quad \sigma = 2M\epsilon \quad \tau = G\gamma \qquad (2.18)$$

which have three material parameters: K is similar to the bulk modulus (areal mod-

ulus for 2D deformation), M is the pure shear modulus (P-wave modulus) and G is the simple shear modulus. By using the stress/strain equations (2.10) and the linear constitutive equations (2.18), a tensile experiment and a general biaxial experiment can be described with proper constitutive equations.

2.5.1 Uniaxial tension

Fibrous composites with a single fiber family are considered. They were pulled in directions that align with and are normal to the fiber orientation.

Traction aligns with fiber direction

In this boundary condition, traction S (force per unit undeformed area) applies to the fiber direction, so $\widetilde{S}_{11} = S$ and $\widetilde{S}_{22} = \widetilde{S}_{12} = 0$. After encoding these conditions into their conjugate values via Eq. (2.12), stress measures can be defined as $\pi = S/n$, $\sigma = S/n$ and $\tau = 0$. Incorporating these stress values with the linear constitutive Eq. (2.18), and combining the conjugate strains into the same equations produce

$$\frac{S}{n} = 4K \ln \sqrt{a^n b^{1/n}}, \qquad \frac{S}{n} = 2M \ln \sqrt{a^n / b^{1/n}} \tag{2.19a}$$

or

$$\frac{S}{n} = 2K \ln a^n b^{1/n}, \qquad \frac{S}{n} = M \ln a^n / b^{1/n} \tag{2.19b}$$

that invert to become

$$\exp\left(\frac{S}{2Kn}\right) = a^n b^{1/n} \qquad \exp\left(\frac{S}{Mn}\right) b^{1/n} = a^n \tag{2.19c}$$

Moving a^n from the right sides of these equations into their left sides leads to

$$\exp\left(\frac{S}{2Kn}-\frac{S}{Mn}\right)=b^{2/n} \quad \text{or} \quad b=\exp\left(\frac{S}{4K}-\frac{S}{2M}\right) \tag{2.20a}$$

and similarly

$$\exp\left(\frac{S}{2Kn}+\frac{S}{Mn}\right)=a^{2n} \quad \text{or} \quad a=\exp\left(\left(\frac{1}{n^2}\right)\left(\frac{S}{4K}+\frac{S}{2M}\right)\right) \tag{2.20b}$$

where extension ratios in the fiber direction a and normal to the fiber orientation b can be described as a function of the Kirchhoff stress S.

Traction normal to fiber direction

In this boundary condition, Traction S (force per unit undeformed area) is applied normal to the fiber direction, so $\widetilde{S}_{22}=S$ and $\widetilde{S}_{11}=\widetilde{S}_{12}=0$. After encoding these conditions into their conjugate values via Eq. (2.12), stress measures can be defined as $\pi=Sn$, $\sigma=-Sn$ and $\tau=0$. Incorporating these stress values into the linear constitutive Eq. (2.18), while combining the conjugate strains into these same equations, produces

$$Sn=4K\ln\sqrt{a^n b^{1/n}}, \qquad -Sn=2M\ln\sqrt{a^n/b^{1/n}} \tag{2.21a}$$

or

$$Sn=2K\ln a^n b^{1/n}, \qquad -Sn=M\ln a^n/b^{1/n} \tag{2.21b}$$

that invert to become

$$\exp\left(\frac{Sn}{2K}\right) = a^n b^{1/n} \qquad \exp\left(-\frac{Sn}{M}\right) b^{1/n} = a^n. \tag{2.21c}$$

Moving a^n from the right-hand sides into their left-hand sides leads to

$$\exp\left(\frac{Sn}{2K} + \frac{Sn}{M}\right) = b^{2/n} \qquad b = \exp\left(n^2\left(\frac{S}{4K} + \frac{S}{2M}\right)\right) \tag{2.22a}$$

. (2.22b)

and similarly

$$\exp\left(\frac{Sn}{2K} - \frac{Sn}{M}\right) = a^{2n} \qquad a = \exp\left(\frac{S}{4K} - \frac{S}{2M}\right) \tag{2.22c}$$

where extension ratios in the fiber direction a and normal to the fiber orientation b can be described as a function of Kirchhoff stress S, which is now applied normal to the fibers. The first nonlinear Hookean model, where strains are exponential functions of traction, was published by Becker [14]. His study was published before Hencky's [15] model whose stresses are logarithmic functions of stretch, cf. Neff *et al.* [16].

2.5.2 Biaxial tension

Boundary conditions are considered where fibrous composites with a single fiber family are loaded under biaxial tractions. Specimens are pulled in fiber and transverse directions. Let the traction applied to the fiber direction be $\widetilde{S}_{11} = S_{11}$ and normal to the fiber direction is $\widetilde{S}_{22} = S_{22}$. After inserting these conditions into Eq.

(2.12), dilation and squeeze stress measures can be described as

$$\pi = \frac{S_{11}}{n} + nS_{22} \quad \sigma = \frac{S_{11}}{n} - nS_{22} \tag{2.23}$$

. Combining these stress measures with constitutive equations (2.18) results in conjugate strain relations

$$4K \ln \sqrt{a^n b^{1/n}} = \frac{S_{11}}{n} + nS_{22} \qquad 2M \ln \sqrt{a^n / b^{1/n}} = \frac{S_{11}}{n} - nS_{22} \tag{2.24a}$$

or

$$2K \ln a^n b^{1/n} = \frac{S_{11}}{n} + nS_{22} \qquad M \ln a^n / b^{1/n} = \frac{S_{11}}{n} - nS_{22} \tag{2.24b}$$

that convert to become

$$a^n b^{1/n} = \exp\left(\frac{\frac{S_{11}}{n} + nS_{22}}{2K}\right) \qquad a^n = \exp\left(\frac{\frac{S_{11}}{n} - nS_{22}}{M}\right) b^{1/n}. \tag{2.24c}$$

Moving a^n from left sides of these equations to their right sides gives

$$b^{2/n} = \exp\left(\frac{\frac{S_{11}}{n} + nS_{22}}{2K} - \frac{\frac{S_{11}}{n} - nS_{22}}{M}\right) \tag{2.24d}$$

After rearranging terms, the stretch normal to fiber direction can be obtain as

$$b = \exp \quad S_{11}\left(\frac{1}{4K} - \frac{1}{2M}\right) + n^2 S_{22}\left(\frac{1}{4K} + \frac{1}{2M}\right)\Bigg) \tag{2.24e}$$

and similarly the stretch along the fiber direction can be found

$$a = \exp \quad \frac{S_{11}}{n^2}\left(\frac{1}{4K} + \frac{1}{2M}\right) + S_{22}\left(\frac{1}{4K} - \frac{1}{2M}\right)\Bigg). \tag{2.24f}$$

These general constitutive equations can easily be applied for equi-biaxial boundary condition by equating $S_{11} = S_{22} = S$. If S_{22} is equal to zero, these biaxial constitutive equations will reduce to the uniaxial equations derived above. Either uniaxial or biaxial constitutive relation can be easily transformed to the isotropic condition by assigning $n = 1$.

3. EXPERIMENTAL PROCEDURE, TESTING PROTOCOLS AND TOOLS FOR DATA ANALYSIS*

In this chapter, specimen preparation, experimental setup, and testing protocols are explained. The genetic algorithm and digital-image correlation methods are also investigated in detail.

3.1 Materials and Specimen Fabrication

Sorta Clear® 40, a white translucent silicone rubber, and 1/16" high-temperature silicone O-ring cord, purchased from McMaster-Carr®, were used as raw materials for the matrix and fiber constituents to produce a silicone/silicone composite capable of large deformations. Matrix silicone has a Shore hardness is 40A; whereas, the fiber silicone has 70A Shore hardness based on manufacturers' technical bulletins. Because the chemistry for matrix and fiber was the same, i.e., silicon, excellent bonding between fiber and matrix was observed.

A 3D printed mold was designed in Solidworks® and used to produce our silicone composite. A smooth surfaced plastic cap was implanted into the bottom of the polylactide (PLA) mold bottom to obtain a gentle surface. Same length fiber rods were inserted into each slot of the mold. A small steel rod was used to push the fibers into their slots to make sure the fiber rods were properly aligned. Figure 3.1 shows the PLA mold, silicone fiber rods, and plastic caps. There is another plastic cap that covers the silicone composite top surface to control thickness and top surface smoothness of the composite material.

*Part of this section is reprinted with permission of ASME from "Experimental Validation of Neo-Hookean Fiber Reinforced Elastic Solids" by Veysel Erel, Mingliang Jiang, Micheal R. Moreno and Alan D. Freed 2018, Conference on Smart Materials, Adaptive Structures and Intelligent Systems, San Antonio, TX, USA, September 10–12, 2018, pp V001T01A019. Copyright 2018 ASME.

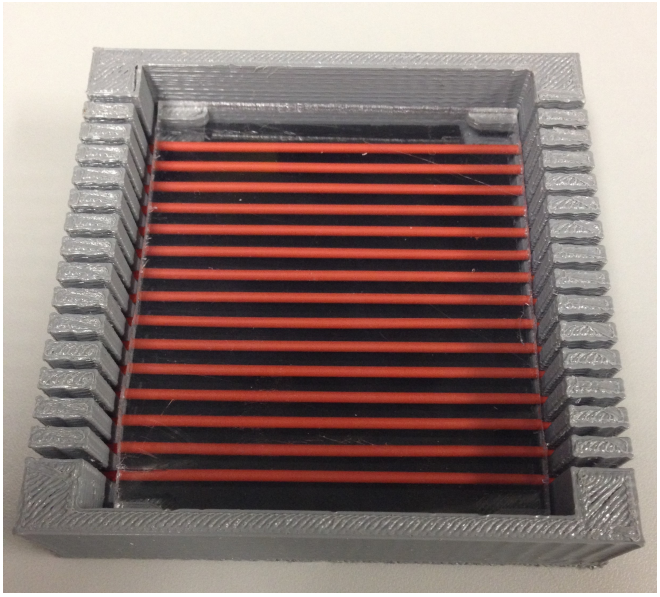

Figure 3.1: 3D printed mold [17]

Sorta Clear part A and part B constituents were combined inside a plastic container to prepare the composite matrix material. The mixture was degassed inside the vacuum oven at 28.5 inches of mercury for around 5 minutes before it was poured into the PLA mold. Then the mixture was degassed for five additional minutes to eliminate any air trapped from pouring. Before the composite material was extracted from the mold, it was allowed to cure for 16 hours. Each casting was cut into three specimens. A typical specimen had around 18% fiber volume fraction. Figure 3.2 shows 0° and 90° silicone/silicone composite tensile specimens. ASTM standard D3039 [18], titled Standard Test Method for Tensile Properties of Polymer Matrix Composite Materials, was adhered to determine the gage section and clamping area of each specimen. Black lines close to the top and bottom show where the specimen is supposed to be clamped; whereas those lines close to the center delineate the gage

section area.

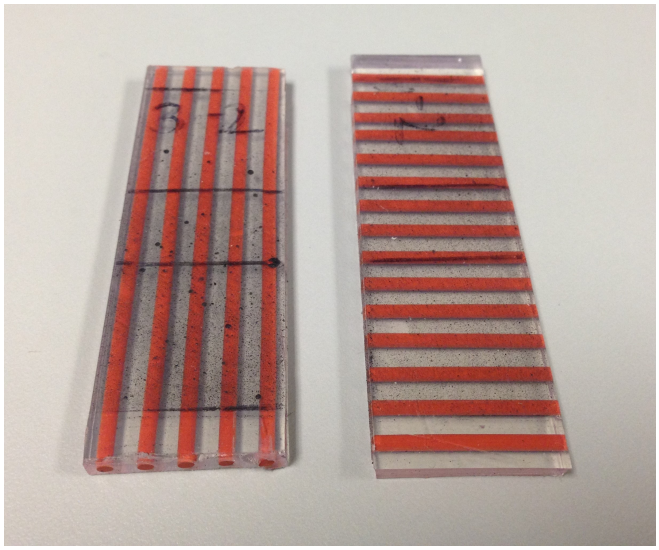

Figure 3.2: 0° and 90° uniaxial tensile specimens

3.2 Experimental Setup and Test Procedure

The biaxial system, located inside the Biomechanical Environments Laboratories in the Mechanical Engineering Department at Texas A&M University, was used to perform the experimental side of this thesis research. This setup is able to provide non-contact measurement of mechanical properties for different types of experiments such as shear, uniaxial and general biaxial tests.

The biaxial mechanical testing system, shown in Fig. 3.3, contains four motorized linear actuators (DS4 series, Kollmorgen Corp.), each impelled by a servo motor (AKM23D, Kollmorgen Corp.), rigidly stabilized on a breadboard table to prevent vibrations. A high resolution camera was installed above the system to observe a specimen surface and record the markers' movement on the specimen. The system

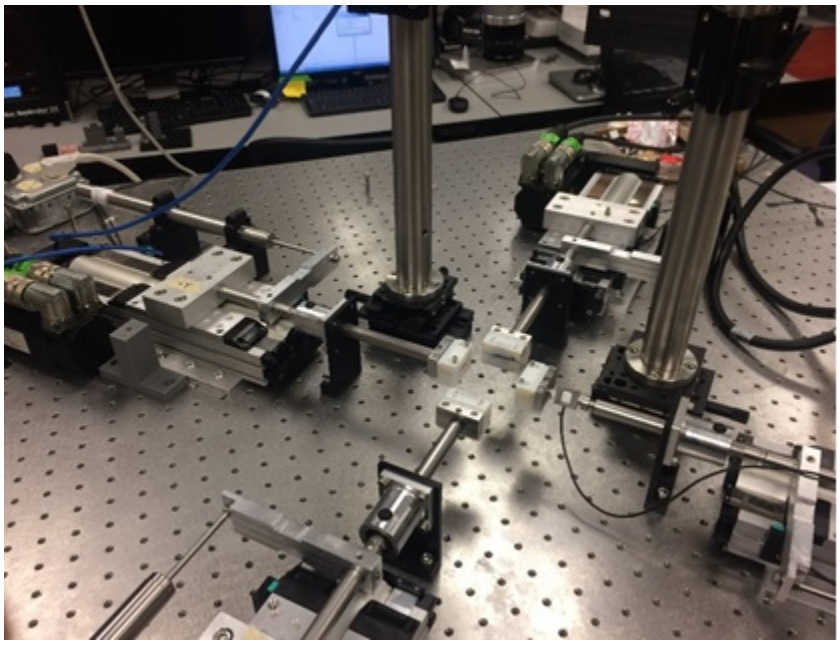

Figure 3.3: Experimental setup

was integrated with a custom made four-axis controller that will allow load, stroke and centroid control of the deformation on each axis. This adjustable system can be configured to perform uniaxial, equi-biaxial, general biaxial, and shear tests as-well-as tests that can measure viscoelastic behaviors.

Linear variable differential transformers (LVDT, MVL7C, Honeywell Sensing and Control) were employed for closed loop control of displacement. All the drives were controlled by a custom made four-axis digital servocontroller (MTI TESTExpress ®, McGaw Technology Inc.) that employs a centroid control algorithm to enable independent and switchable control between load and displacement on each axis.

Displacements are measured by linear actuators which were connected to linear variable differential transformers. An area scan camera (Basler acA1300-200um, Basler AG) fitted with a 25mm lens (HF25HA-1B, Computar) was installed above

the specimen for non-contacting measurement. For load measurement, there were uniaxial tension/compression 10 pound load cells (Model 31, Honeywell Sensing and Control) on each orthogonal axis to measure the forces applied to the specimen.

3.3 Test Procedure

First, a gage length was calculated by subtracting two times the width and clamping distance from the total length, per ASTM testing standard. Each specimen's gage section was drawn with a black marker, and then patterned with small ink dots to enable tracking displacement changes during the deformation. Second, three width, height and thickness measurements were taken with an micrometer from each specimen to determine averaged initial specimen dimensions. Then, each specimen was attached to the set-up using 3D printed toothed clamp, (shown in Fig. 3.3). Each specimen alignment was checked using the Mako G-419B camera before starting the experiment. Load cell initial load values were also recorded. Finally, uniaxial tensile tests were performed at a 1% strain rate on six 0° and six 90° silicone/silicone composite specimens, six fiber specimens, and six matrix specimens for different percent strains. The load data and an image were simultaneously captured at 0.2 second intervals. Axial and transverse displacements were captured through the camera.

3.4 Experiment Analysis

Voltage changes from the load cell and LVDT were recorded by a data acquisition board. These voltage changes were transformed into calibrated load and displacement changes. Stress values were calculated by dividing load with the initial cross-section area, and strain values were calculated by dividing displacement changes with the initial grip distance. Ncorr [19], an open-source digital image-correlation software, was used to quantify longitudinal and transverse Eulerian strain measures. All options were assigned default settings during the image analysis, except for prefering

Table 3.1: Ncorr strain measurement validation.

	Axial Strain Measurement			Transverse Strain Measurement		
	Ncorr	LVDT	Difference	Ncorr	ImageJ	Difference
0° specimen	0.3414	0.345	1.04 %	0.1134	0.1168	2.88 %
90° specimen	0.3518	0.345	1.97 %	0.0997	0.1030	3.26 %

the four-thread multithreading option. Only the surface area within the gage section was used to perform image correlation analysis. The Ncorr axial strain measurements were verified against readings from an LVDT attached to the biaxial experimental system; whereas, their transverse strain measurements were validated with the ImageJ [20] software, which can measure pixel differences between images from an initial frame and a final frame. Table 3.1 presents strain measurements for both the axial and transverse strains, and their differences between the various measurement techniques computed.

3.5 Genetic Algorithms

A genetic algorithm was used to analyze the 10% uniaxial compliant/compliant composite data to obtain optimized, conjugate-pair, material parameters. This algorithm was coded by Dr. Freed, inspired from E. D. Goldberg [21]. In Goldberg's book, he clearly explained what genetic algorithms are:

> "Genetic algorithms are search algorithms based on the mechanics of natural selection and natural genetics. They combine survival of the fittest among string structures with a structured yet randomized information exchange to form a search algorithm with some of the innovative flair of human search. In every generation, a new set of artificial creatures (strings) is created using bits and pieces of the fittest of the old: an

occasional new part is tried for good measure. While randomized, genetic algorithms are no simple random walk. They efficiently exploit historical information to speculate on new search points with expected improved performance."

Goldberg used a simple genetic algorithm that fixed the probabilities for mutation and crossover over the lifetime of the colony; however, Dr. Freed implemented an adaptive genetic algorithm [22] that is able to alter variation of crossover and mutation probability. This is the general objective function that has been used in this algorithm.

$$\epsilon = \frac{1}{R}\sum_{r=1}^{R} e_r \tag{3.1}$$

where R is number of response variables and

$$e_r = a_r(X_r - \Xi), \quad a_r = \frac{1}{\max_{n=1}^{N}(|x_{rn}|)} \tag{3.2}$$

wherein e_r is residual error and a_r is scaling factor. Expected residual error

$$E(\epsilon) = \left(\frac{1}{R}\sum_{r=1}^{R}\Big(E(e_r)\Big)^P\right)^{1/P} \tag{3.3}$$

where P is the number of parameters in a model, $E(e_r) = a_r(E(X_r) - E(\Xi_r))$ is the expected residual error for specific data. This objective function was found by Dr. Freed after many trial and errors. There is no literature behind this function.

Genes reside at the lowest level of genetic algorithm hierarchy, and allele are the possibility value of the genes. During procreation, which is where the first colony of individuals come from, the allele are randomly assigned, whereas in later colonies, allele are assigned through chromosome crossovers with a possible additional gene mutation. In this programming stage, biallelic genes have been used to assign a

dominant gene with 1 and a recessive gene with 0. Mutation may also happen in this stage. The probability of mutation P_m is assigned to each creature after a generation has been fully populated and the fitness of all creatures in that generation are known.

$$P_m = P^m_{max} - \frac{(P^m_{max} - P^m_{min})(f - f_{avg})}{f_{max} - f_{avg}} \quad \text{if} \quad f \geq f_{avg} \quad \text{otherwise} \quad P_m = P^m_{max} \tag{3.4}$$

where P^m_{max} and P^m_{min} are the maximum and minimum probabilities for mutation, while f is the fitness of an individual creatures, f_{avg} is the average fitness of that generation and f_{max} is the fitness of its elite creature. During the reproduction, father and mother's mutation chances become averaged and are to assigned to their offspring's probability of mutation.

Chromosomes are on the second level of a genetic algorithm hierarchy. At this programming stage, each chromosome is correlated with a single model parameter that is desired to be optimized. A one-point chromosome crossover happens at this stage. A random number generator determines where a splice is to take place to complete a crossover. A probability for crossover P_c is assigned to every chromosome of an individual creature after a generation has been fully populated and the fitness of all creatures in that generation are known.

$$P_c = \frac{1}{P}\left(P^c_{max} - \frac{(P^c_{max} - P^c_{min})(f - f_{avg})}{f_{max} - f_{min}}\right) \quad \text{if} \quad f \geq f_{avg} \quad \text{otherwise} \quad P_c = \frac{P^c_{max}}{P} \tag{3.5}$$

where P^c_{max} and P^c_{min} are the maximum and minimum probabilities for crossover happening within a creature, and P corresponds to number of chromosomes that a creature has. During the reproduction, father and mother's crossover chances will be averaged to assign their offspring's probability of crossover.

Schemata are fundamental building blocks in genetic algorithms. A schema is

a combination of genes that is shorter than the chromosome. They carry high performance matchings to successive generations. In schemata, there are some gene expressions are fixed; whereas, others are allowed to vary.

The third level of genetic algorithm hierarchy is the genome, which contains the entire evolution history of a living organism. Genomes are groups of chromosomes, which relate to each model parameter. Thus the number of model parameters corresponds to the number of arrays of chromosomes contained in its genome.

Creatures belong to the level of a physical being, an organism or an individual. This level contains a lot of information such as: a creature's birthID, fitness, parameters, similarity of its parent's genome, and probabilities of mutation and crossover. Each individual associates with an unique set of model parameters that contains both fixed and varied parameters. An individual can come into being from three different ways. *Procreation* is used to create the first colony. This process requires specified upper and lower bounds for each parameter interval. Then initialization starts with an upper level of 11111111 (assuming the chromosome has eight genes) and a lower level of 00000000 span the range of allowed chromosomes which scale with the min and max of parameter's values. The second way an individual can be created is through an *alien migration*. Aliens have a known phenotype (material parameter); whereas, procreated individuals have random (assigned by chance) phenotypes. This process seeds individuals with good fitness into a population. The final way to a create an individual is though *mating* two distinct individuals. This method creates an individual from its parents, and carries mutation and crossover possibilities to its offspring.

Colonies are the highest level in genetic algorithm hierarchy. Creature couples from an existing colony are selected to mate through a process called tournament play to determine whose offspring will constitute the next generation of the colony. The

participants for tournament play are randomly selected from an existing population, and mate with the winner (most-fit) participant from each tournament of play. The number of participants in the tournament is a set that is 2% of the population size. In figure 3.4 each step in the genetic algorithm hierarchy has been summarized;

a) Gene mutation happens at this stage.

b) Crossover occurs at this stage. Each chromosome correlates with a single material parameter.

c) There is a one-to-one correlation between the number of material parameters in a model and the arrays number of chromosomes in its genome.

d) Each individual has an unique assigned set of model parameters which contains all of its genetic information, plus its fitness, mutation and crossover probabilities.

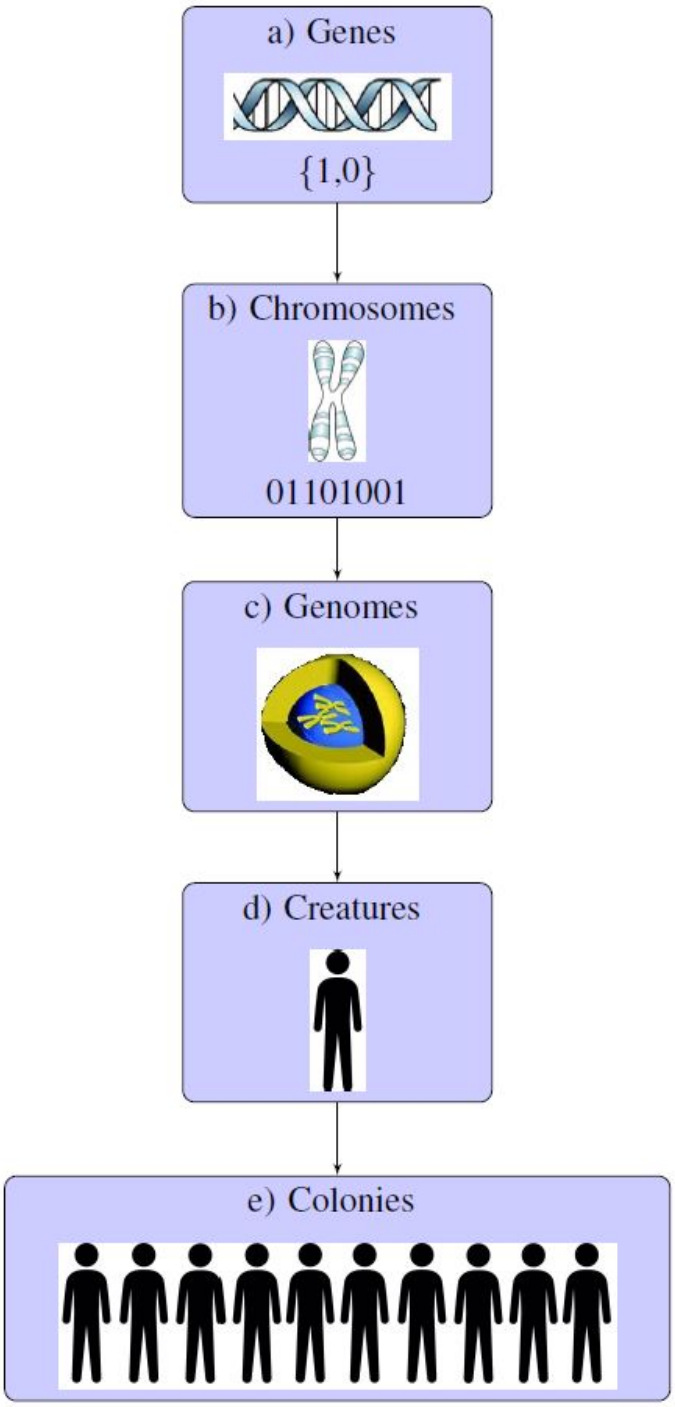

Figure 3.4: Genetic Algorithm Hierarchy

3.6 Digital Image Correlation:Ncorr

Digital image correlation (DIC) uses an image processing technique to obtain non-contact measurements of displacements from which strain fields can be derived. Specimen images are taken during deformation, then compared with an initial (reference) image by obtaining one-to-one mappings between the undeformed image and subsequent deformed images. The planar, stress/stain, conjugate pair, approach requires two-dimensional strain measurements. Thus, the author used Ncorr [19], an open source and digital image correlation software, to analyze his planar deformations. In this section, theory and numerical methods behind the Ncorr software are investigated.

The deformation is aimed to observe within a region of interest (ROI) that is divided into many subsections (subsets). A group of neighboring points can generate a subset as-long-as it contains a center point. The deformation is assumed to be homogeneous inside each subset. Consider a first-order transformation described by

$$\begin{aligned} \tilde{x}_{cur_i} &= x_{ref_i} + u_{rc} + \frac{\partial u}{\partial x_{rc}}(x_{ref_i} - x_{ref_c}) + \frac{\partial u}{\partial y_{rc}}(y_{ref_j} - y_{ref_c}) \\ \tilde{y}_{cur_j} &= y_{ref_j} + v_{rc} + \frac{\partial v}{\partial x_{rc}}(x_{ref_i} - x_{ref_c}) + \frac{\partial v}{\partial y_{rc}}(y_{ref_j} - y_{ref_c}) \end{aligned} \tag{3.6}$$

where x_{ref_i} and y_{ref_j} indicate the location of an initial reference subset point in x and y coordinates, x_{ref_c} and y_{ref_c} express the center of the initial reference subset in the x and y coordinates, x_{cur_i} and y_{cur_j} provide the location of a final (current) subset point in the x and y coordinates, with i and j being symbols used to represent the relative location of subset points with respect to the center of the subset. S is a set that contains all of the subset points. The subscript 'rc' refers to a transformation from the reference to the current coordinate system. $\mathbf{p}$ is a generalized deformation

vector defined as

$$\mathbf{p} = \Big\{ u \quad v \quad \frac{\partial u}{\partial x} \quad \frac{\partial u}{\partial y} \quad \frac{\partial v}{\partial x} \quad \frac{\partial v}{\partial y} \Big\}. \tag{3.7}$$

Equation (3.6) can also be described in a matrix form as

$$\xi_{ref_c} + w(\Delta\xi_{ref}; \mathbf{p}_{rc}) = \begin{bmatrix} x^{\mathrm{T}}_{ref_c} \\ y^{\mathrm{T}}_{ref_c} \\ 1 \end{bmatrix} + \begin{bmatrix} 1 + \frac{\mathrm{d}u}{\mathrm{d}x_{rc}} & \frac{\mathrm{d}u}{\mathrm{d}y_{rc}} & u_{rc} \\ \frac{\mathrm{d}v}{\mathrm{d}x_{rc}} & 1 + \frac{\mathrm{d}v}{\mathrm{d}y_{rc}} & v_{rc} \\ 0 & 0 & 1 \end{bmatrix} \begin{bmatrix} \Delta x^{\mathrm{T}}_{ref} \\ \Delta y^{\mathrm{T}}_{ref} \\ 1 \end{bmatrix} \tag{3.8}$$

where ξ is an augmented vector, $\Delta x = x_{ref_i} - x_{ref_c}$ and $\Delta y = y_{ref_i} - y_{ref_c}$ are distances between points inside the subset the center of the subset, and w is called the warp function. Ncorr allows the reference subset to deform within the reference configuration to achieve computationally more efficient algorithm. This idea is solved using the inverse, compositional, Gauss-Newton numerical, method [23]. Thus

$$\begin{aligned} \tilde{x}_{ref_i} &= x_{ref_i} + u_{rr} + \frac{\partial u}{\partial x_{rr}}(x_{ref_i} - x_{ref_c}) + \frac{\partial u}{\partial y_{rr}}(y_{ref_j} - y_{ref_c}) \\ \tilde{y}_{ref_j} &= y_{ref_j} + v_{rr} + \frac{\partial v}{\partial x_{rr}}(x_{ref_i} - x_{ref_c}) + \frac{\partial v}{\partial y_{rr}}(y_{ref_j} - y_{ref_c}), \ (i,j \in S) \end{aligned} \tag{3.9}$$

where $\tilde{x}_{ref_i}$ and $\tilde{y}_{ref_i}$ indicates location of a final reference subset in x and y coordinates. The 'rr' subscription implicates transformation between the two coordinate systems with respect to the reference configuration (image).

Ncorr uses two different correlation criteria [24] in order to associate similarity (gray-scale value) between the final reference subset and a final current subset. The normalized cross correlation (NCC) equation is used to compute an initial guess at the integer pixel locations, i.e.,

$$C_{cc} = \frac{\sum_{ij} \Big(f(\tilde{x}_{ref_i}, \tilde{y}_{ref_j}) - f_m \Big) \Big(g(\tilde{x}_{cur_i}, \tilde{y}_{cur_j}) - g_m \Big)}{\sqrt{\sum_{ij} \Big[f(\tilde{x}_{ref_i}, \tilde{y}_{ref_j}) - f_m \Big]^2 \sum_{ij} \Big[g(\tilde{x}_{cur_i}, \tilde{y}_{cur_j}) - g_m \Big]^2}}, \quad (i,j \in S) \tag{3.10}$$

where f and g are the reference and current image grayscale intensity functions, respectively, for a specific location (x, y). Functions f_m and g_m correlate with the reference and current subset mean grayscale values, respectively. The procedure to find an initial guess is as follows:

1. Use a reference subset (a small circle inside the ROI) and pad it with zeros to obtain a full size image that is equal in area to current image.

2. Convolve the padded image with the current image to find the array of NCC.

3. Determine the subset location in the current configuration by finding the position of the maximum correlation criteria.

Because an initial guess only provides u and v at integer location $\mathbf{p} = \{$ u, v, 0, 0, 0, 0 $\}$, another correlation criteria C_{LS} is used to refine location at sub-pixel level resolution, specifically

$$C_{LS} = \sum \left[\frac{f(\tilde{x}_{ref_i}, \tilde{y}_{ref_j}) - f_m}{\sqrt{\sum_{ij} \left[f(\tilde{x}_{ref_i}, \tilde{y}_{ref_j}) - f_m \right]^2}} - \frac{g(\tilde{x}_{cur_i}, \tilde{y}_{cur_j}) - g_m}{\sqrt{\left[\sum_{ij} \left[g(\tilde{x}_{cur_i}, \tilde{y}_{cur_j}) - g_m \right]^2 \right.}} \right] \tag{3.11}$$

which is considered as a normalized least square criteria that indicates a good match whenever its value is close to zero whereas the C_{cc} value (normalized cross correlation criteria) is close to one. Subtracting mean components (f_m and g_m) from Eq. (3.10) and (3.11) and dividing by the quantity in the denominator provides a correlation criteria that is invariant to affine shifts in gray scale values.

The starting point of nonlinear, iterative, least square optimization in Ncorr is the Gauss-Newton method, which is widely used to find the roots of a function. This method can be extended to optimization by finding the roots of a function derivative. Furthermore, multi-variable optimization, a more generalized version,

can be obtained by replacing derivatives with gradients, and determining where the norm of the gradient approaches.

In this case, the general form of the iterative equation has been derived by applying the second order Taylor series expansion of C_{LS} around $\mathbf{p}_o$, which contains the initial guess, and then determine where its derivative with respect to $\Delta\mathbf{p}$ is equal to the zero vector, viz.,

$$C_{LS}(\mathbf{p_o}+\Delta\mathbf{p}) \approx C_{LS}(\mathbf{p_o}) + \nabla C_{LS}\mathbf{p_o}(\Delta\mathbf{p}) + \frac{1}{2}(\Delta\mathbf{p})^2\nabla\nabla C_{LS}(\mathbf{p}_o) \tag{3.12}$$

then,

$$\frac{\mathrm{d}C_{LS}(\mathbf{p}_o+\Delta\mathbf{p})}{\mathrm{d}\Delta\mathbf{p}} \approx \nabla C_{LS}(\mathbf{p_o}) + \nabla\nabla C_{LS}(\mathbf{p}_o)\Delta\mathbf{p} = 0 \tag{3.13}$$

where $\nabla C_{LS}(\mathbf{p}_o)$ is the gradient of C_{LS} at $\mathbf{p}_o$ and $\nabla\nabla C_{LS}(\mathbf{p}_o)$ is the Hessian of C_{LS} at $\mathbf{p}_o$. The general form for this optimization equation can be then rewritten as

$$\nabla\nabla C_{LS}(\mathbf{p_o})\Delta\mathbf{p} = -\nabla C_{LS}(\mathbf{p_o}) \tag{3.14}$$

Newton-Raphson iteration is applied to this equation.

Ncorr utilizes an inverse compositional method to update $\mathbf{p}$. With this method, the final reference subset location is allowed to alter; however, $\mathbf{p}_{rr}$ is set to zero at every iteration. On the other hand, the final current subset location is allowed to alter; it is set to $\mathbf{p}_{old}$. This method requires a single Hessian calculation at every iteration. The gradient $\nabla C_{LS}(0)$ and Hessian $\nabla\nabla C_{LS}(0)$ are used to compute $\Delta\mathbf{p}$ from Eq. (3.14). Then $\mathbf{p}_{old}$ is multiplied by Δp^{-1} to obtain a closer approximation to $\mathbf{p}_{rc}$. Ncorr developers also investigated another method (forward additive Gauss-Newton) to obtain update for $\mathbf{p}$ that are equal to $\mathbf{p}_{old}+\Delta\mathbf{p}$. For this method, the Hessian matrix needs to be calculated after every iteration, which is a computational

expensive.

To calculate the gradient $\mathrm{d}C_{LS}(0)/\mathrm{d}\Delta\mathbf{p}$ and Hessian $\mathrm{d}^2C_{LS}(0)/\mathrm{d}\Delta\mathbf{p}^2$, the functions below have to be known;

$$\frac{\partial}{\partial\tilde{x}_{ref_i}}f(\tilde{x}_{ref_i},\tilde{y}_{ref_j}),\quad \frac{\partial}{\partial\tilde{y}_{ref_j}}f(\tilde{x}_{ref_i},\tilde{y}_{ref_j}),\quad g(\tilde{x}_{cur_i},\tilde{y}_{cur_j}) \tag{3.15}$$

Ncorr uses biquantic B-spline interpolation [25], to mitigate DIC error caused by interpolating signals with high frequency content, and thereby being able to compute the functions shown in Eq. (3.15). B-splines have a very favorable property in that they are separable. In other words, 2D interpolation can be decomposed into a series of 1D interpolations, which can be computed faster than 2D interpolations. This 1D interpolation can be described as:

$$g(x)=\sum_{k\epsilon Z}c(k)\beta^n(x-k) \tag{3.16}$$

where $c(k)$, $\beta^n(x-k)$ and $g(x)$ are the B-spline coefficients at integer k and kernel $x-k$ values, and interpolated signal value at x, respectively. Ncorr developers adopted a B-spline kernel of order five with Z denoting the integer set. The kernel equation was defined as

$$\beta^n(x)=\frac{1}{n!}\sum_{k=0}^{n+1}\binom{n+1}{k}(-1)^k(x-k+\tfrac{n+1}{2})^2. \tag{3.17}$$

B-spline coefficients can be found through deconvolution. In this case, a discrete Fourier transform is applied to Eq. (3.16) giving

$$F\{c\}=\frac{F\{g\}}{F\{\beta^n\}} \tag{3.18}$$

that upon taking the inverse direct Fourier transform of Eq. (3.18) will provide the

B-spline coefficients. Now we need to interpolate the gray scale value from these 1D B-spline coefficient values $[\mathrm{c}]_{(x_f,y_f)}$.

$$g(\tilde{x}_{cur},\tilde{y}_{cur}) = [1\ \Delta y\ \Delta y^2\ \Delta y^3\ \Delta y^4\ \Delta y^5]^{\mathrm{T}}[QK][c]_{(x_f,y_f)}[QK]^{\mathrm{T}} \begin{bmatrix} 1 \\ \Delta x \\ \Delta x^2 \\ \Delta x^3 \\ \Delta x^4 \\ \Delta x^5 \end{bmatrix} \tag{3.19}$$

where $\Delta x = \tilde{x}_{cur} - x_f$ and $\Delta y = \tilde{y}_{cur} - y_f$,

$$[QK] = \begin{bmatrix} \frac{1}{120} & \frac{13}{60} & \frac{11}{20} & \frac{13}{60} & \frac{1}{120} & 0 \\ -\frac{1}{24} & -\frac{5}{12} & 0 & \frac{5}{12} & \frac{1}{24} & 0 \\ \frac{1}{12} & \frac{1}{6} & -\frac{1}{2} & \frac{1}{6} & \frac{1}{12} & 0 \\ -\frac{1}{12} & \frac{1}{6} & 0 & -\frac{1}{6} & \frac{1}{12} & 0 \\ \frac{1}{24} & -\frac{1}{6} & \frac{1}{4} & -\frac{1}{6} & \frac{1}{24} & 0 \\ -\frac{1}{120} & \frac{1}{24} & -\frac{1}{12} & \frac{1}{12} & -\frac{1}{24} & \frac{1}{120} \end{bmatrix}$$

and

$$[c]_{(x_f,y_f)} = \begin{bmatrix} c_{x_f-2,y_f-2} & c_{(x_f-1,y_f-2)} & c_{(x_f,y_f-2)} & c_{(x_f+1,y_f-2)} & c_{(x_f+2,y_f-2)} & c_{(x_f+3,y_f-2)} \\ c_{(x_f-2,y_f-1)} & c_{(x_f-1,y_f-1)} & c_{(x_f,y_f-1)} & c_{(x_f+1,y_f-1)} & c_{(x_f+2,y_f-1)} & c_{(x_f+3,y_f-1)} \\ c_{(x_f-2,y_f)} & c_{(x_f-1,y_f)} & c_{(x_f,y_f)} & c_{(x_f+1,y_f)} & c_{(x_f+2,y_f)} & c_{(x_f+3,y_f)} \\ c_{(x_f-2,y_f+1)} & c_{(x_f-1,y_f+1)} & c_{(x_f,y_f+1)} & c_{(x_f+1,y_f+1)} & c_{(x_f+2,y_f+1)} & c_{(x_f+3,y_f+1)} \\ c_{(x_f-2,y_f+2)} & c_{(x_f-1,y_f+2)} & c_{(x_f,y_f+2)} & c_{(x_f+1,y_f+2)} & c_{(x_f+2,y_f+2)} & c_{(x_f+3,y_f+2)} \\ c_{(x_f-2,y_f+3)} & c_{(x_f-1,y_f+3)} & c_{(x_f,y_f+3)} & c_{(x_f+1,y_f+3)} & c_{(x_f+2,y_f+3)} & c_{(x_f+3,y_f+3)} \end{bmatrix}$$

Here the inverse compositional method has a work-flow that is an extension of the Lucas Kanade algorithm published by S. Baker [23].

1. Entire DIC Analysis Computation (Optional)

   (a) Precompute $[QK][c]_{(x_f,y_f)}[QK]^{\mathrm{T}}$ for the entire current image.

   (b) Compute $\frac{\partial}{\partial \tilde{x}_{ref_i}} f(\tilde{x}_{ref_i}, \tilde{y}_{ref_j})$ and $\frac{\partial}{\partial \tilde{y}_{ref_j}} f(\tilde{x}_{ref_i}, \tilde{y}_{ref_j})$ for the entire reference image.

   2. A subset computation

      (a) Compute $\frac{\mathrm{d}}{\mathrm{d}\Delta\mathbf{p}} f\Big(\xi_{ref_c} + w(\Delta\xi_{ref}; 0)\Big)$

      (b) Compute Hessian $\nabla\nabla C_{LS}(0)$

      (c) Set the initial $\mathbf{p}_{old}$ value to the initial guess from NCC

      3. Computation for each subset iteration

         (a) Compute $g(\tilde{x}_{cur}, \tilde{y}_{cur})$ by utilizing the B-spline method

         (b) Compute the gradient $\nabla C_{LS}(0)$

         (c) Compute $\Delta\mathbf{p}$ using the known Hessian and gradient of C_{LS}

         (d) Update $\mathbf{p}_{old}$

         (e) Exit when the norm of $\Delta\mathbf{p}$ is small.

Ncorr utilized a reliability-guided digital image correlation method [26] to obtain full field displacements. This method begins with selecting a seed point that is at the center location of the first reference subset. This is a special subset, because it is the one that uses NCC correlation to obtain an initial guess. The rest of the subsets inside the region of interest use neighboring information as an initial guess. After selecting a seed point, the neighboring points C_{LS} are computed. The algorithm then

moves in the direction of the lowest C_{LS} value, computing neighboring point least squares correlation C_{LS} again, and finally moving on to the next lowest correlation value until the queue is empty. This method helps to protect wrong computation due to area and/or deformation discontinuity. In other words, leaving the least correlated values (best match) at the end of entire computation will help prevent to the propagation of error, i.e., the bad points do not affect subsequent calculations.

Calculating strains is more difficult than calculating displacements due to differentiation. Any noise in displacement field will magnify errors in the strain field. B. Pan [27] proposed another idea that utilizes a two-dimensional Savitzky-Golay digital differentiator, rather than a reliability guided method. The basic idea behind this differentiator method is to fit a 2D polynomial function to a local subregion of the displacement field. Then to determine the unknown polynomial coefficients by using the least squares method. Finally, to take derivatives of the found polynomial displacement function with respect to x and y to obtain Lagrangian/Eulerian strain components.

4. ANISOTROPIC SMALL STRAIN CONJUGATE PAIRS*

4.1 Small Strain Validation

Linear anisotropic vinylester data [28] are used to validate our transversely isotropic conjugate stress/strain pairs theory. A set of experimental results comprised of five 0° and six 90° specimens was used to compare experiment with both the conventional and conjugate-pair models. The 0° specimens were loaded in the fiber direction and are numbered from 1 to 5. The 90° specimens were loaded normal to the fiber direction and are numbered from 6 to 11.

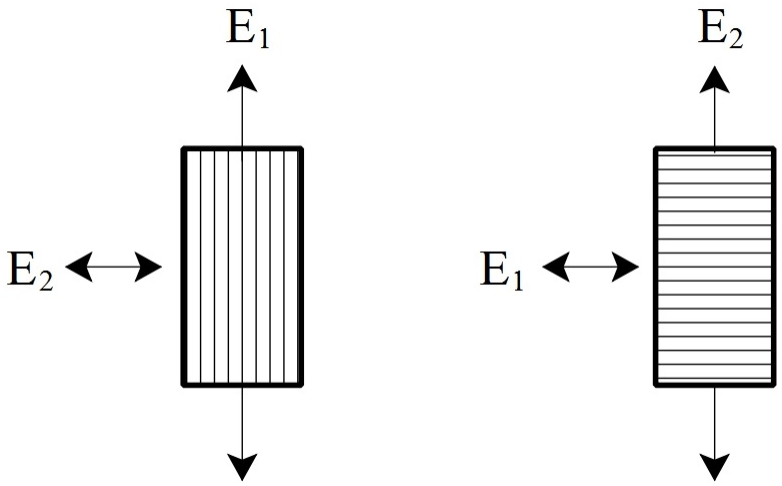

Figure 4.1: 0° fiber and 90° fiber

*Part of this section is reprinted with permission from "Stress/strain basis pairs for anisotropic materials." by Veysel Erel and Alan D. Freed 2017, Composites Part B: Engineering 120 (2017): 152-158. Copyright 2017 Elsevier Ltd. All rights reserved.

4.1.1 Data Analyzing

Raw datum [28] were obtained from Dr. Muliana, Texas A&M University Mechanical Engineering Department. Axial stress was quantified by dividing the axial force by the reference cross-sectional area. If the first strain value was not zero in an experimental data set, then small digits were added or subtracted to round the first strain values to zero. There were two strain probes placed at each side of specimen that measured strain at micro strain resolution. Strains from the first probe were used for calculations.

In the conventional Spencer model, the elastic modulus is determined by calculating the slope of the stress/strain curve data in both the pulling and transverse directions. The negative ratio of the transverse strain vs. pulling direction strain gives the Poisson ratio for the material. Linear regression was used to find the slope of the curves, with optimal lines enforced to pass through the origin.

Elongation ratios a and b were converted into percent strain values in an engineering sense for plotting purposes. A code written in C++ was used to analyze the data.

4.1.2 Specimen Comparision

In the figures that follow, Figs. 4.2 - 4.31, the graphs at the left demonstrate the elastic modulus in the pulling direction for both the 0° and 90° specimens. Small figures close to curves indicate the fiber and pulling directions. Graphs at the right show a axial/transverse strain ratio for both the 0° and 90° specimens.

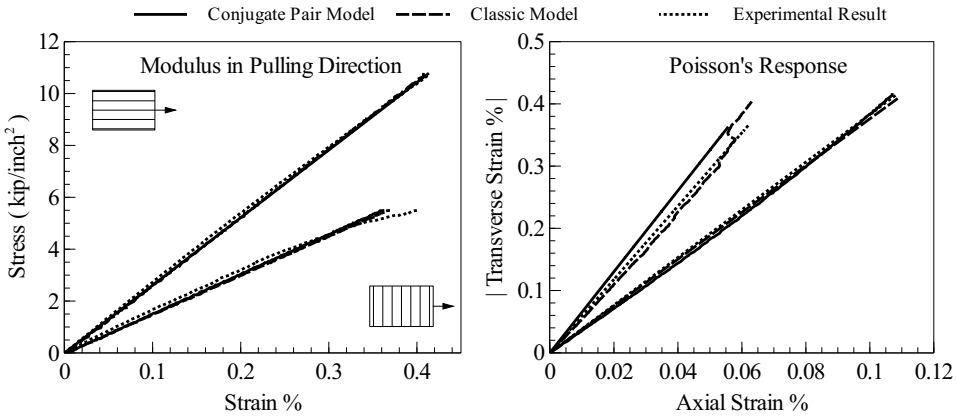

Figure 4.2: 0° specimen 1 vs 90° specimen 6

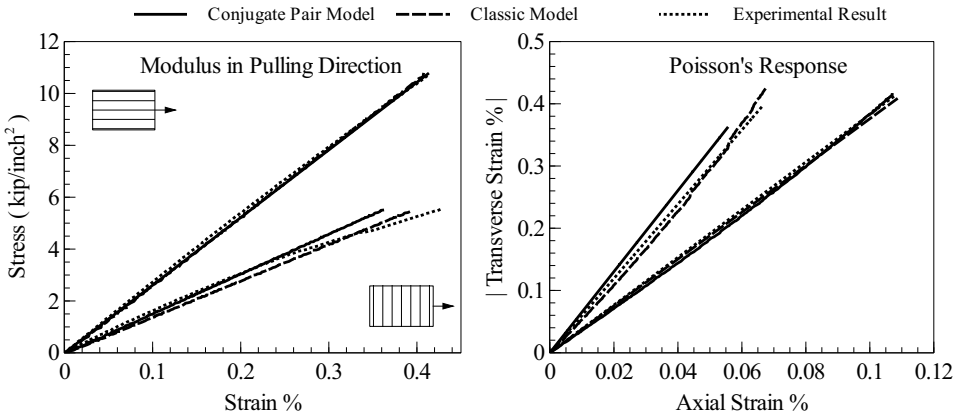

Figure 4.3: 0° specimen 1 vs 90° specimen 7

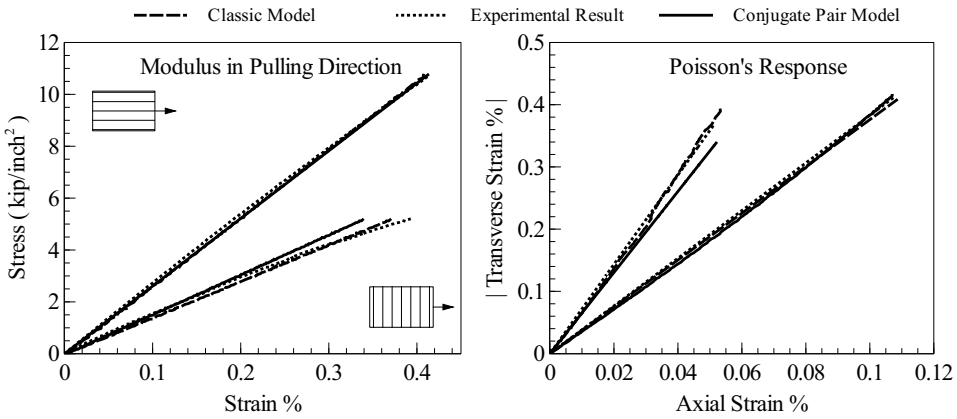

Figure 4.4: 0° specimen 1 vs 90° specimen 8

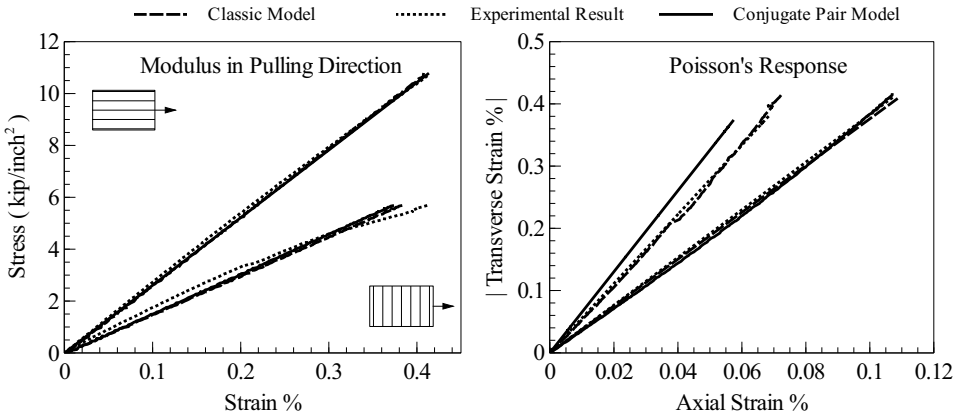

Figure 4.5: 0° specimen 1 vs 90° specimen 9

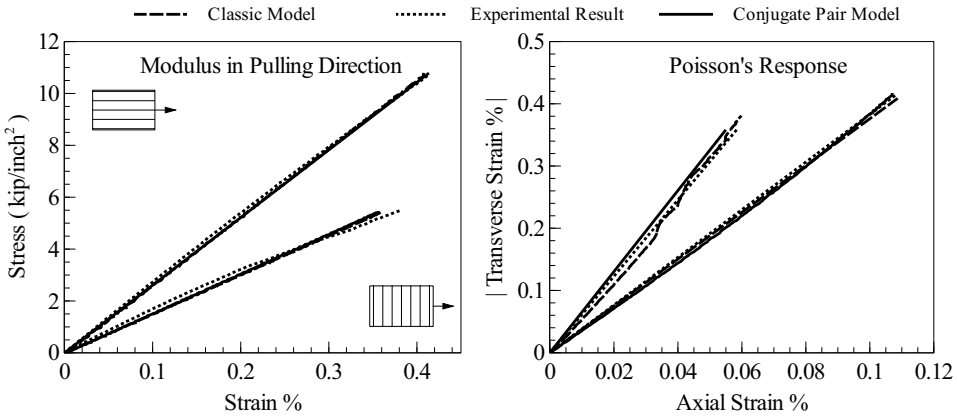

Figure 4.6: 0° specimen 1 vs 90° specimen 10

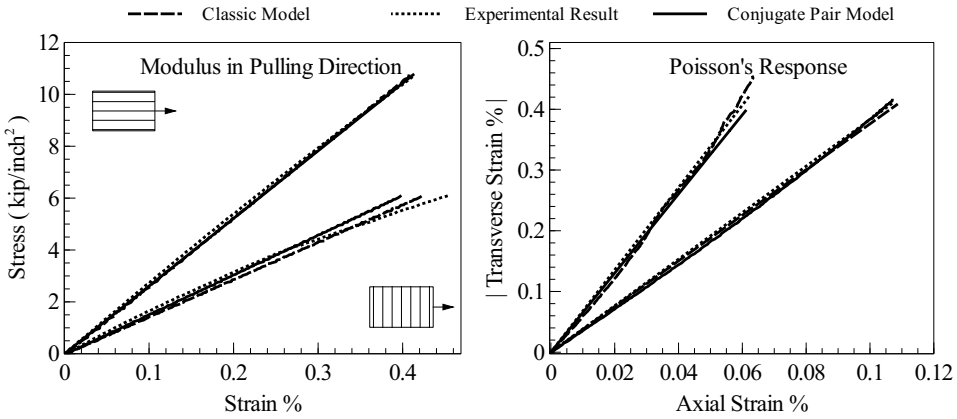

Figure 4.7: 0° specimen 1 vs 90° specimen 11

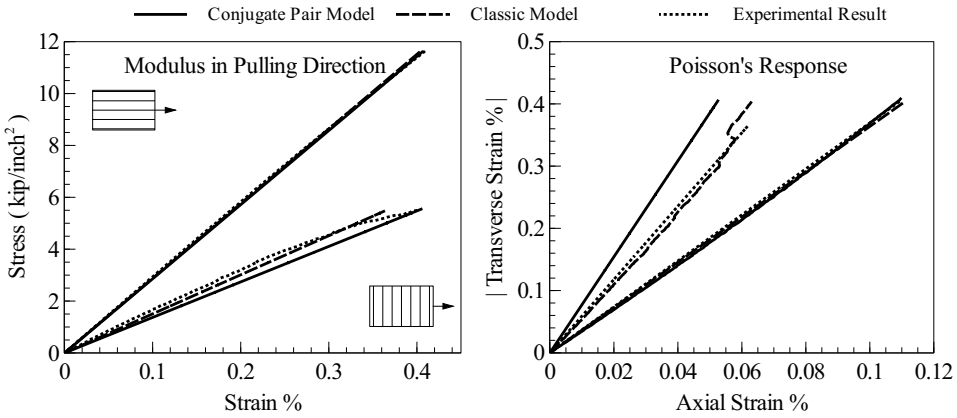

Figure 4.8: 0° specimen 2 vs 90° specimen 6

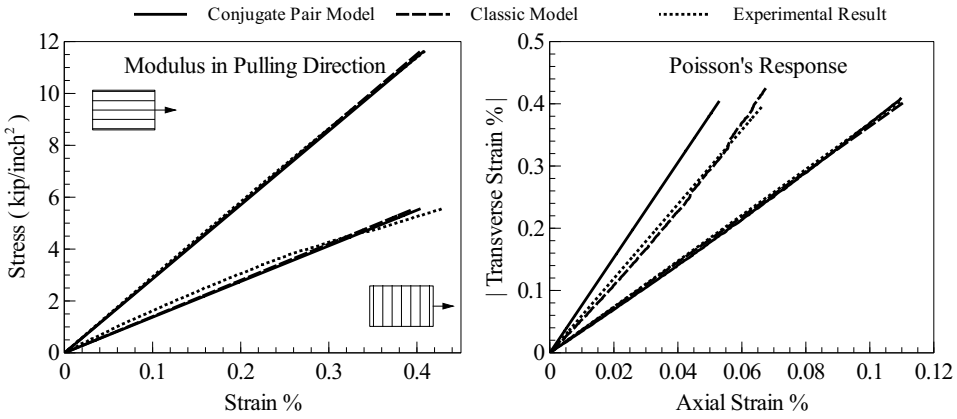

Figure 4.9: 0° specimen 2 vs 90° specimen 7

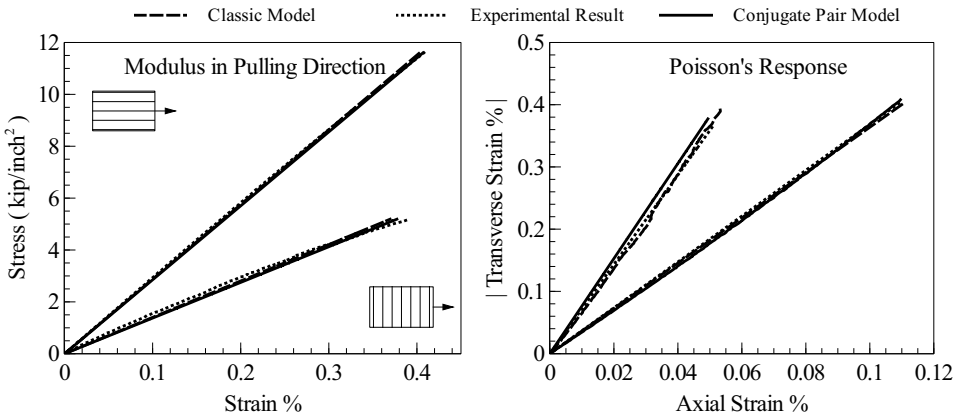

Figure 4.10: 0° specimen 2 vs 90° specimen 8

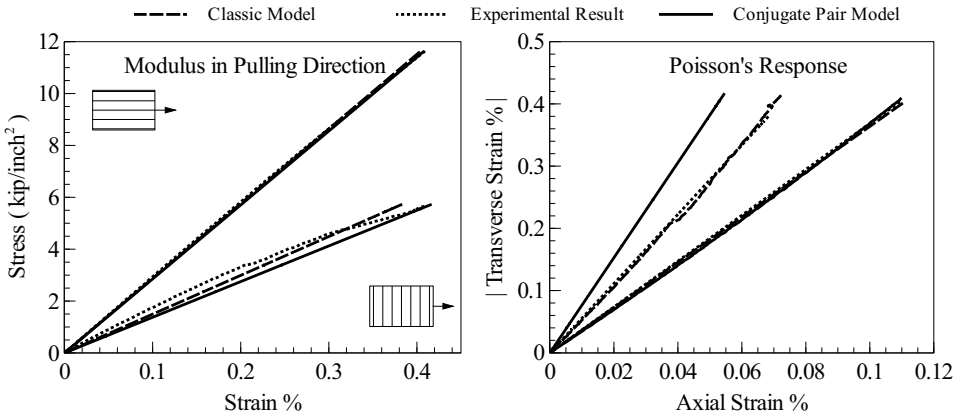

Figure 4.11: 0° specimen 2 vs 90° specimen 9

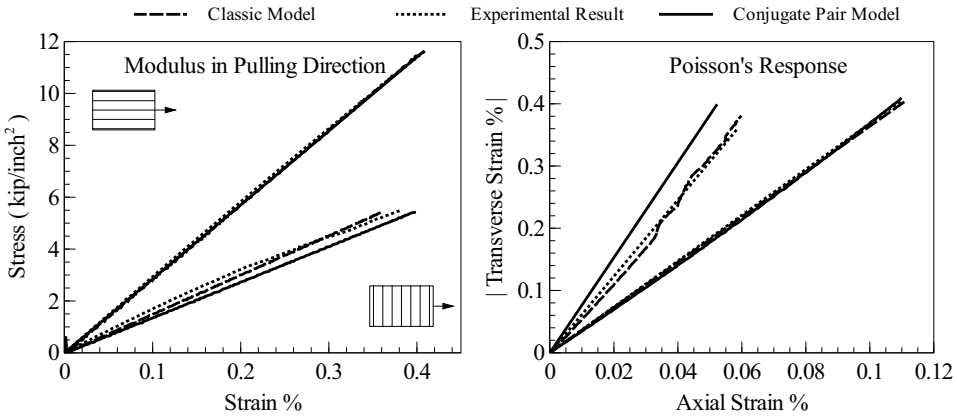

Figure 4.12: 0° specimen 2 vs 90° specimen 10

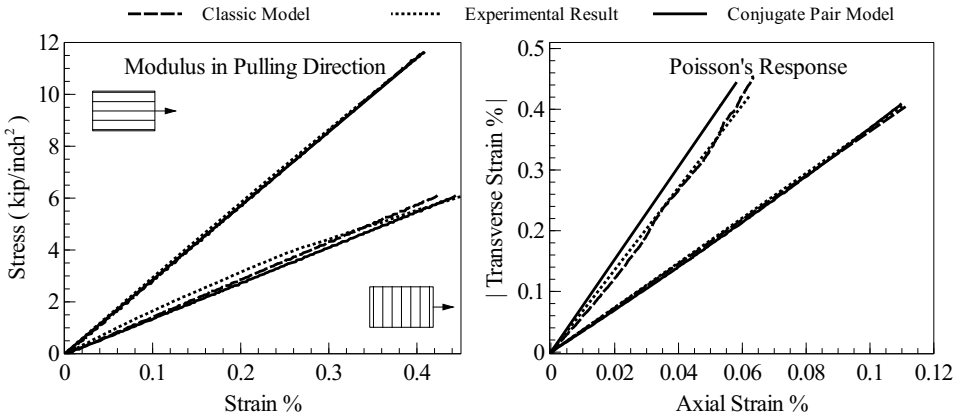

Figure 4.13: 0° specimen 2 vs 90° specimen 11

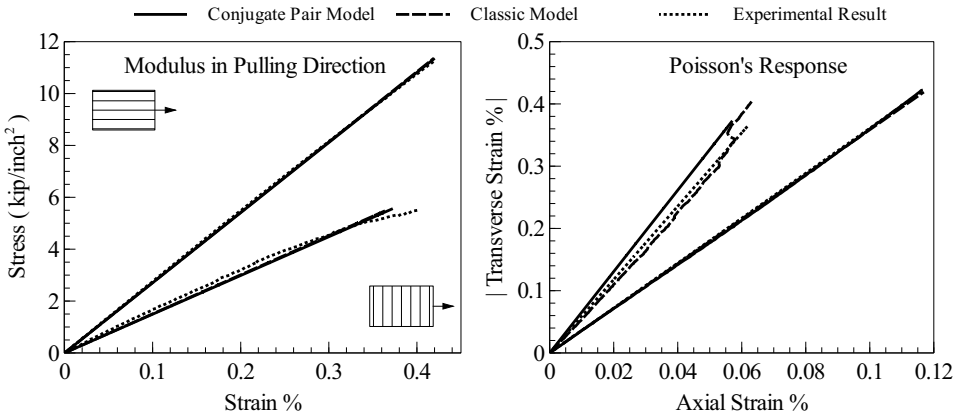

Figure 4.14: 0° specimen 3 vs 90° specimen 6

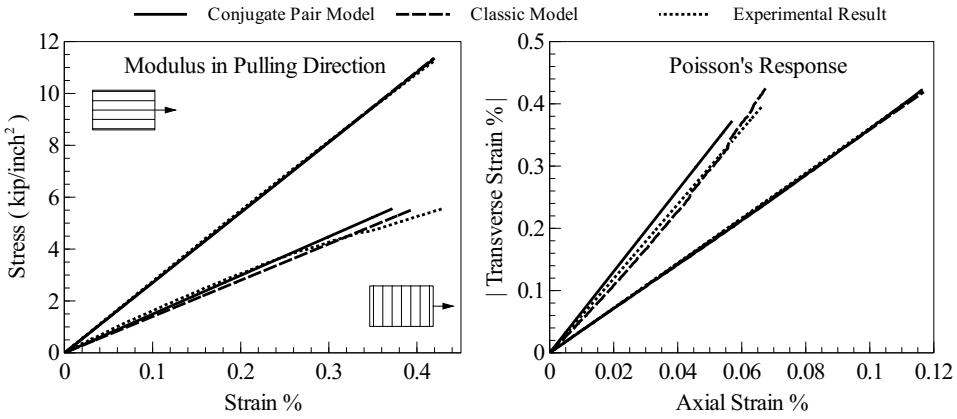

Figure 4.15: 0° specimen 3 vs 90° specimen 7

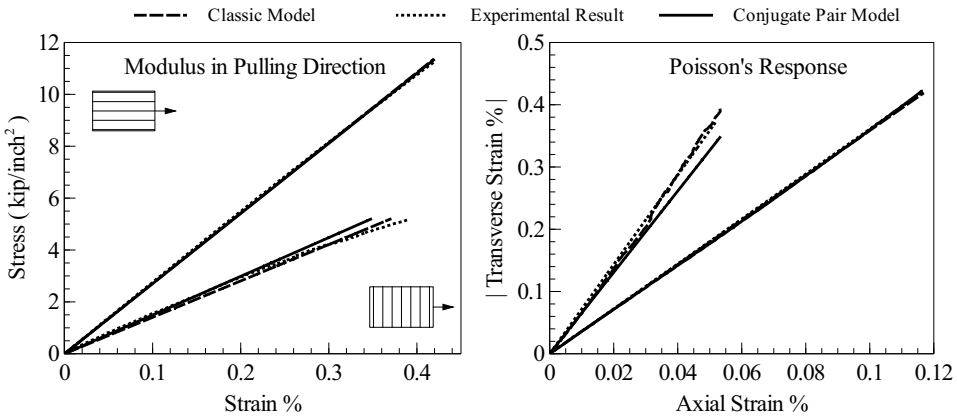

Figure 4.16: 0° specimen 3 vs 90° specimen 8

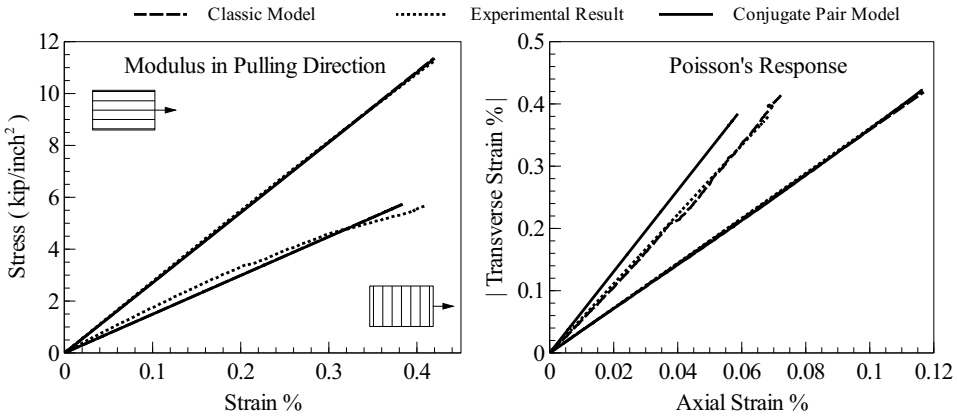

Figure 4.17: 0° specimen 3 vs 90° specimen 9

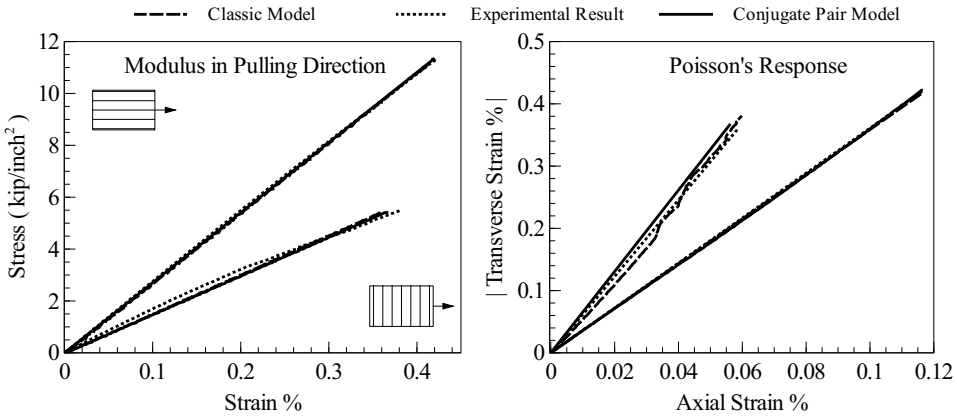

Figure 4.18: 0° specimen 3 vs 90° specimen 10

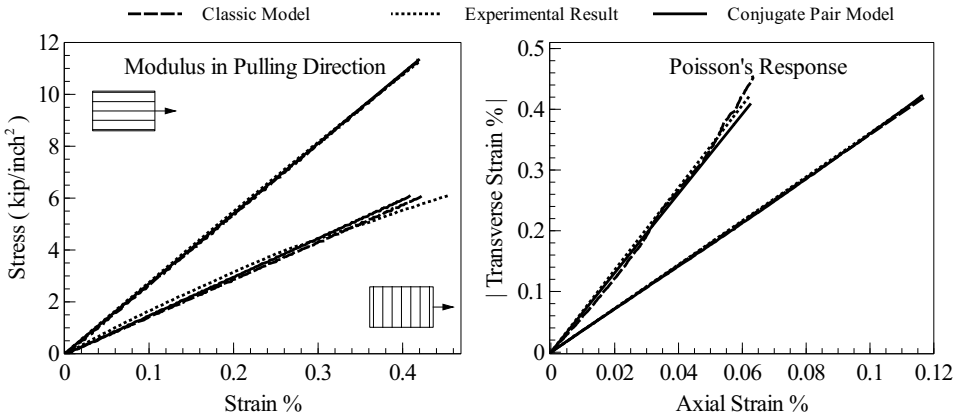

Figure 4.19: 0° specimen 3 vs 90° specimen 11

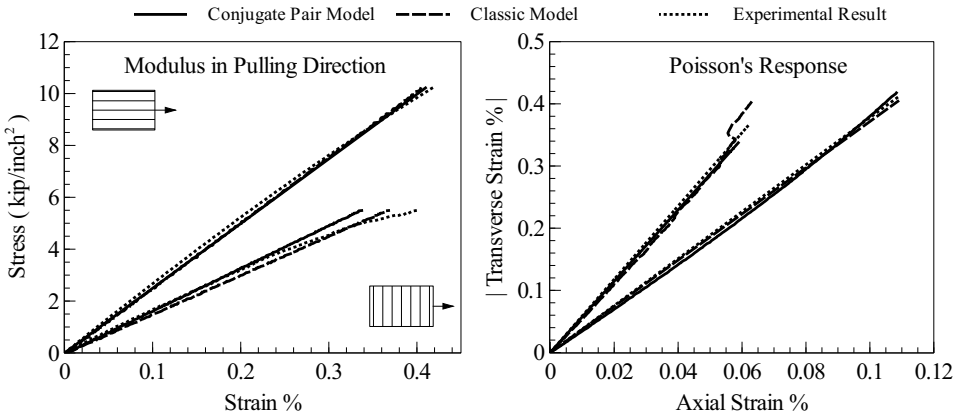

Figure 4.20: 0° specimen 4 vs 90° specimen 6

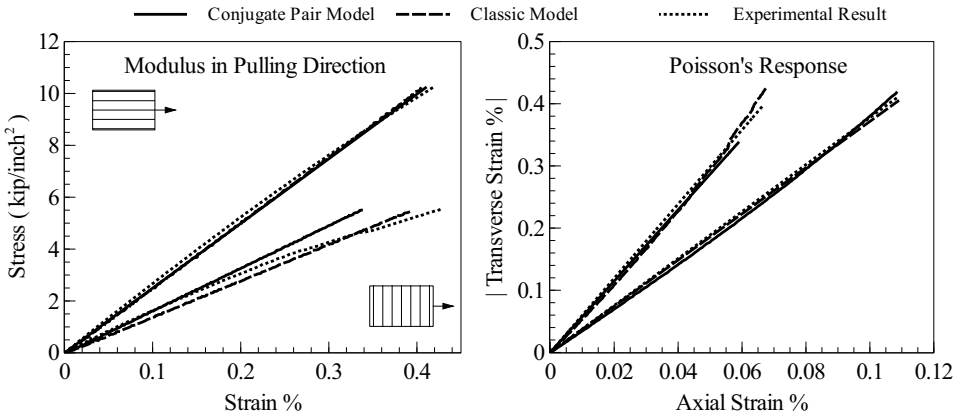

Figure 4.21: 0° specimen 4 vs 90° specimen 7

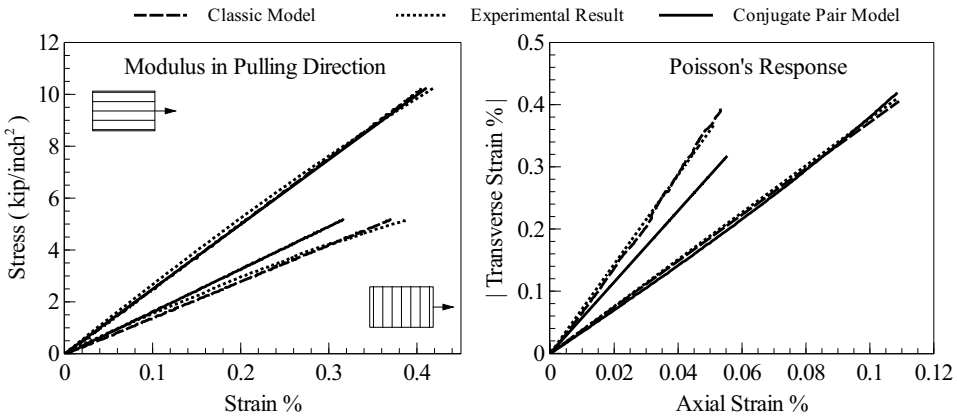

Figure 4.22: 0° specimen 4 vs 90° specimen 8

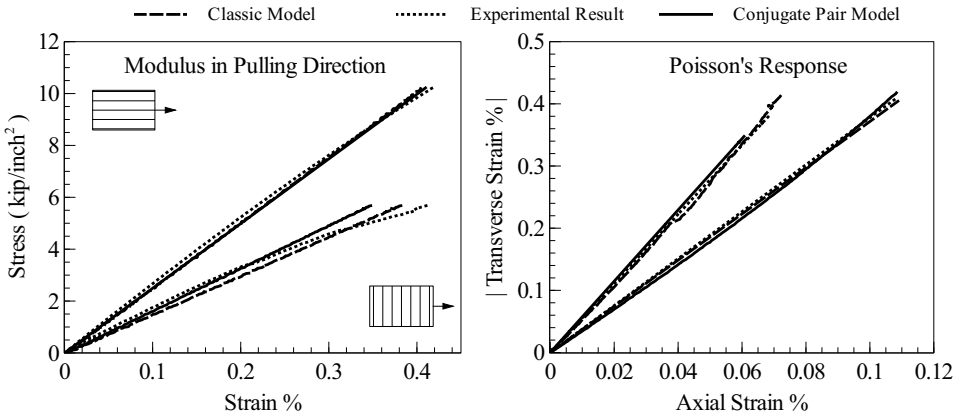

Figure 4.23: 0° specimen 4 vs 90° specimen 9

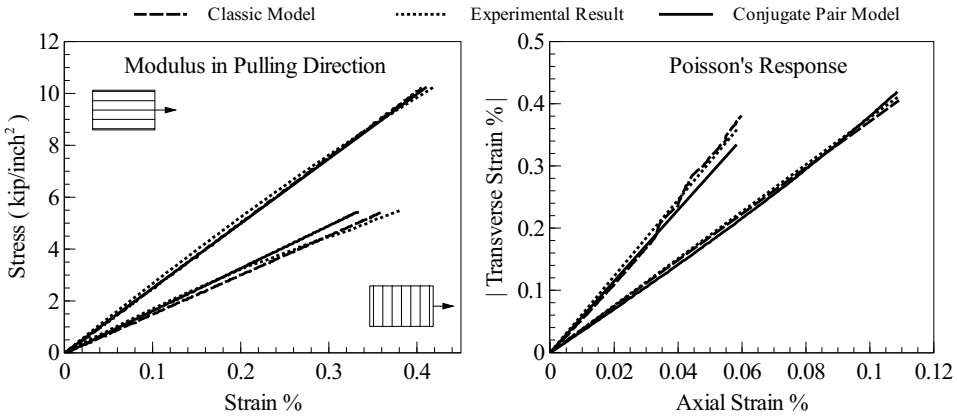

Figure 4.24: 0° specimen 4 vs 90° specimen 10

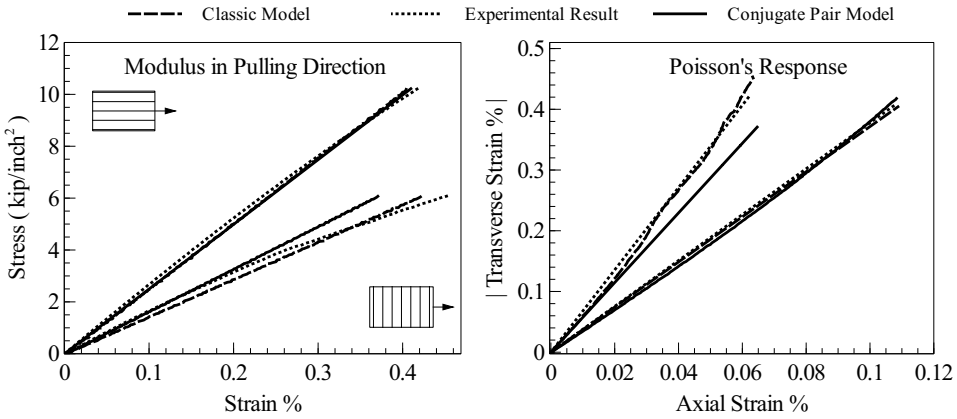

Figure 4.25: 0° specimen 4 vs 90° specimen 11

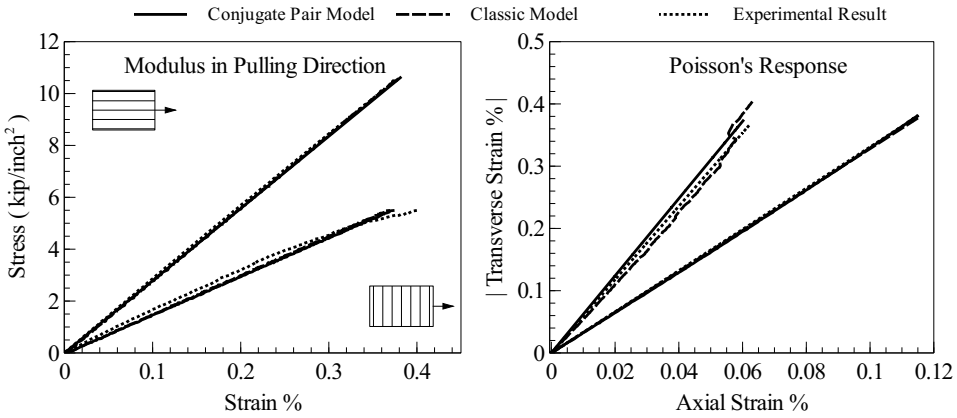

Figure 4.26: 0° specimen 5 vs 90° specimen 6

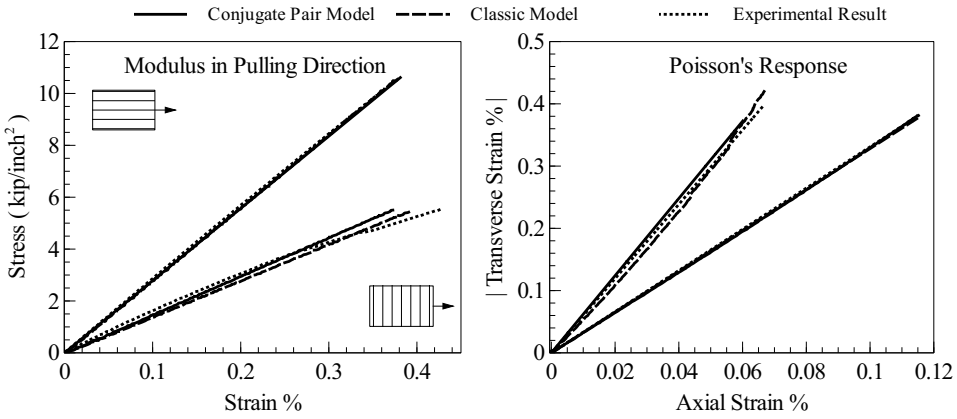

Figure 4.27: 0° specimen 5 vs 90° specimen 7

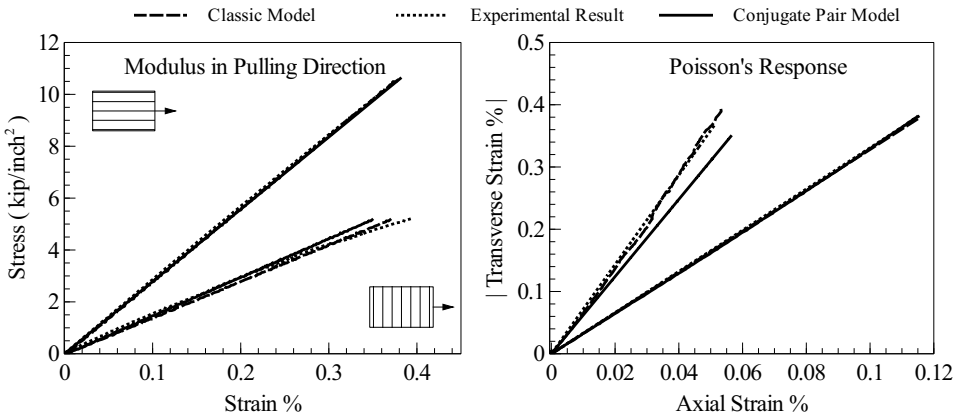

Figure 4.28: 0° specimen 5 vs 90° specimen 8

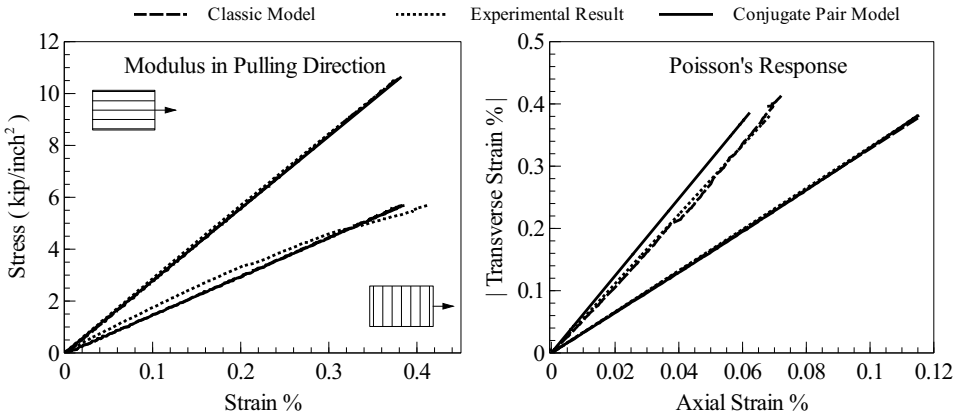

Figure 4.29: 0° specimen 5 vs 90° specimen 9

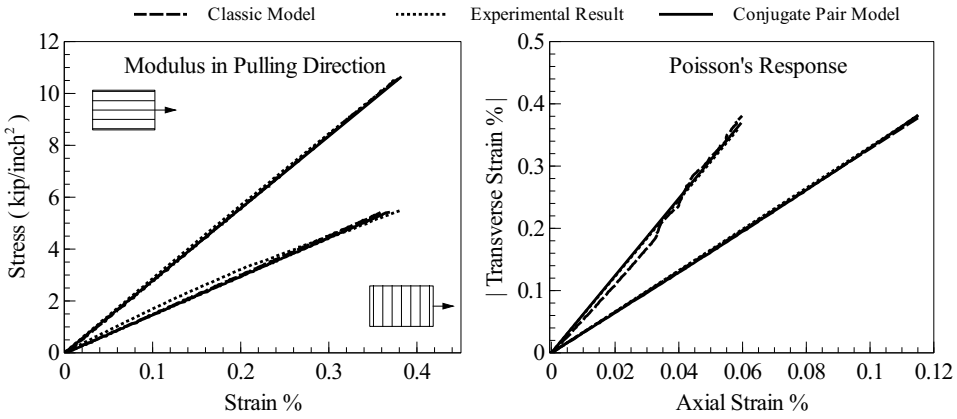

Figure 4.30: 0° specimen 5 vs 90° specimen 10

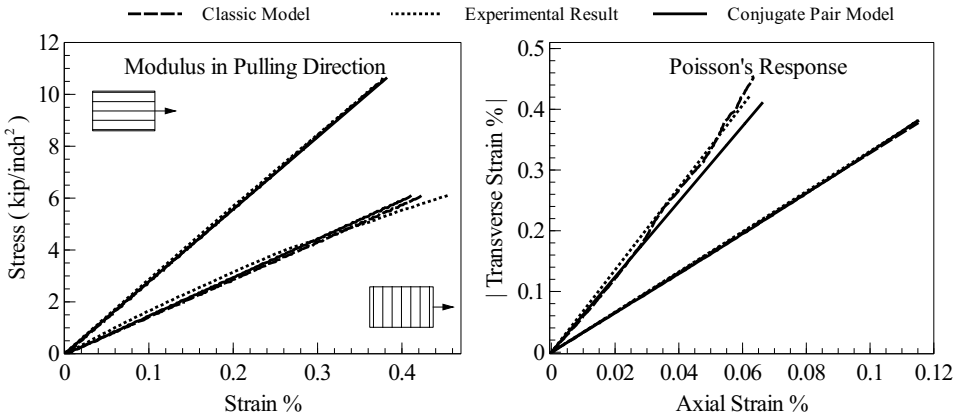

Figure 4.31: 0° specimen 5 vs 90° specimen 11

Both the classical model and the conjugate pair model describe linear responses for transversely isotropic behavior. It can be clearly seen in the graphs from the proceeding figures that the 0° fiber specimens response in the pulling direction is mostly linear; however, a few specimens' experimental results did not match with either theoretical approach due to material non-linearity. Some of the 90° specimens have a response in the pulling direction that is also a nonlinear response. The conjugate pair model fit better than the classical model for the 90° pulling direction response. It fits the linear regions of these response curves.

Most 0° Poisson responses are linear. Thus both models fit the data well for this type of response. Some 90° specimens demonstrate nonlinear behavior. Linear regression was used to fit the classical model to data; however, the conjugate pair model assumes isotropic behavior, even in the off-fiber direction. In the presence of non-linearity the classical, model may generate a better fit. Some 90° specimens, viz. (Fig. 4.30), show isotropic behavior described well by both models.

4.2 Classic Model and Conjugate Pair Models: A Comparison

The capability of our model is contrasted against that of the classic fiber (transversely isotropic) model of Spencer [9] which was derived (in Chapter 1.3) from invariant theory. These two models are outlined and compared in Table 4.1.

The 0° and 90°, one-preferred fiber direction composite plates were used to compare the two different models' numerical results. Three different types of stress/strain behaviors were examined in this study. Specimens were pulled along with fiber direction and normal to fiber direction. Parameters K, M and n correlate to the 0° elastic modulus E_1, and the 90° elastic modulus E_2. The relationship is written below.

Table 4.1: Model comparison table. [2]

Spencer's Model (Conventional)	Conjugate Base-Pair Model (New)
$\begin{Bmatrix} \epsilon_{11} \\ \epsilon_{22} \\ \gamma_{12} \end{Bmatrix} = \begin{bmatrix} \frac{1}{E_1} & \frac{-\nu_{21}}{E_2} & 0 \\ \frac{-\nu_{12}}{E_1} & \frac{1}{E_2} & 0 \\ 0 & 0 & \frac{1}{G_{12}} \end{bmatrix} \begin{Bmatrix} T_{11} \\ T_{22} \\ T_{12} \end{Bmatrix}$	$\begin{Bmatrix} \delta \\ \epsilon \\ \gamma \end{Bmatrix} = \begin{bmatrix} \frac{1}{4K} & 0 & 0 \\ 0 & \frac{1}{2M} & 0 \\ 0 & 0 & \frac{1}{G} \end{bmatrix} \begin{Bmatrix} \frac{S_{11}}{n} + nS_{22} \\ \frac{S_{11}}{n} - nS_{22} \\ \frac{a}{b} S_{12} \end{Bmatrix}$
This model has 5 parameters to describe material behavior: E_1, E_2, G_{12}, ν_{12} and ν_{21}.	This model has 4 parameters to describe material behavior: K, M, G and n.
Off diagonal terms imply a coupling between strains in terms of stresses.	No coupling effect. Each conjugate strain is independent of the other conjugate stresses.
Constitutive equations are derived from a strain-energy density described in terms of strain invariants.	Constitutive equations are derived from a strain-energy density described in terms of thermodynamic conjugate pairs.

$$\frac{1}{n^2}\Big(\frac{1}{4K}+\frac{1}{2M}\Big)=\frac{1}{E_1},\quad n^2\Big(\frac{1}{4K}+\frac{1}{2M}\Big)=\frac{1}{E_2} \tag{4.1}$$

In the conjugate pair model parameters K, M and n have unique values for data from this set of specimens. Parameters n and K changed in value after 0° specimen was changed. For the conventional model, each specimen pair associates with a different elastic modulus and different Poisson ratio, because they represents material parameters. So, to; the optimal parameters were not found to be unique when the data were parameterized against the classic model derived from invariant theory. In contrast, the optimal parameters were unique for our new theory of elastic anisotropy constructed from thermodynamic conjugate pairs.

Model parameters obtained from all twenty-five sets of data are tabulated in Table 4.2. In that table, modulus M was intentionally held fixed, while modulus K was allowed to vary. Because the data sets investigated did not contain shear experiments, responses governed by the shear moduli, viz., Spencer's G_{12} and our G, could not be compared.

Table 4.2: Parameterization the classic invariant model and our conjugate-pair model. [2]

0° vs. 90°	n	K	M	E_1	E_2	ν_{12}	ν_{21}
Spec. 1 vs. Spec. 6	1.14	1250	1670	2640	1510	0.265	0.169
Spec. 1 vs. Spec. 7	1.14	1250	1670	2640	1400	0.265	0.167
Spec. 1 vs. Spec. 8	1.14	1250	1670	2640	1400	0.265	0.139
Spec. 1 vs. Spec. 9	1.14	1250	1670	2640	1500	0.265	0.179
Spec. 1 vs. Spec. 10	1.14	1250	1670	2640	1510	0.265	0.162
Spec. 1 vs. Spec. 11	1.14	1250	1670	2640	1440	0.265	0.147
Spec. 2 vs. Spec. 6	1.20	1220	1670	2880	1510	0.274	0.169
Spec. 2 vs. Spec. 7	1.20	1220	1670	2880	1400	0.274	0.167
Spec. 2 vs. Spec. 8	1.20	1220	1670	2880	1400	0.274	0.139
Spec. 2 vs. Spec. 9	1.20	1220	1670	2880	1500	0.274	0.179
Spec. 2 vs. Spec. 10	1.20	1220	1670	2880	1510	0.274	0.162
Spec. 2 vs. Spec. 11	1.20	1220	1670	2880	1440	0.274	0.147
Spec. 3 vs. Spec. 6	1.16	1270	1670	2710	1510	0.278	0.169
Spec. 3 vs. Spec. 7	1.16	1270	1670	2710	1400	0.278	0.167
Spec. 3 vs. Spec. 8	1.16	1270	1670	2710	1400	0.278	0.139
Spec. 3 vs. Spec. 9	1.16	1270	1670	2710	1500	0.278	0.179
Spec. 3 vs. Spec. 10	1.16	1270	1670	2710	1510	0.278	0.162
Spec. 3 vs. Spec. 11	1.16	1270	1670	2710	1440	0.278	0.147
Spec. 4 vs. Spec. 6	1.11	1290	1670	2530	1510	0.269	0.169
Spec. 4 vs. Spec. 7	1.11	1290	1670	2530	1400	0.269	0.167
Spec. 4 vs. Spec. 8	1.11	1290	1670	2530	1400	0.269	0.139
Spec. 4 vs. Spec. 9	1.11	1290	1670	2530	1500	0.269	0.179
Spec. 4 vs. Spec. 10	1.11	1290	1670	2530	1510	0.269	0.162
Spec. 4 vs. Spec. 11	1.11	1290	1670	2530	1440	0.269	0.147
Spec. 5 vs. Spec. 6	1.17	1310	1670	2820	1510	0.304	0.169
Spec. 5 vs. Spec. 7	1.17	1310	1670	2820	1400	0.304	0.167
Spec. 5 vs. Spec. 8	1.17	1310	1670	2820	1400	0.304	0.139
Spec. 5 vs. Spec. 9	1.17	1310	1670	2820	1500	0.304	0.179
Spec. 5 vs. Spec. 10	1.17	1310	1670	2820	1510	0.304	0.162
Spec. 5 vs. Spec. 11	1.17	1310	1670	2820	1440	0.304	0.147

4.2.1 Statistical analysis

Variations in the moduli from both models, the Poisson ratios, and the n parameter have been investigated for all data sets. Results from statistical analyses are tabulated in Table 4.3. The strength of anisotropy parameter n in our model and the Poisson ratios ν_{12} and ν_{21} of the invariant model have minimal variation, while our modulus K has less variation than the classic moduli E_1 and E_2.

Table 4.3: Mean and standard deviation values for material parameters. [2]

Parameters	n	K	E_1	E_2	ν_{12}	ν_{21}
Mean	1.15	1270	2720	1460	0.278	0.160
Standard deviation	0.03	30	130	50	0.004	0.013

5. LARGE STRAIN LINEAR AND NONLINEAR CONJUGATE PAIR*

Transversely isotropic conjugate pair theory has been extended for large linear and nonlinear deformation in this chapter. The physical meaning of anisotropy parameter n (the strength of anisotropy) has been obtained and implemented to uniaxial silicone/silicone composite material behavior.

5.1 The Strength of Anisotropy

Anisotropy parameters have been widely used to describe behavior difference from axial to transverse direction. In 2008, Shivakumar [29] proposed a new, universal, anisotropy index for elastic single crystals by relating stiffness matrix components (the moduli C_{11}, C_{12} and C_{44}) from cubic cystal symmetry. Another anisotropic parameter introduced [30] to describe the ratio between the horizontal and vertical velocities of seismic waves is P-wave anisotropy. In addition to these, an anisotropic index definition, similar to what is described here, has been presented by Cheney [31]. He states the surface anisotropy is a ratio of the tangent moduli measured parallel and perpendicular to elastin fibers. In this section, we utilize the anisotropic conjugate-pair approach to find a relationship between these Young's moduli and the strength of anisotropy parameter n.

Constitutive formulæ describing an uniaxial extension of anisotropic materials were derived in terms of our anisotropic, stress/strain, basis pairs in the third chapter. Let us assume a_1 and a_2 are elongations in the fiber direction, while b_1 and b_2 are elongations normal to the fiber direction in 0° and 90° composites, respectively. Stress S_1 is an applied traction in the fiber direction for 0° specimens, whereas stress

*Part of this section is reprinted with permission from "Anisotropic Conjugate Stress/Strain Base Pair Approach for Laminates Undergoing Large Deformations" by Veysel Erel and Alan D. Freed 2019. Copyrigh 2019 Acta Materialia Inc. Published by Elsevier Ltd. All rights reserved.

S_2 is an applied traction normal to the fiber direction for 90° specimens [2]. Then,

$$a_1 = \exp\Big(\frac{1}{n^2}\Big(\frac{S_1}{4K} + \frac{S_1}{2M}\Big)\Big), \qquad b_1 = \exp\Big(\frac{S_1}{4K} - \frac{S_1}{2M}\Big) \tag{5.1a}$$

$$a_2 = \exp\Big(\frac{S_2}{4K} - \frac{S_2}{2M}\Big), \qquad b_2 = \exp\Big(n^2\Big(\frac{S_2}{4K} + \frac{S_2}{2M}\Big)\Big) \tag{5.1b}$$

where K is the areal modulus, and M is the pure shear modulus in 2D space. Shear modulus G does not arise in these formulæ because their boundary conditions are shear free.

Here a formula to quantify parameter n is derived. By using Eq. (5.1), which contains parameter n, we select

$$a_1 = \exp\Big(\frac{1}{n^2}\Big(\frac{S_1}{4K} + \frac{S_1}{2M}\Big), \qquad b_2 = \exp\Big(n^2\Big(\frac{S_2}{4K} + \frac{S_2}{2M}\Big)\Big) \tag{5.2a}$$

that invert to become

$$\frac{n^2 \ln a_1}{S_1} = \Big(\frac{1}{4K} + \frac{1}{2M}\Big), \qquad \frac{\ln b_2}{S_2 n^2} = \Big(\frac{1}{4K} + \frac{1}{2M}\Big) \tag{5.2b}$$

which when equated lead to the following expression for n

$$n = \sqrt[4]{\frac{S_1 \ln b_2}{S_2 \ln a_1}}. \tag{5.2c}$$

By using Eq. (19) in Ref. [2], a useful relationship follows,

$$n = \sqrt[4]{\frac{S_1 \ln b_2}{S_2 \ln a_1}} = \sqrt[4]{\frac{E_1}{E_2}} \tag{5.2d}$$

where E_1 and E_2 are the elastic moduli aligned with the fiber and transverse-fiber

directions, respectively. R. W. Ogden [32] and T. J. Pence [33] have used a parameter (γ) with the neo-Hookean model to describe the anisotropic portion of mechanical behavior; however, their parameter doesn't have any physical meaning, unlike our parameter n defined in this thesis which does.

As seen above, parameter n can be calculated without knowing the other conjugate-pair material parameters viz., K and M. With this method, constitutive equations can easly be solved and material parameter calculation becomes straight forward. It describes how much the fibers increase material stiffness in the preferred direction. If $n > 1$, then the 1-direction will be stiffer than the 2-direction, and if $n < 1$, then the 2-direction will be stiffer than the 1-direction, while isotropy exists whenever $n = 1$. In addition, we conclude that parameter n arises from decoding/encoding maps, and not the constitutive equation itself [2]. In other words, n does not appear in either the stiffness or compliance matrices. A comparison for the strength of anisotropy (n) for different composite materials is discussed in later sections.

5.2 Large Strain Conjugate Pair for Linear Behavior

In Figure 5.1 curves in the left plot describe an average stress/strain response for 0° and 90° composite specimens, while curves in the right plot demonstrates the axial/transverse strain response for both the 0° and 90° specimens. The 0° specimens show higher stress/strain and Poisson values than the 90° specimens. Stress and the axial and transverse strain measurements are averaged from six specimens. The solid line represents the 0° composite responses, while dashed line presents 90° composite response with maximum and minimum bounds shown. Figure 5.2 demonstrates fiber, 0° and 90° silicone fiber-matrix composite, and matrix material uniaxial response.

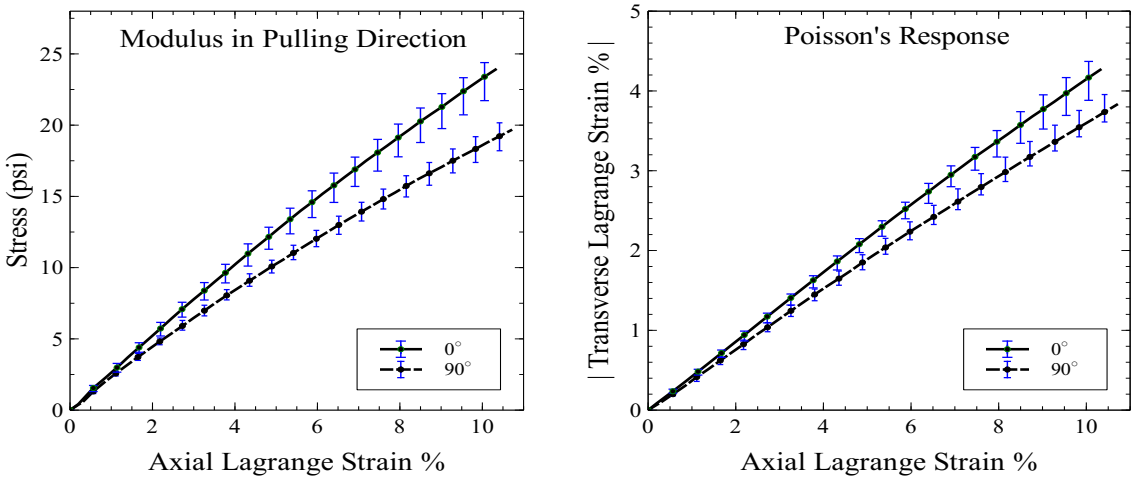

Figure 5.1: 0° silicone/silicone fiber-matrix composite material Stress vs. axial strain, and transerve vs. axial strain graphs. Barrents show the stress variation observed from six specimens. [17]

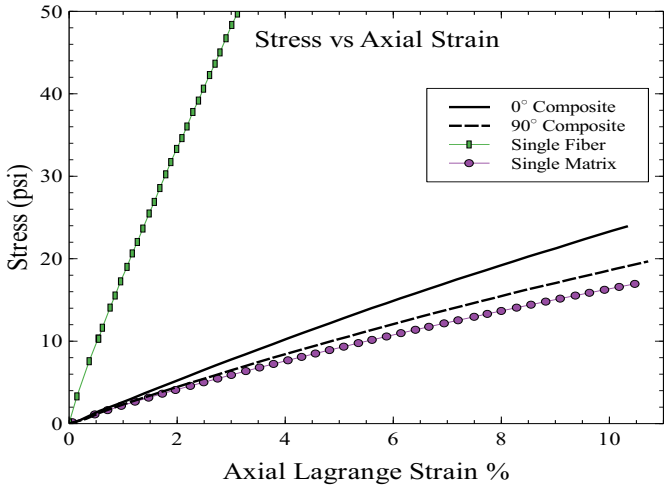

Figure 5.2: From top to bottom: fiber, 0° and 90° silicone fiber-matrix composite, and matrix material stress/strain responses. [17]

5.2.1 Data Analysis

A genetic algorithm optimization technique [21] was used to find optimum material parameters. Six 0° and six 90° stress/strain data sets generated 36 combinations of response, e.g., specimen 1 (0°) vs. specimen 7 (90°) and so on. First, material parameters (n, K, M) were obtained for the 36 individual combinations. Then average values for the three material parameters were calculated. Second, the six 0° stress/strain responses were combined by taking their average. Then the same procedure was applied to the six 90° responses. Both the 0° and 90° averaged stress/strain responses were used for parameter estimation. Third, each 0° and 90° data set was optimized by itself. After these parameter optimizations were completed. A statistical analyses was performed to gain a better understanding of the conjugate-pair material parameters.

Figure 5.3 shows parameter n, which represents the strength of anisotropy, as a box and whisker plot of the data for all optimization cases. The first two optimization cases and the 90° individual fits provide similar n mean values, while the 90° individual optimization demonstrates higher variation. Figure 5.4 shows parameter K and M, as box and whisker plots of the data for all optimization cases. The mean and variations show similarity for parameter K, while only the combined optimization demonstrates similar optimization results for parameter M. All mean and standard deviations are tabulated in Table 5.1, with an addition of the coffecient of determination (R-squared analysis). Because the R-squared values do not represent reliable measures for the different goodness of curve fitting, the authors added z-test and t-test statistical analyses to compare the different optimization cases.

Z-tests and t-tests were performed to compare whether two samples have the same mean or the same variance, respectively. The 0° and 90° averaged response

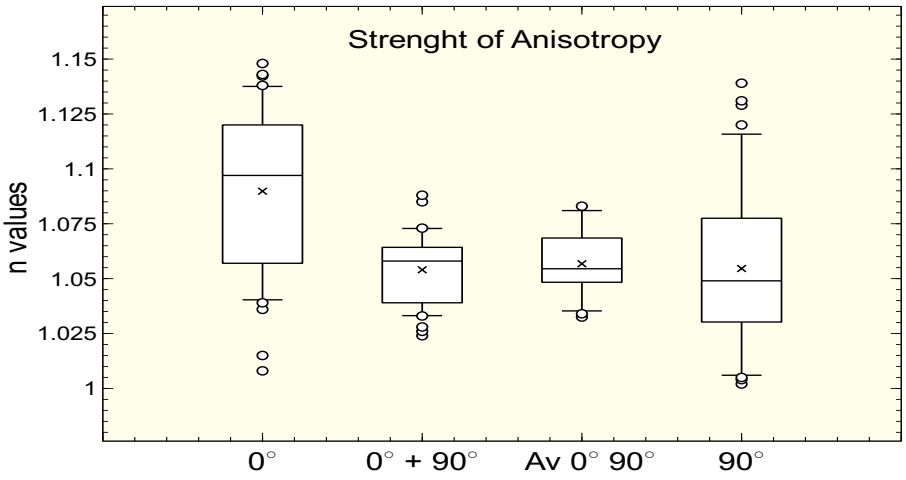

Figure 5.3: Parameter n box and whisker plot of the data for all optimization cases. [17]

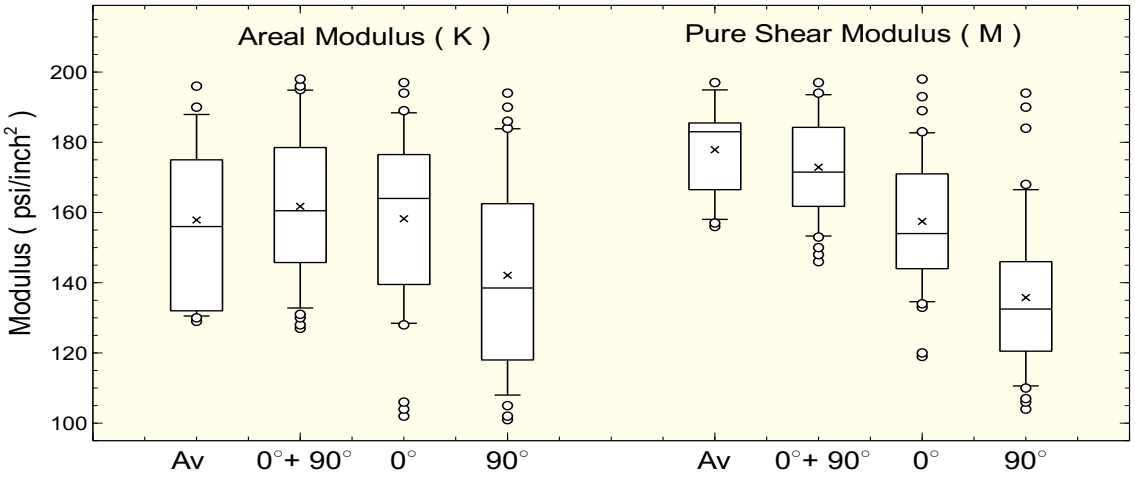

Figure 5.4: Parameter K and M box and whisker plots of the data for all optimization cases. [17]

Table 5.1: Optimization table for model parameters. [17]

		n	K	M	0° R^2	90° R^2
0° and 90° Average	Mean	1.056	157.86	177.76	0.998968	0.9997954
	Standard Deviation	0.015	22.74	12.05	3.527E-5	7.798E-5
0° and 90° All	Mean	1.054	161.75	172.88	0.998932	0.997840
	Standard Deviation	0.016	20.83	14.35	4.449E-4	8.18E-4
0° All	Mean	1.089	158.22	157.47	0.998908	
	Standard Deviation	0.037	25.04	19.38	4.419E-4	
90° All	Mean	1.054	142.11	135.77		0.997825
	Standard Deviation	0.036	27.63	22.29		8.36E-4

(optimization case two) was used to compare with other optimization cases in terms of material parameters. Table 5.2 presents the p-values used to determine if the data are statistically significant or not. Bolded values corresponding to less than 0.05 means there is a difference between the mean or the variance in a statistical sense. Only when each combination of all specimens are optimized (case one) are all p-values satisfied, i.e., there is insufficient statistical evidence to support the hypothesis that they are different.

Table 5.2: Z-test and t-test analyses were performed to compare mean and variance values. [17]

		p values		
selected p-value: 0.05		n	K	M
z test: Two sample assuming same means	0° and 90° All	0.574	0.565	0.22
	0° All	**8.93E-6**	0.96	**1.22E-5**
	90° All	0.767	**0.03**	**7.96-5**
t test: Two sample assuming same variance	0° and 90° All	0.586	0.563	0.2615
	0° All	**0.002**	0.962	**0.0006**
	90° All	0.828	0.061	**1.89E-8**

Three material parameters arise from the conjugate-pair approach. They have been calculated and compared with E-glass/vinylester material parameters [2]. Table 5.3 presents differences between compliant (silicone) and stiff (E-glass/vinylester) composites. Parameters K and M for the stiff composite are around an order in magnitude larger than those of the compliant composite.

Parameter n, as calculated by using elastic moduli via Eq. (7d), is compared with n values obtained through optimization in Table 5.4. A big difference can only be

Table 5.3: Stiff and compliant composites: conjugate-pair material comparison [17]

Conjugate parameters	n	K	M
E-glass/vinylester composite	1.15	1270	1670
Silicone/silicone composite	1.055	142	191

Table 5.4: An n value of 1.055 arises from the elastic modulus ratio, Eq. (7d), compared with statistical n values. [17]

	n	Difference from theoretical n	Variance
0° and 90° Average	1.056	0.1%	0.000254
0° and 90° All	1.054	0.1%	0.000262
0° All	1.89	3.2%	0.00138
90° All	1.054	0.1%	0.00132

seen for the 0° individual fits for the n value, while only the analysis that uses both 0° and 90° experimental results shows similar variance. By definition, n describes strength differences between the 0° and 90° specimens.

The goal of this work, proven in figure 5.5, was to validate an anisotropic, conjugate, stress/strain pairs approach for laminates undergoing large deformation. Compliant silicone/silicone fiber-matrix composite specimens were studied under uniaxial tension loading conditions. The author's anisotropic, conjugate, stress/strain basis theory has been successfully implemented for large deformations using three material parameters. A genetic algorithm was used to optimize the parameter estimation. Statistical methods like R-squared, z-test, and t-test were then used to gain a deeper understanding of the material parameters. Evidence suggests that the combined 0° and 90° data should be used to obtain less varied material parameters. Of particular interest is that the anisotropy parameter n, formulated in terms of Young's moduli, has a physical meaning, unlike classical anisotropic parameters such as γ.

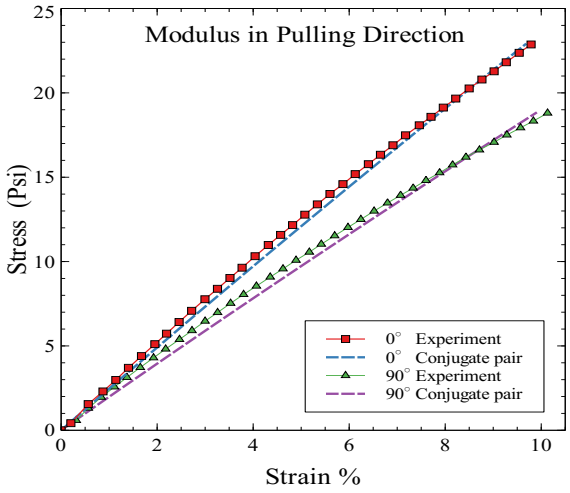

Figure 5.5: Correlation of experimental results with a conjugate-pair model for 0° and 90° composite specimens. [17]

5.3 Large Strain Conjugate Pair for Nonlinear Behavior

The same experimental setup and testing procedures have been used to perform 60% uniaxial tensile experiments on a silicone/silicone composite material. Due to 90° specimen delamination, Gom Correlate commercial DIC software was used to verify strain results obtained through Ncorr. Each specimen comparison for axial and transverse percent strain values can be seen in Tables 5.5 and 5.6. Strain differences between these two softwares are in the acceptable range. Explicit conjugate pair models have been used to model experimental results and compared with conventional (Neo-Hookean) transversely isotropic models that were proposed by Pence, and Ogden. A constraint caused by transverse direction boundary condition has been implemented into a genetic algorithm for obtaining material parameters.

Table 5.5: Ncorr vs. GOM Axial Percent Strain Comparison

0° degree			90° degree		
Specimen	Ncorr	GOM	Specimen	Ncorr	GOM
1-1	58.9874	59.4085	3-1	58.164	60.8837
1-2	59.1136	59.9767	3-2	58.7275	61.0505
1-3	57.5182	58.3475	3-3	57.7671	60.5215
2-1	58.9951	62.9051	4-1	59.4908	59.1700
2-2	57.6887	58.1328	4-2	61.1311	62.3756
2-3	58.9174	60.1433	4-3	59.4756	57.9016
Average	58.8649	59.8425	Average	59.1260	60.3171
Difference	1.66%		Difference	2.02%	

Table 5.6: Ncorr vs. GOM Transverse Percent Strain Comparison

0° degree			90° degree		
Specimen	Ncorr	GOM	Specimen	Ncorr	GOM
1-1	-19.6426	-19.3992	3-1	-17.8706	-18.8505
1-2	-20.1462	-20.7243	3-2	-17.7676	-18.3283
1-3	-19.4583	-20.1714	3-3	-16.3703	-19.0631
2-1	-19.9068	-19.6378	4-1	-18.2945	-17.6873
2-2	-19.2425	-19.3998	4-2	-17.4043	-17.4879
2-3	-20.1857	-20.1599	4-3	-18.2129	-18.4824
Average	-19.878	-20.553	Average	-17.6534	-18.3166
Difference	3.4%		Difference	3.75%	

5.3.1 Conventional Nonlinear Transversely Isotropic Theories

Neo-Hookean transversely isotropic theories, have historically been used to describe rubber-like behavior, which were studied by T.J. Pence [33], J. Merodio and R.W. Ogden [32], and others as an application of fiber-reinforced, nonlinear, elastic solids. Single-axis, continuous, fiber reinforcement provides transverse anisotropy, which can be described in terms of a forth and fifth strain invariant [9]. In a proceeding paper [34] published by the author contains a different Neo-Hookean transversely isotropic models comparison and uniaxial boundary condition derivation. In that study the author concluded that a constitutive equation which uses the 4th invariant provides better results, and that silicone/silicone composite material is compressible. Thus, the same constitutive equations have been used to obtain material parameters for the 0° and 90° silicone/silicone material.

5.3.2 Constraint Condition

Constitutive equations derived from invariant theory introduce constraint conditions arising in the transverse direction. The contracted direction should have a zero stress value with a constant material parameter and varying strain input. Consider a compressible Neo-Hookean transversely isotropic constitutive equation that was proposed by Thomas Pence, which uses the 4th invariant to describe anisotropic

behavior. The 0° composite nominal stress can be found as [34]

$$\begin{aligned} N_{11} &= \mu J^{-1}\Big[-\frac{\lambda_1^2+\lambda_2^2}{2\lambda_1}+\lambda_1\Big]+2D_1(J-1)\lambda_2+2\mu\gamma\lambda_1(\lambda_1^2-1) \\ &= \frac{\mu}{2}J^{-1}\Big[\lambda_1-\frac{J^2}{\lambda_1^3}\Big]+2D_1(J-1)\lambda_2+2\mu\gamma\lambda_1(\lambda_1^2-1) \qquad (5.3a) \\ N_{22} &= \mu J^{-1}\Big[-\frac{\lambda_1^2+\lambda_2^2}{2\lambda_2}+\lambda_2\Big]+2D_1(J-1)\lambda_1=0 \\ &= \frac{\mu}{2}J^{-1}\Big[\lambda_2-\frac{J^2}{\lambda_2^3}\Big]+2D_1(J-1)\lambda_1 \\ &= \frac{\mu}{2}J^{-1}\Big[\frac{J}{\lambda_1}-\frac{\lambda_1^3}{J}\Big]+2D_1(J-1)\lambda_1 \qquad (5.3b) \end{aligned}$$

The N_{22} stress value is equal to zero due to the reason mentioned above. To obtain material parameters, this constraint condition has also to be satisfied. A sequential least square algorithm was used for this purpose, which is in the implemented in the Scipy library.

Consider the Conjugate Pair dilation and squeeze stress terms, which are

$$\pi = \frac{S_{11}}{n}+nS_{22}, \quad \text{and} \quad \sigma = \frac{S_{11}}{n}-S_{22}n. \qquad (5.4)$$

For uniaxial tensile boundary condition, S_{11} =S and S_{22} =0. After inserting these stress values into the conjugate pair stress terms one gets

$$\pi = \frac{S_{11}}{n}, \quad \text{and} \quad \sigma = \frac{S_{11}}{n} \qquad (5.5)$$

with this relations, and the constraint conditions are been satisfied. Thus, the conjugate pair approach does not require nonlinear optimization with a constrain condition to find optimal material parameters.

5.3.3 Material Parameter Optimization

A transversely isotropic Neo-Hookean model was parameterized using 0 degree and 90 degree silicone/silicone uniaxial data. A sequential, nonlinear, least-squares (SLSQP) program from the SciPy Python library was used to quantify these material parameters. Constraint conditions (Eqs. 21b and 22a) arise from the traction-free boundary condition that exists in the transverse direction, and were also applied to the least-squares algorithm. A simultaneous least-squares algorithm was also used to obtain material parameters for Qiu and Pence's model. Figure 5.6 demonstrates the Neo-Hookean model fits to the author's experimental results, and Table 5.7 shows these material parameters.

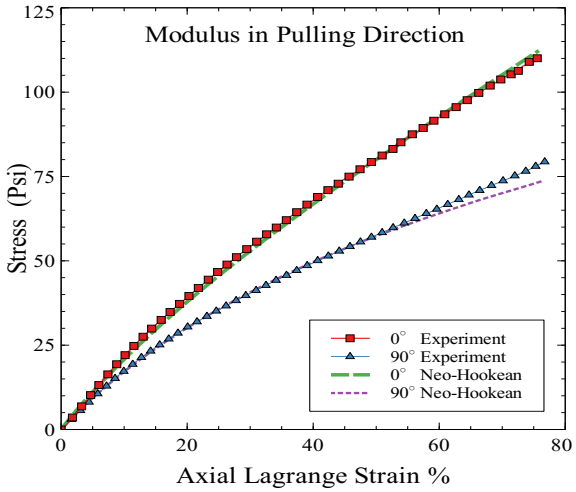

Figure 5.6: Uniaxial tensile 0° and 90° composite specimens response and the transversely isotropic Neo-Hookean model

Table 5.7: 60 % Neo-Hookean material parameters

Neo-Hookean model parameters	μ	D_1	γ
Silicone/silicone composite	69.8192	83.486	0.1297

5.3.4 Conjugate Pair Model

The same uniaxial experimental results were used with transversely isotropic conjugate pair approach (explicit dilation and squeeze equations) to obtain material parameters. First the anisotropic parameter n was calculated through Eq. 5.2. Then the First PK and stretch measurements were used to plot the dilation and squeeze responses. Unlike the Neo-Hookean response, the explicit conjugate pair models provide a linear response for both dilation and squeeze. Figure 5.7 and 5.8 show the dilation and squeeze responses respectively. Material parameters can been seen in Table 5.8.

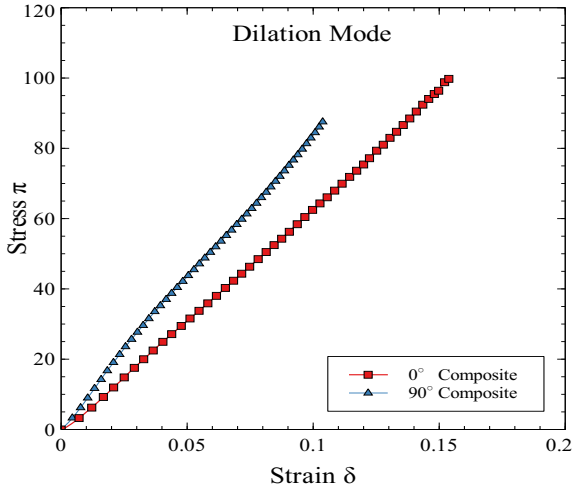

Figure 5.7: Uniaxial tensile 0° and 90° composite specimens dilation response

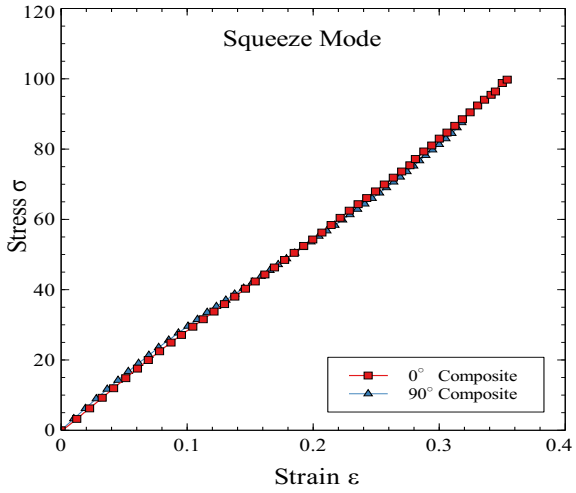

Figure 5.8: Uniaxial tensile 0° and 90° composite specimens squeeze response

Table 5.8: 60 % Conjugate pair material parameters

Conjugate parameters	n	K_0	K_{90}	M
Silicone/silicone composite	1.098	643.04	826.53	270.13

6. FINITE ELEMENT IMPLEMENTATION

Hyperelastic materials utilize a strain energy density function to derive constitutive equations. Professor Ronald Rivlin, who was one of the creators of large strain elasticity theory, published a series of papers between 1948 and 1952 entitled 'large elastic deformations of isotropic elastic materials'. He luculently explained that the strain energy density for an isotropic elastic solid can be stated as a function of deformation tensor invariants [35]. The Neo-Hookean model, derived from statistical mechanics by Treloar [36] and others, is a special case of Rivlin's invariant theory at the continuum level. Models by Mooney-Rivlin, Ogden, Fung and numerious others have been proported, often given the name of their developers. Most material models are derived from a strain energy function, a feature that finite element software has widely adopted.

Finite element analysis is a method that solves engineering and physics problems numerically. The working principle of a finite element solver is to first process the deformation gradient to obtain either a Lagrangian or an Eulerian strain measure. Then use either the Green deformation or the Finger deformation tensor invariants to calculate stress values, which are gradients of the strain energy density function. Lastly, a tangent (stifness) matrix is calculated using material parameters. It is comprised of second derivatives of the strain energy density. There are many commercial finite element softwares available to simulate a material response. These codes are commonly used for solid and fluid material applications. Biological materials such as bones, tissues, ligaments and muscles, due to anisotropy, non-homogeneity, and viscoelastic behavior of these materials, are more challenging to implement into code.

FEBio is an open-source, nonlinear, finite element software specifically constructed

for biomechanical applications. Abaqus/CAE is a commercial finite element analysis software. Both packages offer plugin options that provide a means for users to expand upon the existing material model library without a need of recompile the whole source code. Plugins for FEBio can be written in C++ or Fortran77, the latter being used for Abaqus/CAE. Tangent (Jacobian) and stress functions are the two main matrices that need to be defined for our application. The conjugate pair approach constructs its stress and tangent functions in the experimentor's coordinate frame, after which they need to be rotated into the spatial frame. Even if there is no rotation during deformation, our stress/strain measure still requires to be transformed. There is no rotation between frames, and the fiber directions are parallel to the x direction are the assumptions made to calculate the stress and a tangent function.

The stress function takes a deformation gradient to calculate the conjugate strain measures. A root finding algorithm is required to determine the conjugate stress values because the constitutive equations are nonlinear. The false position method has been implemented for this purpose. Finally, values for stress are calculated via known stress relations. Rotations between the experimentor's frame to the Lagrangian and Eulerian frames should be considered as final steps. A flow chart demonstrates all calculations to get Cauchy stress, in detail.

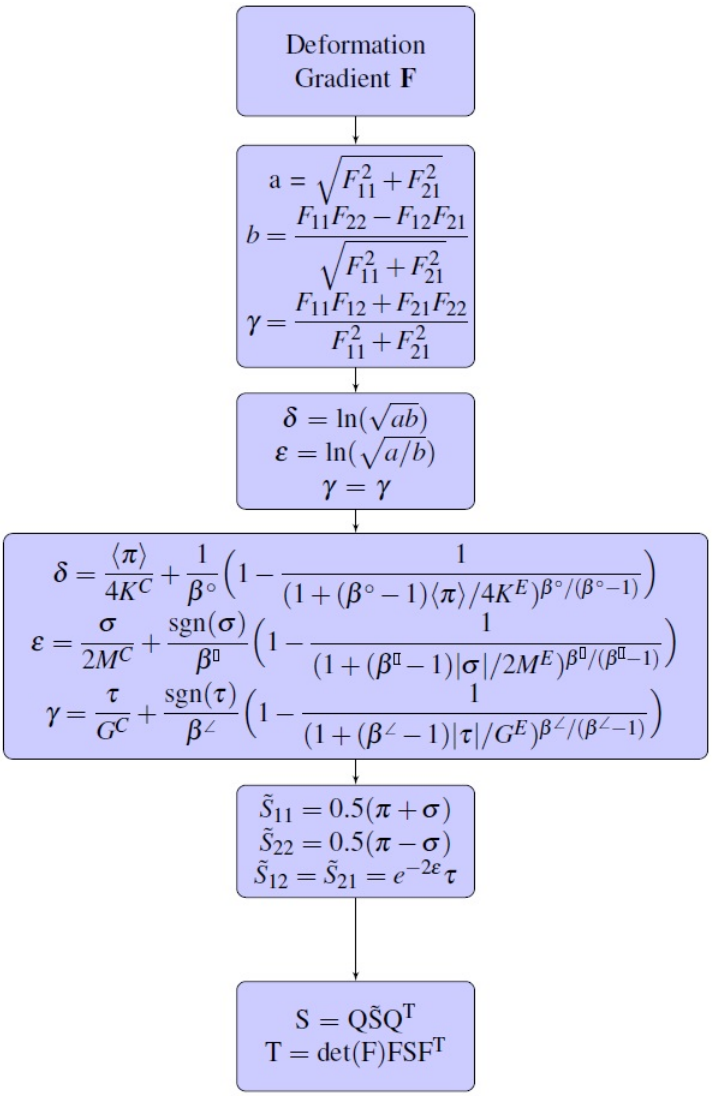

Figure 6.1: Cauchy stress calculation

6.1 Tangent Modulus Calculation from Experimentor's Frame to Spatial Frame

The most general tangent equation is dS = M:dE where S is the PK stress and E is Almansi strain, which is a general constitutive equation expressed in the Eulerian frame. The tangent function requires some transformation, because the conjugate approach uses conjugate stress/strain pairs that need to be converted into Eulerian stress/strain measures. A chain rule and a compliance matrix were used to reduce complicated calculations. The compliance matrix equation for the Experimentor's frame can be separated as below

$$\tilde{C} = \frac{\mathrm{d}\tilde{E}}{\mathrm{d}\tilde{S}} = \frac{\partial \tilde{E}}{\partial \Lambda} : \frac{\mathrm{d}\Lambda}{\mathrm{d}\Omega} : \frac{\mathrm{d}\Omega}{\mathrm{d}\Sigma} : \frac{\partial \Sigma}{\partial \tilde{S}} \tag{6.1}$$

where $\Lambda = \{a, b, \gamma\}$ is set of stretch components , $\Sigma = \{\pi, \sigma, \tau\}$ is set of conjugate stresses and $\Omega = \{\delta, \epsilon, \gamma\}$ is set of conjugate strains.

Lets investigate each term in the chain; and begin with the relation between stretch and Almansi strain that can be found in Eq. 8a [7]. The aim is to find tangent modulus for the spatial configuration.

$$\tilde{E} = \frac{1}{2}(I - \tilde{b}^{-1}), \quad \tilde{b}^{-1} = \tilde{F}^{-T}\tilde{F}^{-1}, \quad \tilde{F}^{-1} = \begin{bmatrix} 1/a & -\gamma/b \\ 0 & 1/b \end{bmatrix} \tag{6.2a}$$

and

$$\begin{bmatrix} \tilde{E}_{11} & \tilde{E}_{12} \\ \tilde{E}_{21} & \tilde{E}_{22} \end{bmatrix} = \frac{1}{2}\begin{bmatrix} 1 - 1/a^2 & \gamma/ab \\ \gamma/ab & 1 - (\gamma^2+1)/b^2 \end{bmatrix} \tag{6.2b}$$

We need to take the derivative of stretch components (a, b, γ) with respect to $\tilde{E}_{11}$,

$\tilde{E}_{22}$, and $\tilde{E}_{12}$

$$\frac{\partial \tilde{E}_{11}}{\partial a} = \frac{1}{a^3} \tag{6.3a}$$

$$\frac{\partial \tilde{E}_{22}}{\partial b} = \frac{1+\gamma^2}{b^3}, \quad \frac{\partial \tilde{E}_{22}}{\partial \gamma} = -\frac{\gamma}{b^2} \tag{6.3b}$$

$$\frac{\partial \tilde{E}_{12}}{\partial a} = \frac{-\gamma}{2a^2 b}, \quad \frac{\partial \tilde{E}_{12}}{\partial b} = \frac{-\gamma}{2ab^2}, \quad \frac{\partial \tilde{E}_{12}}{\partial \gamma} = -\frac{1}{2ab} \tag{6.3c}$$

Secondly, the relation between stretch and conjugate stress can be seen as

$$\delta = ln\sqrt{ab}, \quad \epsilon = ln\sqrt{a/b}, \quad \gamma = \gamma \tag{6.4}$$

Their derivatives with respect to conjugate strains are quite straight forward.

$$\frac{\partial \delta}{\partial a} = \frac{1}{2a}, \quad \frac{\partial \delta}{\partial b} = \frac{1}{2b}, \quad \frac{\partial \epsilon}{\partial a} = \frac{1}{2a}, \quad \frac{\partial \epsilon}{\partial b} = -\frac{1}{2b}, \quad \frac{\partial \gamma}{\partial \gamma} = 1 \tag{6.5a}$$

We need to take the inverses of these matrices to find stretch derivatives with respect to these conjugate strains.

Thirdly, the derivative of conjugate stress pairs with respect to conjugate strain pairs means a material models' derivatives. These come from constitutive equations. These relations can be derived by using equations 22 [7].

$$\frac{\mathrm{d}\delta}{\mathrm{d}\pi} = \frac{1}{4K^C} + \frac{1}{4K^E(\frac{\pi(\beta^\circ - 1)}{4K^E} + 1)^{(2\beta^\circ - 1)/(\beta^\circ - 1)}} \tag{6.6a}$$

$$\frac{\mathrm{d}\epsilon}{\mathrm{d}\sigma} = \frac{1}{2M^C} + \frac{sign(\sigma)}{2M^E(\frac{\sigma(\beta^\square - 1)}{2M^E} + 1)^{(2\beta^\square - 1)/\beta^\square - 1}} \tag{6.6b}$$

$$\frac{\mathrm{d}\gamma}{\mathrm{d}\tau} = \frac{1}{G^C} + \frac{sign(\tau)}{G^E(\frac{\tau(\beta^\angle - 1)}{G^E} + 1)^{(2\beta^\angle - 1)/(\beta^\angle - 1)}} \tag{6.6c}$$

Lastly, the relation between conjugate pair stresses and Kirchhoff stress $\tilde{S}$ can be

found in the Freed, Erel and Moreno paper Eq 11b.

$$\frac{\partial \tilde{S}}{\partial \Sigma} = \begin{bmatrix} 1 & 1 & 0 \\ 1 & -1 & 0 \\ 0 & 0 & e^{2\epsilon} \end{bmatrix} \tag{6.7}$$

A multiplication of these 4 matrices can be seen below

$$\begin{bmatrix} 1/a^3 & 0 & 0 \\ 0 & (1+\gamma^2)/b^3 & -\gamma/b^2 \\ -\gamma/2a^2b & -\gamma/2ab^2 & -1/2ab \end{bmatrix} \begin{bmatrix} a & a & 0 \\ b & -b & 0 \\ 0 & 0 & 1 \end{bmatrix} \begin{bmatrix} \frac{\mathrm{d}\delta}{\mathrm{d}\pi} & 0 & 0 \\ 0 & \frac{\mathrm{d}\epsilon}{\mathrm{d}\sigma} & 0 \\ 0 & 0 & \frac{\mathrm{d}\gamma}{\mathrm{d}\tau} \end{bmatrix} \begin{bmatrix} 1 & 1 & 0 \\ 1 & -1 & 0 \\ 0 & 0 & e^{-2\epsilon} \end{bmatrix} \tag{6.8}$$

All these multiplications produce a compliance matrix in the experimentor's coordinate frame. A matrix inversion and a tensor transformation are done to finally obtain a tangent modulus for the spatial configuration. There is no rotation between frames and fiber directions are parallel to the x direction assumptions were made to calculate this tangent matrix.

6.2 FEBio and Abaqus, Comparisions with Experimental Results

The specimen dimensions (25mm x 25mm) taken from reference paper [37] are used to simulate a dilation and squeeze experiment. FEBio is a new finite element package compared to Abaqus, so it has some limitations, e.g., load driven simulations are nonstable for some cases. A plane stress condition has been selected with a prescribed displacement boundary condition. Material parameters have been taken from a conjugate pairs paper presenting a planar analysis of biological tissues [7]. Figure 6.2 shows simulation results which are very close to the experimental results. There are small mismatching regions because constitutive equations cannot perfectly represent experimental results.

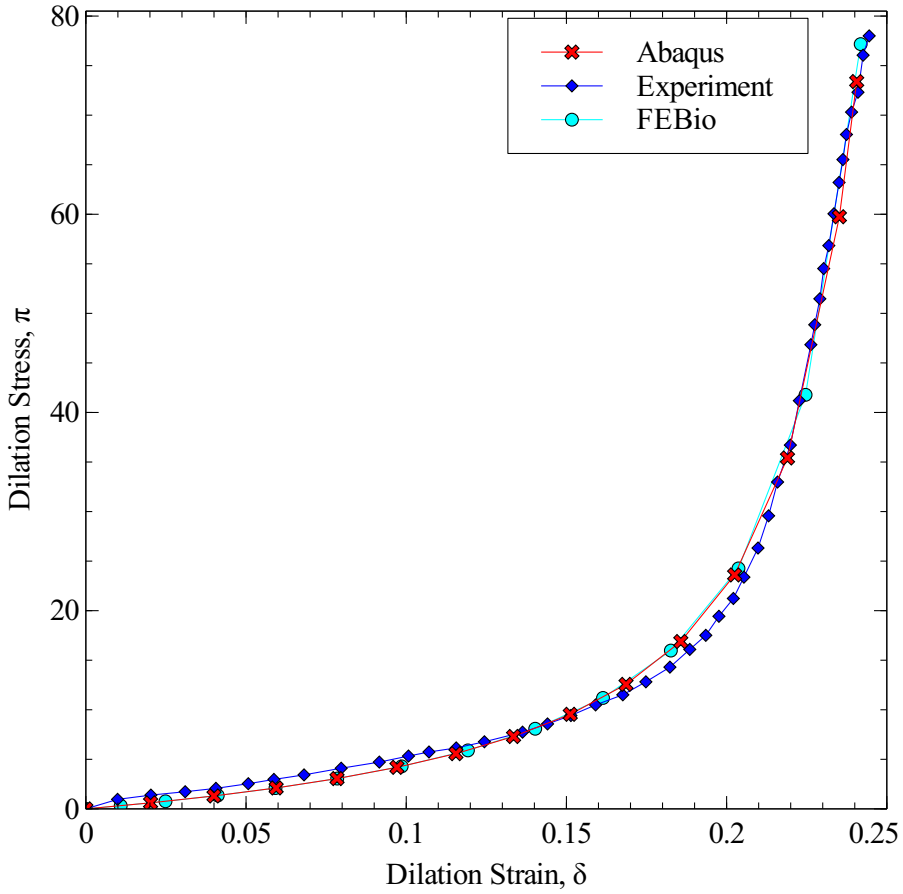

Figure 6.2: FEBio and Abaqus simulations are compared with experimental results

7. CONCLUSION

This study presents linear and nonlinear transversely isotropic material models. Theoretical models validated with experimental results and material parameters have been found through optimization techniques such as a genetic algorithm and a sequential least square algorithm. Advantages of newly proposed models can be summarized as follows

1. Isotropic and anisotropic constitutive equations can be derived from the same strain energy function. In other words, the conjugate base pairs obey the law of thermodynamics.

2. The anisotropic conjugate stress/strain model, which doesn't require invariant theory, has parameters that are more general than Spencer's model. It requires four material parameters to describe material behavior: K, M, G and n vs. five for Spencer's model.

3. Strength of anisotropy parameter (n), formulated in terms of Young's moduli, has a physical meaning and is readily extracted from basic experiments done on composites.

4. Constraint conditions like traction free are automatically satisfied, unlike the Neo-Hookean model, due to the nature of dilation and squeeze equations. Constraint optimization techniques are required to obtain Neo-Hookean material parameters.

5. Conjugate pair approach provides an opportunity to describe nonlinear, rubber like behavior as a linear response.

6. Anisotropic, conjugate, stress/strain basis theory has been successfully implemented for small and large deformation. From 0.1% to 60 % percent uniaxial behavior can be described with unique constitutive equations.

REFERENCES

[1] Veysel Erel, Mingliang Jiang, and Alan D. Freed. Conjugate stress/strain pair approach for anisotropic materials. In *Proceedings of the American Society for Composites - Thirty-Third Technical Conference on Composite Materials*. DEStech Publications, 2018.

[2] Veysel Erel and Alan D. Freed. Stress/strain basis pairs for anisotropic materials. *Composites Part B: Engineering*, 120:152 – 158, 2017.

[3] Raymond W Ogden. *Non-linear elastic deformations*. Courier Corporation, 1997.

[4] Junuthula Narasimha Reddy. *Energy principles and variational methods in applied mechanics*. John Wiley & Sons, 2017.

[5] A.R.Srinivasa. On the use of the upper triangular (or **QR**) decomposition for developing constitutive equations for green-elastic materials. *Journal of Engineering Scince*, 60:1–12, 2012.

[6] JC Simo and TJR Hughes. Computational inelasticity, interdisciplinary applied mathematics vol. 7,(Springer-Verlag, new york, 1998).

[7] Alan D. Freed, Veysel Erel, and Micheal R. Moreno. Conjugate stress/strain base pairs for planar analysis of biological tissues. *Journal of Mechanics of Materials and Structures*, 2016.

[8] Alan D. Freed and A.R. Srinivasa. Logarithmic strain and its material derivative for a QR decomposition of the deformation gradient. *Acta Mechanica*, 226:2645–2670, 2015.

[9] A. J. M. Spencer. *Deformations of fibre-reinforced materials*. Oxford Science Research Papers. 1972.

[10] Alan D. Freed. *Soft solids : a primer to the theoretical mechanics of materials*. Modeling and Simulation in Science, Engineering and Technology. 2014.

[11] C. Caratheodory. Investigations into the foundations of thermodynamics. *The Second Law of Thermodynamics*, 5:229–256, 1976.

[12] AG McLellan. Finite strain coordinates and the stability of solid phases. *Journal of Physics C: Solid State Physics*, 9(22):4083, 1976.

[13] Kumbakonam R Rajagopal. On implicit constitutive theories. *Applications of Mathematics*, 48(4):279–319, 2003.

[14] G. F. Becker. The finite elastic stress-strain function. *American Journal of Science*, 46:337–356, 1893.

[15] H. Hencky. The law of elasticity for isotropic and quasi-isotropic substances by finite deformations. *Journal of Rheology*, 2:169–176, 1931.

[16] P. Neff, I. Münch, and R. Martin. Rediscovering G. F. Becker's early axiomatic deduction of a multiaxial nonlinear stress-strain relation based on logarithmic strain. *Mathematics and Mechanics of Solids*, 21(7):856–911, 2016.

[17] Veysel Erel, Mingliang Jiang, Michael R Moreno, and Alan D Freed. Anisotropic conjugate stress/strain base pair approach for laminates undergoing large deformations. *Materialia*, 6:100318, 2019.

[18] ASTM D3039/D3039M-17 Standard Test Method for Tensile Properties of Polymer Matrix Composite Materials. *ASTM International*.

[19] J Blaber, B Adair, and A Antoniou. Ncorr: open-source 2D digital image correlation Matlab software. *Experimental Mechanics*, 55(6):1105–1122, 2015.

[20] Johannes Schindelin, Curtis T Rueden, Mark C Hiner, and Kevin W Eliceiri. The ImageJ ecosystem: An open platform for biomedical image analysis. *Molecular Reproduction and Development*, 82(7-8):518–529, 2015.

[21] DE Goldberg. Genetic Algorithms in Search, Optimization, and Machine Learning (1989). *New York, Addison-Wesley.*

[22] SN Sivanandam and SN Deepa. *Introduction to Genetic Algorithms*. Springer, 2008.

[23] Simon Baker and Iain Matthews. Lucas-Kanade 20 years on: A unifying framework. *International journal of computer vision*, 56(3):221–255, 2004.

[24] Bing Pan, Huimin Xie, and Zhaoyang Wang. Equivalence of digital image correlation criteria for pattern matching. *Applied optics*, 49(28):5501–5509, 2010.

[25] Philippe Thévenaz, Thierry Blu, and Michael Unser. Image interpolation and resampling. *Handbook of medical imaging, processing and analysis*, 1(1):393–420, 2000.

[26] Bing Pan. Reliability-guided digital image correlation for image deformation measurement. *Applied optics*, 48(8):1535–1542, 2009.

[27] Bing Pan, Huimin Xie, Zhiqing Guo, and Tao Hua. Full-field strain measurement using a two-dimensional Savitzky-Golay digital differentiator in digital image correlation. *Optical Engineering*, 46(3):033601, 2007.

[28] Anastasia Hanifah Muliana. *Integrated Micromechanical–Structural Framework for the Nonlinear Viscoelastic Behavior of Laminated and Pultruded Composite Materials and Structures*. PhD thesis, Citeseer, 2003.

[29] Shivakumar I Ranganathan and Martin Ostoja-Starzewski. Universal elastic anisotropy index. *Physical Review Letters*, 101(5):055504, 2008.

[30] John Milsom. *Field geophysics*, volume 25. John Wiley and Sons, 2007.

[31] Jorn A Cheney, Nicolai Konow, Andrew Bearnot, and Sharon M Swartz. A wrinkle in flight: the role of elastin fibres in the mechanical behaviour of bat wing membranes. *Journal of The Royal Society Interface*, 12(106):20141286, 2015.

[32] J Merodio and RW Ogden. Mechanical response of fiber-reinforced incompressible non-linearly elastic solids. *International Journal of Non-Linear Mechanics*, 40(2-3):213–227, 2005.

[33] GY Qiu and TJ Pence. Remarks on the behavior of simple directionally reinforced incompressible nonlinearly elastic solids. *Journal of Elasticity*, 49(1):1–30, 1997.

[34] Veysel Erel, Mingliang Jiang, Michael R Moreno, and Alan D Freed. Experimental validation of neo-hookean fiber reinforced elastic solids. In *ASME 2018 Conference on Smart Materials, Adaptive Structures and Intelligent Systems*. American Society of Mechanical Engineers Digital Collection, 2018.

[35] A. J. M. Spencer. Ronald Rivlin and invariant theory. *International Journal of Engineering and Science*, 47.

[36] Leslie Ronald George Treloar. *The physics of rubber elasticity*. Oxford University Press, USA, 1975.

[37] Alan D Freed, Jun Liao, and Daniel R Einstein. A membrane model from implicit elasticity theory: application to visceral pleura. *Biomechanics and modeling in mechanobiology*, 13(4):871, 2014.